

1976

Hydraulics of ice covered channels.

Mohamed Reda Ibrahim. Haggag
University of Windsor

Follow this and additional works at: <http://scholar.uwindsor.ca/etd>

Recommended Citation

Haggag, Mohamed Reda Ibrahim., "Hydraulics of ice covered channels." (1976). *Electronic Theses and Dissertations*. Paper 2336.

This online database contains the full-text of PhD dissertations and Masters' theses of University of Windsor students from 1954 forward. These documents are made available for personal study and research purposes only, in accordance with the Canadian Copyright Act and the Creative Commons license—CC BY-NC-ND (Attribution, Non-Commercial, No Derivative Works). Under this license, works must always be attributed to the copyright holder (original author), cannot be used for any commercial purposes, and may not be altered. Any other use would require the permission of the copyright holder. Students may inquire about withdrawing their dissertation and/or thesis from this database. For additional inquiries, please contact the repository administrator via email (scholarship@uwindsor.ca) or by telephone at 519-253-3000ext. 3208.

INFORMATION TO USERS

THIS DISSERTATION HAS BEEN
MICROFILMED EXACTLY AS RECEIVED

This copy was produced from a microfiche copy of the original document. The quality of the copy is heavily dependent upon the quality of the original thesis submitted for microfilming. Every effort has been made to ensure the highest quality of reproduction possible.

PLEASE NOTE: Some pages may have indistinct print. Filmed as received.

Canadian Theses Division
Cataloguing Branch
National Library of Canada
Ottawa, Canada K1A 0N4

AVIS AUX USAGERS

LA THESE A ETE MICROFILMEE
TELLE QUE NOUS L'AVONS RECUE

Cette copie a été faite à partir d'une microfiche du document original. La qualité de la copie dépend grandement de la qualité de la thèse soumise pour le microfilmage. Nous avons tout fait pour assurer une qualité supérieure de reproduction.

NOTA BENE: La qualité d'impression de certaines pages peut laisser à désirer. Microfilmée telle que nous l'avons reçue.

Division des thèses canadiennes
Direction du catalogage
Bibliothèque nationale du Canada
Ottawa, Canada K1A 0N4

HYDRAULICS OF ICE COVERED CHANNELS

A Thesis

Submitted to the Faculty of Graduate Studies Through
The Department of Civil Engineering in Partial
Fulfillment of the Requirements of the
Degree of Master of Applied Science,
at the
University of Windsor

by

Mohamed Reda Ibrahim Haggag
B.Sc. (Honours)

Windsor, Ontario, Canada
1976

© Mohamed Beda Ibrahim Haggag 1976

To my wife,

With all the love that ones heart can bear,
thank you very much.

ABSTRACT

The problem of the flow in ice covered channels was treated theoretically and experimentally.

The theoretical treatment includes the prediction of the velocity profile, the separation surface as well as the computation of the composite roughness.

A rigid simulated ice cover with different thicknesses was tested experimentally. Also, the fluid turbulence at the front of the cover was studied. The underside configurations for loose covers were also observed in the laboratory.

There was good agreement between the theory and both the experimental and field data.

ACKNOWLEDGEMENTS

The writer is greatly indebted to his advisor, Dr. S.P. Chee, Professor of Civil Engineering for his sincere, patient guidance throughout this study. His valuable suggestions and comments were truly helpful, and his kindness, support and continuous encouragement are sincerely appreciated.

The writer wishes to express his thanks to Dr. J.A. McCorquodale, Professor of Civil Engineering for his comments, concern and encouragement.

The aid of Mr. P. Feimer and Mr. G. Michalczuk during the experimental work is highly appreciated.

Finally, the writer is grateful to the financial support provided by the National Research Council of Canada, and the Civil Engineering Department at the University of Windsor including the use of the hydraulics laboratory.

TABLE OF CONTENTS

	PAGE
APPROVAL PAGE	iii
DEDICATION	iv
ABSTRACT	v
ACKNOWLEDGEMENTS	vii
TABLE OF CONTENTS	x
LIST OF FIGURES	xiii
LIST OF TABLES	xiii
CHAPTER 1. INTRODUCTION	1
1.1 Introduction	2
1.2 Definition of the Problem	3
CHAPTER 2. LITERATURE SURVEY	4
2.1 Introduction	5
2.2 Underside of Ice Covers	5
2.3 Composite Roughness of Ice Covered Channels	7
CHAPTER 3. THEORETICAL ANALYSIS	33
3.1 Introduction	34
3.2 Theoretical Assumptions	34
3.3 On the Flow Equation	35
3.4 The Shear Distribution	39
3.4.1 Velocity Distribution	40
3.4.2 Velocity Distribution Characteristics	46
3.5 The Dividing Surface Equation	48
3.6 The Composite Roughness Equation	50
3.7 Methods of Solution	52
3.8 Practical Applications	53
CHAPTER 4. EXPERIMENTAL ARRANGEMENT AND RESULTS	54
4.1 Introduction	55
4.2 The Test Equipment	55
4.2.1 Laboratory Facilities	55
4.2.2 Bedforms	57
4.2.3 Simulated Ice Covers	57
4.2.4 Ice Traps	60
4.3 Measurement Equipment	60
4.3.1 Point Gauges	60
4.3.2 Pitot-tube	63
4.3.3 Loose Cover Underside Configuration	63
4.3.4 The Shear Apparatus	63

	PAGE
CHAPTER 4. cont'd	
4.4 Experimental Arrangement, Procedure and Results	63
4.4.1 Seven Different Groups of Experiments	63
4.4.2 Evaluation of the Channel Roughness .	65
4.4.3 Evaluation of Cover Roughness	65
4.4.4 Effect of the Ice Cover Front	65
4.4.5 Verification	65
4.4.6 Composite Roughness	67
4.4.7 Loose Ice Cover Configuration	67
4.5 Experimental Errors	67
CHAPTER 5. DISCUSSION OF THE EXPERIMENTAL RESULTS	68
5.1 The Effects of the Front Zone	69
5.1.1 Cover Front Effect on Velocity Distribution	69
5.1.2 Effect of Cover Front on Shear Distribution	73
5.1.3 General Conclusions	77
5.2 The Velocity Distribution	81
5.3 Checking for λ Value	83
5.4 Composite Roughness: Experimental Data	89
5.5 Composite Roughness: Field Data Verification	93
5.5.1 Application to Uzuner's Data	93
5.5.2 Comparison of Developed Theory with Carey's Equation	93
5.5.3 Comparison of Known Relations for Computation of Composite Roughness ..	97
5.6 Loose Cover Underside Configuration	99
5.6.1 The Longitudinal Configuration	99
5.6.2 The Lateral Configuration	100
CHAPTER 6. DIMENSIONAL ANALYSIS	103
6.1 Introduction	104
6.2 The Factors Affecting the Problem	104
A. Geometric	104
B. Kinematic	105
C. Dynamic	105
6.3 Dimensional Analysis	108
6.4 General Solution	109
6.4.1 Solution for λ	109
6.4.2 Solution for Composite Roughness	111
6.5 Experimental Data Fitting	113
CHAPTER 7. CONCLUSIONS	114
APPENDIX A. GRAPHICAL SOLUTION OF THE COMPOSITED ROUGHNESS PROBLEM	117

	PAGE
APPENDIX B. COMPUTATION OF RATING CURVES, NUMERICAL EXAMPLE	127
APPENDIX C. DESIGN OF ICE COVERED CHANNELS, NUMERICAL EXAMPLE	132
APPENDIX D. EXPERIMENTAL ERRORS	137
APPENDIX E. EXPERIMENTAL RESULTS	141
NOMENCLATURE	153
LIST OF REFERENCES	157
VITA AUCTORIS	160

LIST OF FIGURES

FIGURE		PAGE
2.1	Definition Sketch	8
2.2	Dimensionless Composite Roughness Plot (after Larsen 1966).....	16
2.3	21
2.4	21
2.5	21
2.6	21
2.7	Comparison of Literature Equations as Given by the Numerical Example	31
3.1	37
3.2	Channel Cross-Section	37
3.3	Body Force	37
3.4	Shear Distribution	41
3.5	Definition of ϵ_1/ϵ_2	41
3.6	Velocity & Dimensionless Velocity Functions	44
3.7	Variation of Velocity Distribution With the Cover and Channel Roughnesses	47
4.1	Details of Testing Flume with the Arrangements Made for Rigid Ice Covers	56
4.2	Arrangement of Loose Ice Cover Simulation with Fixed Dune Bedforms	58
4.3	Typical Dimensions of Dune Fixed Bedform	59
4.4	Standard Rigid 1" and 2" Blocks Used to Simulate Rigid Ice Cover	61
4.5	Standard Polyethylene Plastic Pellet Used to Simulate Loose Ice Cover	61

FIGURE	PAGE
4.6 Ice Traps and Its Arrangement	62
4.7 Shear Apparatus	64
4.8 Lined Channel Used in Evaluation of Ice Cover Roughness	66
5.1 Separation Zones and Stability Forces	70
5.2 Breakup of Ice Covers	70
5.3 Velocity Profiles Underneath the Ice Cover	71
5.4 Dimensionless Velocity Ratios at Cover Entrance	72
5.5 Integrated Shear and Shear Velocity Distribution	74
5.6 Shear Distribution	75
5.7 Dimensionless Shear Distribution	76
5.8 Integrated Shear Variation With the Discharge at Different Distances	78
5.9 Variations in Shear Stress with Discharge Along the Ice Cover Front	79
5.10 The Variation of the Shear and the Dimension- less Shear Velocity with Reynolds Number	80
5.11 Comparison Between Theoretical and Measured Dimensionless Velocity Distributions	82
5.12	84
5.13	86
5.14 Indirect Verification of λ Assumption	86
5.15	88
5.16	88
5.17 Comparison of Theoretical and Measured Composite Manning's Roughness Coefficients	91
5.18 Comparison Between the Theoretical and Measured Discharges	92

FIGURE	PAGE
5.19 Comparison Using Uzuner's Data	95
5.20 Comparison of the Developed Theory with the Known Equations in the Literature	98
5.21 Lateral Configurations Underside Loose Ice Cover	101
A.1	121
A.2	122
A.3	123
A.4	124
A.5	125
A.6 With and Without Ice Cover Discharge Ratio	126
B.1 Channel Cross-Section	131
B.2 Rating Curves	131
C.1 Definition Sketch	136
C.2 Dimensions of the Design Cross-Section	136
E.1 Measured Velocity Profiles for Experiments E1, E2 and E3	144
E.2.1	147
E.2.2	148
E.2.3	149
E.2.4	150
E.2.5	151
E.3 Calibration Curve of the Flow Meter	152

LIST OF TABLES

TABLE	PAGE
2-1 Non-dimensional Composite Roughness Relations for Ice Covered Channels	24
2-7 Illustrated Example	30
3-1 Assigned Notations	36
5-1	94
6-1 The Dimensional Matrix	106
6-2 The Matrix of Solution	107
B-1	129
E-1 Evaluation of Channel Manning's Roughness n_1 ...	142
E-2 Evaluation of Cover Manning's Roughness n_2	142
E-3 Effect of Cover Front on Velocity Profiles	143
E-4 Effect of Cover Front on Shear Distribution	143
E-5 Verification of Velocity Profiles	145
E-6 Verification of Composite Roughness	146

CHAPTER 1
INTRODUCTION

1.1 Introduction

Much of the earth's surface experiences annually recurring periods of low temperatures which result in partial or total freezing of a great number of natural bodies of water.

The ice cover can seriously impede the utilization of these water bodies for many usages such as water supply for human needs, irrigation, power generation, transportation and many other purposes.

Since the beginning of the 20th century, the rapid increasing demands placed upon our water resources require hydraulic engineers to continuously evolve methods to solve these new problems.

Ice covered channels cause many problems such as increasing the friction factors, thereby decreasing the water carrying capacity of the channel leading to flooding of surrounding land.

The lack of knowledge of the different factors that cause the problems such as ice properties, underside cover configuration, and the difficulty to find any data in the literature complicate the progress to solve this problem. This was the motive to utilize this study as a first step to solve one of the most important problems caused by ice covers.

1.2 Definition of the Problem

The problem of the flow in an ice covered channel can be considered as three separate problems.

The first one deals with the formation of the ice cover in which the time of freeze up and the time of break up are important. Prediction of the thickness of the ice cover, its growth conditions and break up are mainly climatological factors.

The second aspect of the problem is to evaluate the roughness of the underside of the ice cover. This refers to the bottom form of the ice cover and the influence of the upstream edge of the cover. The process that shapes the cover front and the underside of the cover are generally due to both hydraulic and thermal effects.

The third aspect of the problem is the utilization of the previously determined data to estimate the total composite roughness of a channel with an ice cover in order to estimate the depth discharge relation.

This study mainly deals with the third aspect of the problem, that is, to estimate the composite roughness of an ice covered channel and hence the total discharge of the channel.

The study also sheds some light on the second aspect of the problem but only from the hydraulic point of view.

CHAPTER 2
LITERATURE SURVEY

2.1 Introduction

It is commonly agreed that an ice cover forms after sufficient heat has been transferred, principally to the atmosphere, to reduce the water temperature to near freezing or slightly below. The other way is by the accumulation of drifting ice blocks.

With regard to the underside configuration of an ice cover one can find only mathematical studies based on thermodynamic analysis.

On the other hand, the composite roughness problem and the discharge estimation have attracted more researchers and some 20 different equations can be found each with different assumptions.

2.2 Underside of Ice Covers

During the two succeeding winters of 1965-66 and 1966-67, Carey published in 1966-67 field data measured at St. Croix River, Wisconsin as the first attempt to study the underside configuration of an ice cover. He reported 19 measurements, 12 in the first winter and 7 in the second winter. Carey's observations can be summarized as follows:

1. A non similar, sharp crested dune formation was observed accompanied with some roughly oriented transverse flow ripples.

2. The dunes have no standard profile, the wave lengths ranged from 0.5 - 1.0 ft. with crests ranging from 0.03 - 0.14 ft. The greatest amplitudes did not necessarily occur with the greatest wave lengths. Also, the upstream face slopes are steeper than the downstream slopes.

As a result Carey introduced the hypothesis that the variations in the intensity of turbulence from point to point within the flow results in differential temperature gradients causing intermittent freezing or melting in the different formations and that these formations are related to the cover underside roughness.

In 1972, Ashton and Kennedy, based on Carey's hypothesis introduced a mathematical model relating the local heat flux to the normal component of the turbulent velocity near the boundary. But they studied the thermodynamic factors only.

In 1973, Larsen developed some field data from both the Kilforsen and Gailjaur channels in Mid-Sweedden. He introduced the bed effect but only as a factor in the heat transfer process. He also showed that the cover is thicker near the banks than at the mid-channel with a gradual variation in between.

No other literature was found for this aspect of ice cover formation nor any dealt with the hydraulic factors more deeply.

2.3 Composite Roughness of Ice Covered Channels

2.3.1 The computation of the composite roughness of an ice covered channel as given in the literature is based on three basic assumptions:

1. The cross-section can be divided into two parts, one section exerting shear on the bed, and the other section exerting shear on the underside of the ice cover.

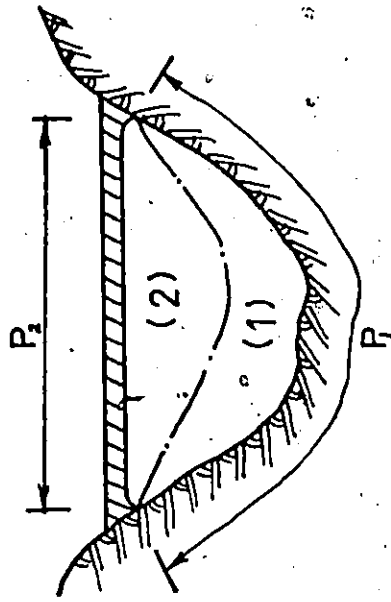
2. The boundary between the bed section and the ice cover section is considered as the locus of a surface of zero shear within the flow. As such, this boundary is not included in either wetted perimeter.

3. The formulas relating the discharge to the hydraulic radius and Manning's n can be applied to each section as if it were a channel by itself.

Fig. (2.1) shows a definition sketch of a cross-section in an ice covered channel. The bed section is denoted by 1, and the cover section is denoted by 2. The area, wetted perimeter and hydraulic radius are A_1 , P_1 , R_1 , A_2 , P_2 and R_2 for the respective sections and A , P and R for the composite section. The shear, Darcy's friction factors and Manning's coefficients are τ_1 , f_1 , n_1 ; τ_2 , f_2 , n_2 ; τ , f , n , for the bed, cover and compound sections respectively.

The following geometric relations are frequently used.

$$R_i = A_i / P_i \quad i = 1, 2 \quad (2.1)$$



- (1) channel subsection
- (2) cover subsection

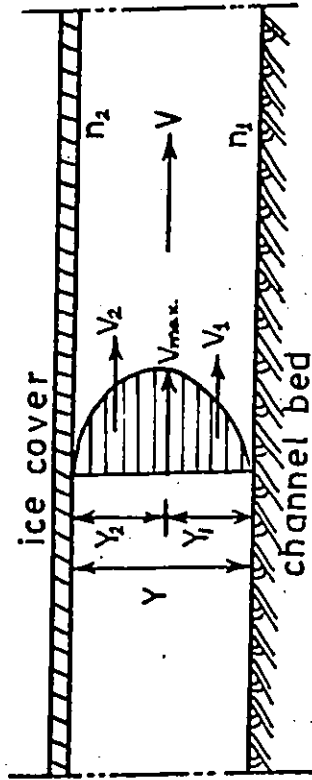


FIG. (2.1). Definition Sketch.

$$A = A_i, \quad i = 1, 2 \quad (2.2)$$

$$A = P_i, \quad i = 1, 2 \quad (2.3)$$

and $R = A/P \quad (2.4)$

with the known Manning, Darcy and the continuity equations. Moreover, the dimensionless parameter (a) defined as P_2/P_1 will also be used.

2.3.2 In 1931 Pavlovskiy was the first to investigate the composite roughness problem. He equated the gravity force along the channel to the sum of the shear forces exerted by the boundaries. He further introduced Manning's equation to compute the shear for each subsection. Pavlovskiy assumed the equality of the hydraulic radii and mean velocities of the two sections to those of the compound section, i.e.

$$R = R_1 = R_2 \quad (2.5)$$

and $V = V_1 = V_2 \quad (2.6)$

He obtained the equation for composite roughness in the form

$$\frac{n}{n_1} = \left(\frac{1 + a(n_2/n_1)^2}{1 + a} \right)^{1/2} \quad (2.7)$$

where $a = P_2/P_1 \quad (2.8)$

In 1933, Lotter applied both the continuity and Chezy's relations to the problem. Then, utilizing the assumption of equal hydraulic radii as shown in Eqn. (2.5) he developed the following relation for composite Chezy's coefficient,

$$C = (C_1 + a C_2)/(1 + a) \quad (2.9)$$

which in terms of Manning's n's becomes

$$\frac{n}{n_1} = (1 + a)/(1 + a \frac{n_1}{n_2}) \quad (2.10)$$

In 1938 Belokon adopted a power law velocity distribution applied to the two subsections. Introducing the equality of the different velocities as shown by Eqn. (2.6) together with the continuity equation gives

$$\sqrt{\frac{n}{n_1}} = (1 + a (\frac{n_2}{n_1})^{3/2})^{2/3} \quad (2.11)$$

which is not valid for the limiting case of n_1 equals n_2 and P_1 equals P_2 where it yields a composite roughness of $1.6 n_1$.

In 1948 Sabaneev modified Belokon's work to improve the relationship between Chezy's C and Manning's n in the general form

$$C_i = 1.486 R_i^r / n_i, \quad i = 1, 2 \quad (2.12)$$

where r is a dimensionless power having a value of 1/6.

Then solving for the area and following the geometric relation of Eqn. (2.2) produces the composite roughness as

$$\frac{n}{n_1} = \left((1 + a \left(\frac{n_2}{n_1}\right)^{\frac{2}{2r+1}}) / (1 + a) \right)^{\frac{2r+1}{2}} \quad (2.13)$$

which when r equals $1/6$ becomes Bolokon's Eqn. (2.11) with a correction factor of $(1 + a)^{-2/3}$. Sabaneev also utilized the assumption of equal velocities.

In 1948 Levi took the first step towards correcting the two common assumptions, namely, Eqns. (2.5) and (2.6) of equal hydraulic radii and mean velocities. He applied the known logarithmic velocity distribution to each subsection in the form

$$u_i(y) = \frac{1}{\kappa} \sqrt{gYS} \ln \frac{y}{d_i}, \quad i = 1, 2 \quad (2.14)$$

where κ is von Karman's constant and d is the hydraulic roughness height. Equating the maximum velocity computed from both sides at Y_1 and Y_2 , Fig. (2.1), with Eqn. (2.2) yields

$$Y_i = d_i \cdot Y / E d_i, \quad i = 1, 2 \quad (2.15)$$

Then applying the continuity equation and Chezy's relation for the composite C yields

$$c = \frac{1}{\sqrt{g}} \left(\ln \frac{Y}{2d_m} - 1. \right) \quad (2.16)$$

Or in terms of Manning's n as

$$n = \frac{\kappa}{\sqrt{g}} \cdot \left(\frac{Y}{2} \right)^{0.25} / \left(\ln \frac{Y}{2d_m} - 1. \right) \quad (2.17)$$

where d_m is defined as the arithmetic mean of both d_1 and d_2 and is given by the relation

$$d_m = \frac{Y}{2} \text{EXP} \left(-1 - \frac{\kappa}{\sqrt{gn_0}} \left(\frac{Y}{2} \right)^{0.25} \right) \quad (2.18)$$

Levi suggested using n_1 and n_2 respectively in Eqn. (2.18) to produce d_1 and d_2 and d_m can be determined.

Although Levi's assumptions are good and realistic, but relating the velocity distributions to an average shear velocity, \sqrt{gYS} in Eqn. (2.14) together with the method suggested to estimate d_m makes the relation theoretically open to question.

In 1959 Ven-Te-Chow followed Pavlovskiy's momentum balance theory and also utilized the assumption for equal velocities. He applied the known relation of Chezy's C and Manning's n to develop the relation

$$\frac{n}{n_1} = \frac{1}{\sqrt{1+a}} \left(\frac{R}{R_1} \right)^{1/6} \left(1 + \left(\frac{R_1}{R_2} \right)^{1/3} \left(\frac{n_2}{n_1} \right)^2 \right)^{1/2} \quad (2.19)$$

Then, introducing an assumption in the form

$$R = R_1 + R_2 \quad (2.20)$$

Ven-Te-Chow proposed that for the case of maximum discharge, a condition of

$$\frac{dn}{d\varepsilon} = 0 \quad (2.21)$$

where $\varepsilon = R_1/R_2$ (2.22)

should be applied. Simplifying, he developed a composite roughness relation of

$$\frac{n}{n_1} = \frac{1}{\sqrt{1+a}} \left(1 + a^{3/4} \left(\frac{n_2}{n_1} \right)^{3/2} \right)^{2/3} \quad (2.23)$$

For the limiting case of $a = 1$ and n_2 equals n_1 ,

(2.23) yields

$$n = 1.122 n_1$$

which did not appear valid. In order to estimate the composite discharge, he assumed that

$$R = R_0/2 \quad (2.24)$$

where R and R_0 are the hydraulic radii with and without ice cover to obtain the discharge ratio

$$\frac{Q}{Q_0} = 0.63 \frac{n_1}{n} \quad (2.25)$$

In 1965 Sinotin proceeding from Nikitins velocity distribution, and applying it to the two subsections derived a relation for what he called the hydraulic division ratio or α_{h_1} which he defined according to Fig. (2.1) as

$$\alpha_{h_1} = Y_1/Y \quad (2.26)$$

which is only valid for wide channels as

$$\alpha_{h_1} = 0.6 \text{Log}_{10} \frac{n_2}{n_1} + 0.5 \quad (2.27)$$

Then he concluded with a composite roughness value of

$$\frac{n}{n_1} = 0.6 / \left((0.6 \text{Log}_{10} \frac{n_2}{n_1} + 0.5)^{1.75} \left(\frac{n_1}{n_2} + 1. \right) \right) \quad (2.28)$$

The equation underestimated values for the composite roughness, although Sinotin was the first to evaluate the hydraulic division ratio.

In 1966 Larsen presented his analysis for wide, and constant depth channels. He adapted a logarithmic velocity profile for each subsection as

$$u_i(y) = 2.5U_* \text{Ln} 30 \frac{y_i}{k_i}, \quad i = 1, 2 \quad (2.29)$$

where U_i is the point velocity, U_{*i} is the shear velocity and k_i is the roughness element height. Equating the maximum velocities as computed from each side along with the average velocities as calculated similarly together with the average velocities relations a hydraulic division ratio of Y_1/Y_2 can be derived as

$$\frac{Y_1}{Y_2} = \left[\frac{\text{Ln } 30 \frac{Y_2}{K_2} (\text{Ln } 30 \frac{Y_2}{K_2} - 1)}{\text{Ln } 30 \frac{Y_1}{K_1} (\text{Ln } 30 \frac{Y_1}{K_1} - 1)} \times \frac{n_1}{n_2} \right]^{3/2} \quad (2.30)$$

Applying the continuity equation Larsen reached a composite roughness n given by

$$\frac{n}{n_1} = \left(\frac{1}{2}\right)^{2/3} \frac{\frac{Y_2}{Y_1} + 1}{\frac{Y_2}{Y_1} \cdot \frac{n_1}{n_2} + 1} \quad (2.31)$$

Larsen stated that in practice $\text{Ln } 30 Y_i/K_i$ is considerably greater than unity, so n/n_1 can be related directly to n_2/n_1 . Such a relation is shown in Fig. (2.2). Larsen stated that this relation is valid only for $0.2 < n_1/n_2 < 1.0$ in channels of water depth not less than 5.0 ft.

In 1966 Carey applied the friction factor analysis based on the Karman-Prandtl resistance equation for turbulent flow in pipes in the form

$$\frac{V_1}{\sqrt{8gR_1S}} = 2 \text{ Log } 2 \frac{R_1}{k_1} + 1.74 \quad (2.32)$$

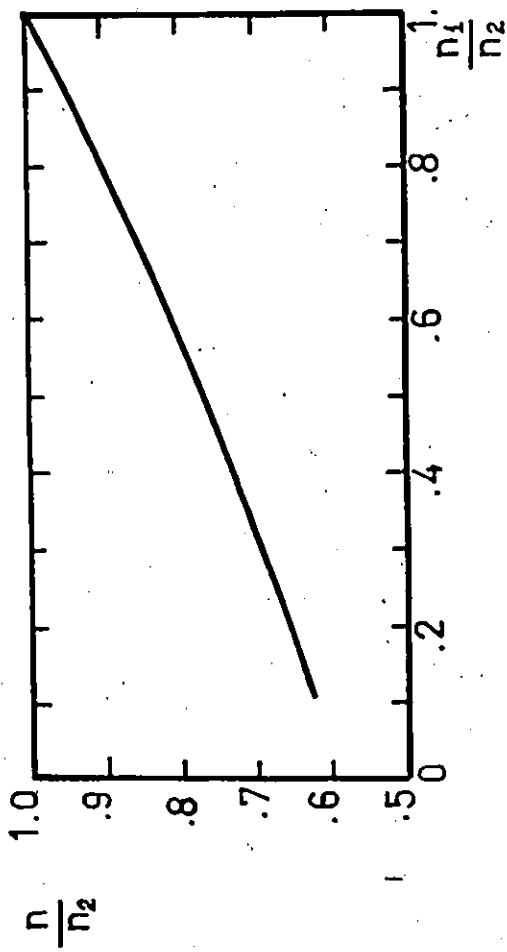


FIG.(2.2). Dimensionless Composite Roughness Plot (after Larsen 1966).

He also utilized the velocity assumption of Eqn. (2.6):

$$V = V_1 = V_2 \quad (2.6)$$

which equals the measured average velocity. Then from the measured channel cross-section a trial and error solution employing Darcy's friction factor relation of

$$f_i = 8gR_i S / V^2, \quad i = 1, 2 \quad (2.33)$$

can be used in evaluating the composite roughness and compound discharge.

In his work, Carey was trying to develop a framework of analysis and presentation of his data, rather than derivation of a predictive technique.

Following his work in 1966, Carey presented in 1967 two different approaches to the problem. Both of the two approaches were based upon field data measured at St. Croix River, Wisconsin. In his first approach, he suggested a modified Darcy-Weisbach friction factor to be given in

$$Q = \sqrt{\frac{8g}{f_{MOD}}} A R^{3/2} S^{1/2} \quad (2.34)$$

The second approach is the stage-fall-relation method based on an analogy between ice covered streams

and streams having variable slopes caused by backwater during periods of open water. The method requires firstly, the development of a stage-discharge curve for fixed conditions, then a discharge ratio-fall ratio relation based upon particular fixed conditions as used initially.

It is clearly seen that Carey's analysis is very practical and it cannot be generalized. This application should be limited to the range of measurements and the site at which this data was obtained.

In 1967 Komora and Sumbal followed the same assumptions of Pavlovskiy together with the Manning-Strickler equation they obtained two different equations. First they derived the hydraulic division ratio α_{h_1} known from Eqn. (2.26) as

$$\alpha_{h_1} = \frac{n_1^{3/2}}{n_1^{3/2} + n_2^{3/2}} \quad (2.35)$$

which they used to derive for the composite roughness a very simple relation given by

$$\frac{n}{n_1} = \left(\frac{\left(\frac{n_2}{n_1}\right)^{3/2} + 1}{2} \right)^{2/3} \quad (2.36)$$

In the second method, they stated a more general relation for the hydraulic division in the form

$$\sqrt{1-\alpha_{h_1}} \left(\frac{6\sqrt{Y}}{n_2} \sqrt{1-\alpha_{h_1}} + \frac{\sqrt{g}}{k} \right) = \sqrt{\alpha_{h_1}} \left(\frac{6\sqrt{Y}}{n_1} \sqrt{\alpha_{h_1}} + \frac{\sqrt{g}}{k} \right) \quad (2.37)$$

with κ as von Karmen's constant. They presented a nomograph which helped in solving Eqn. (2.41) which can be substituted in the relation

$$\frac{n}{n_1} = 0.5^{2/3} / \left(\alpha_{h_1}^{5/3} + \frac{n_1}{n_2} (1 - \alpha_{h_1})^{5/3} \right) \quad (2.38)$$

to calculate the composite roughness n .

In another publication in the same year the two investigators generalized Eqn. (2.35) to apply to a general channel cross-section to give

$$n = \frac{\sum n_i^{3/2} P_i}{\sum P_i} \quad (2.39)$$

They stated that the equation is valid for any channel. They also recommended Eqn. (2.39) to be used due to its simplicity and generality.

The three Eqns. (2.35), (2.38) and (2.39), according to the investigators, have the same degree of accuracy.

In 1967 Hancu applied the velocity defect law assuming wide, rectangular duct with unequal wall roughness using the friction factor λ known to be related to the Darcy's f as

$$\lambda = 0.25 f \quad (2.40)$$

and given by the relation

$$\lambda_i^{-1/2} = 4 \text{ Log } \frac{Y_i}{K_i} + 4.25 \quad (2.41)$$

Then employing the continuity, shear balance and pressure gradient he obtained the relation

$$\lambda = \frac{1}{2} \left(\left(\frac{V_1}{V} \right)^2 \lambda_1 + \left(\frac{V_2}{V} \right)^2 \lambda_2 \right) \quad (2.42)$$

which is shown graphically in Fig. (2.3). Transforming to Manning's n yields the relation

$$\frac{n}{n_1} = \frac{1}{2} \left(\frac{Y}{Y_1} \right)^{1/3} \left(\left(\frac{V_1}{V} \right)^2 + \left(\frac{V_2}{V} \right)^2 \left(\frac{n_2}{n_1} \right)^2 \left(\frac{Y_1}{Y_2} \right)^{1/3} \right) \quad (2.43)$$

where Y/Y_1 , V_1/V and V_2/V are given by the relations shown in Figs. (2.4), (2.5) and (2.6) in relation with the roughness ratio λ_2/λ_1 for different λ_1 values.

Hancu was the first to avoid the assumptions given by Eqns. (2.5) and (2.6).

In 1968 Yu, Graf and Livien produced their semiempirical relation, based on a modified Manning relation of the form

$$V_i = \frac{1.49}{n_1} \left(\frac{A_i}{P_i^z} \right)^{0.5+r} S^{1/2} \quad (2.44)$$

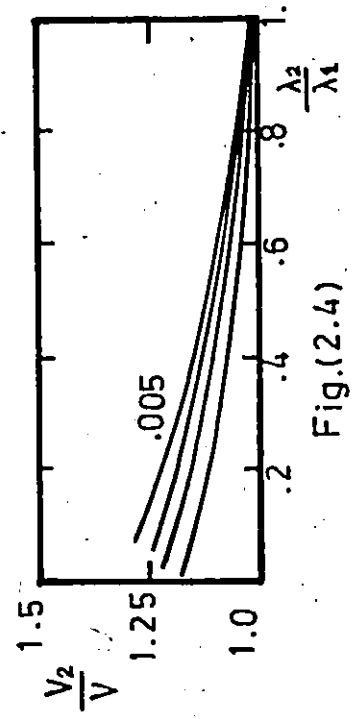


Fig.(2.4)

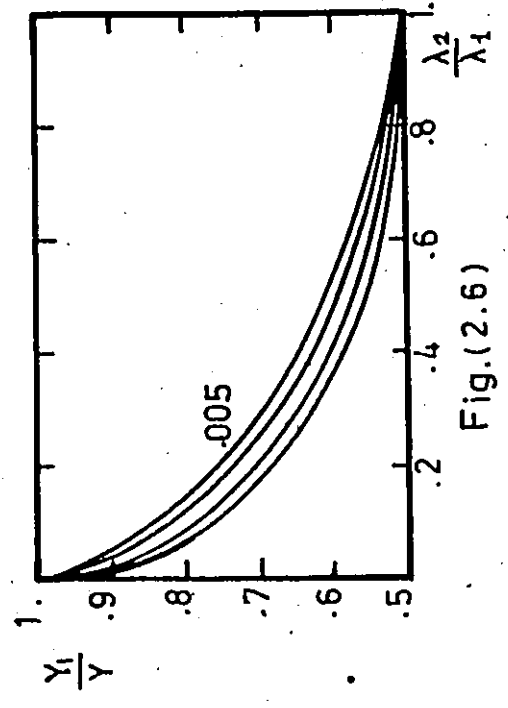


Fig.(2.6)

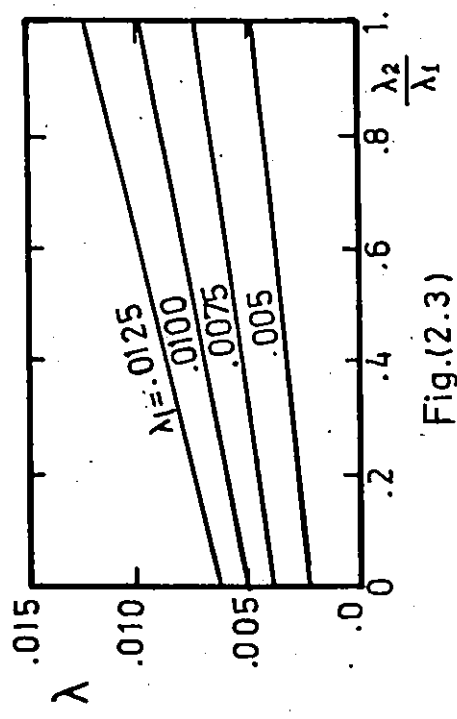


Fig.(2.3)

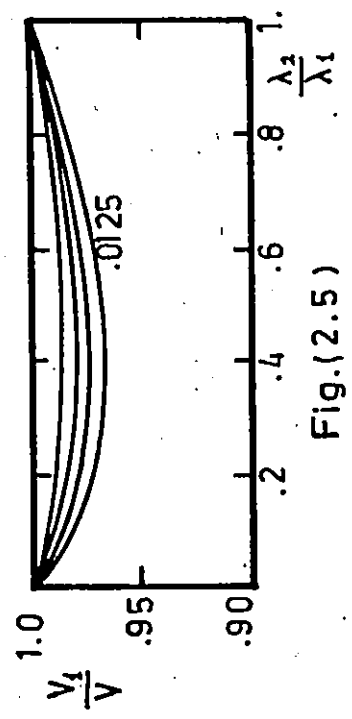


Fig.(2.5)

where r and z are experimental indexes. Applying once more the assumption given by Eqn. (2.6), they obtained n as

$$\frac{n}{n_1} = \frac{1 + a^z (n_2/n_1)^{3/2}}{1 + a^z} \quad (2.45)$$

recommending the value of $1/6$ for r and a z value of

$$z = \left(\frac{n_2}{n_1}\right)^r \quad (2.46)$$

They claimed Eqn. (2.45) to be an advantageous relation as it satisfies the limiting case of $n_2 = 0$.

In 1972 Krishnamurthy and Christensen generalized Larsen's relation. Using different values for the constants in his logarithmic velocity distribution with the continuity, shear and the Manning-Strickler equation they ended up with the general relation

$$n = \text{EXP} \frac{\sum (P_i Y_i^{3/2} \text{Ln } n_i)}{\sum (P_i Y_i^{3/2})} \quad (2.47)$$

which when applied to an ice covered channel yields

$$\frac{n}{n_1} = \left(\frac{n_2}{n_1}\right)^{1/1+a\left(\frac{d_1}{d_2}\right)^{3/2}} \quad (2.48)$$

applicable to any kind of channel section.

Lastly, in 1975 Uzuner developed a graphical solution applied to Carey's trial and error solution of the relation (2.32) or

$$\frac{V_1}{\sqrt{8gR_1S}} = 2 \text{ Log } 2 \frac{R_1}{k_1} + 1.74 \quad (2.32)$$

utilizing a mean depth H defined as A/P , with the dimensionless ratio α as $\sqrt{R_1/H}$. He also introduced a mean Froude number,

$$F = V_1/\sqrt{gH} \quad (2.49)$$

and Eqn. (2.32) becomes

$$\frac{F}{\sqrt{S}} = -4\sqrt{2\alpha} \text{ Log } \frac{k_i}{2H} + 8\sqrt{2\alpha} \text{ Log } \alpha + 3.48\sqrt{2\alpha} \quad (2.50)$$

which can be solved with the aid of a dimensionless plot.

Discussion of the Literature Survey

One can easily see that each investigator utilizes his own approach. In Table (2.3) is summarized the principal formulae developed by all the investigators in the period 1931 to 1975 that are known to the author together with the main underlying assumptions incorporated into each.

It is seen that most of the equations based on assumptions related to the hydraulic radii or the main

TABLE 2-1. NON-DIMENSIONAL COMPOSITE ROUGHNESS RELATIONS FOR ICE COVERED CHANNELS.

Author	Non-Dimensional Formula for Composite n	Assumptions. & Remarks
PAVLOVSKIY (1931)	$\frac{n}{n_1} = \left(\frac{1 + a(n_2/n_1)^2}{1 + a} \right)^{1/2}$	$R = R_1 = R_2$ $V = V_1 = V_2$ $\tau P = \tau_1 P_1 + \tau_2 P_2$
LOTTER (1933)	$\frac{n}{n_1} = \frac{1 + a}{1 + a(n_1/n_2)}$	$R = R_1 = R_2$ $V = V_1 = V_2$ $AV = A_1 V_1 + A_2 V_2$
BELOKON (1938)	$\frac{n}{n_1} = (1 + a(n_2/n_1)^{3/2})^{2/3}$	Power vel. dist. for each section $V = V_1 = V_2$ not correct for limiting case $n_1 = n_2$, $P_1 = P_2$
SABANEV (1948)	$\frac{n}{n_1} = \left(\frac{1 + a \frac{n_2^2}{n_1} \frac{2r+1}{2}}{1 + a} \right)^{2/3}$	$V = V_1 = V_2$ $C_i = 1.486 R_i^2/n_i$, $r = 1/6$ $AV = A_1 V_1 + A_2 V_2$ OR $A = A_1 + A_2$

TABLE 2-1. Cont.

Author	Non-Dimensional Formula for Composite n	Assumptions & Remarks
LEVI (1948) Modified HAGGAG (1975)	$\frac{n}{n_1} = \frac{K(Y/2)^k}{n_1 \sqrt{g} \ln \frac{Y}{2d_m} - 1}$	$d_m = 0.5(d_1 + d_2)$ $d_i = \frac{Y}{2} \exp -i - \frac{K}{n_1 \sqrt{g}} \left(\frac{Y}{2}\right)^k$ $i = 1, 2$
	$\frac{n}{n_1} = C / \ln k(e^C + e^{\frac{C}{n_2/n_1}})$	$C = - \frac{K \left(\frac{Y}{2}\right)^k}{n_1 \sqrt{g}}$
CHOW (1959)	$\frac{n}{n_1} = \frac{1}{\sqrt{1+a}} \frac{n_2}{n_1} \left(a^{3/4} + \left(\frac{n_1}{n_2}\right)^{3/2} \right)^{2/3}$	$R = R_1 + R_2$ $\tau P = \tau_1 P_1 + \tau_2 P_2$ $dn/d(R_1/R_2) = 0$ <p>max. discharge conditions not valid for limiting case $n_1 = n_2$</p>
SINOTIN (1965)	$\frac{n}{n_1} = \frac{0.6}{\left(0.6 \log \frac{n_1}{n_2} + 0.5\right)^{1.75} + \frac{n_1}{n_2}}$	<p>Nikitin's logarithmic velocity distribution, $V = V_1 = V_2$ for wide channels only.</p>
LARSEN (1966)	$\frac{n}{n_1} = \frac{0.63(1 + Y_2/Y_1)}{1 + \frac{n_1}{n_2} \left(\frac{Y_2}{Y_1}\right)^{5/3}}$	$V_i(Y) = 2.50 * \ln \frac{30}{K_i} Y_i$ $V_j = 2.50 + j \left(\ln \frac{30 Y_i}{K_j} - 1 \right)$ $j = 1, 2$ $AV = A_1 V_1 + A_2 V_2$

.....cont.

TABLE 2-1. Cont.

Author	Non-Dimensional Formula for Composite n	Assumptions & Remarks
CAREY (1966)	<p>1966 No. Prediction for n_0 or f_0 Uzuner curves for R_1 then continue substitutions in known eqns.</p>	<p>$V = V_1 = V_2$ $V_1 = 2 \log \frac{2R_1}{K_i} + 1.74$ $H = A/P$</p>
1967	$\frac{n}{n_1} = \frac{1.49}{n_1} R^{2/3} \frac{S^{1/2}}{Q}$	<p>$Q = \frac{(162800)10 \cdot 148GB}{(10^{3330S} + 11.19)^{1/2}} S^k$ or from stage fall method very limited application</p>
KOMORA and SUMBAL (1967)	$\frac{n}{n_1} = \frac{1 + (n_2/n_1)^{3/2}}{2} \quad 2/3$ $\frac{n}{n_1} = (k)^{2/3} / ((1-\alpha_h)^{S/3} + \frac{n_1}{n_2} \alpha_h)$ $\frac{n}{n_1} = \sum_{i=1}^N \frac{(n_i/n_1)^{3/2} P_i}{i} \quad 2/3 \quad N$	<p>$V = V_1 = V_2$, wide channel only Logarithmic vel. dist. $V = V_1 = V_2$, wide channel Nomographs for hydraulic division α_h</p>
HANCU (1967)	$\frac{n}{n_1} = \frac{1}{\sqrt{2}} \left(\frac{R}{R_1} \right)^{1/6} \left(\left(\frac{V_1}{V} \right)^2 + \left(\frac{V_2}{V} \right)^2 \right)$ $\times \left(\frac{n_2}{n_1} \right)^2 \left(\frac{R_1}{R_2} \right)^{1/3} \quad k$	<p>Velocity defect law $\frac{y_i}{Y_1}$ $V_{max} - V_i(y) = U_* i \frac{1}{k} \ln \frac{Y_1}{y_i}$ $YV = V_1 Y_1 + V_2 Y_2$ wide channels only graphs for V_1/V, V_2/V, R_1/R_2</p>

TABLE 2-1. Cont.

Author	Non-Dimensional Formula for Composite n	Assumptions & Remarks
YU, GRAF and LEVINE (1968)	$\frac{n}{n_1} = \left(\frac{1 + a^2 (n_2/n_1)^{3/2}}{(1 + a)z} \right)^{2/3}$	$V_i = 1.49/n_i (A_i/P_i)^{2/3} r^{1/3}$ $S_i^{1/2} = \text{const.}$ $A = A_1 + A_2$ $V = V_1 = V_2$ $AV = A_1 V_1 + A_2 V_2$ $z = (n_2/n_1)^{1/6}$
KRISHNAMURTHY and CHRISTENSEN (1972)	$\frac{n}{n_1} = \frac{n_2}{n_1} \frac{1}{(1 + P_1/P_2 (d_1/d_2)^{3/2})^{3/2}}$ $\frac{n}{n_1} = \frac{n_2}{n_1} \frac{1}{(1 + (d_1/d_2)^{3/2})^{3/2}}$	$V_i = U * i \quad 8.48 + 2.5 \text{ Ln} \frac{.368 d_i}{K_i}$ $i = 1, 2$ $Q = AV = A_1 V_1 + A_2 V_2$ <p>side slopes are too small</p> <p>n = 0.0342 K^{1/6} Manning-Strickler</p> <p>same assumptions but for wide channels</p>

velocities of each of the sub-channels and/or the whole cross-section. These assumptions are examined below:

1. Hydraulic Radii $R = R_1 = R_2$

which require $\frac{A}{P} = \frac{A_1}{P_1} = \frac{A_2}{P_2} = \frac{A_1 + A_2}{P_1 + P_2}$

or $A_1/A_2 = P_1/P_2$ (2.51)

regardless of the roughness of each individual boundary.

Eqn. (2.51) appears valid when n_1 equals n_2 .

2. The assumption utilized by Chow where

$$R_0 = R_1 + R_2$$

which implies that

$$\frac{A_0}{P_0} = \frac{A_1 + A_2}{P_1 + P_2} = \frac{A_1}{P_1} + \frac{A_2}{P_2}$$

or simplifying yields

$$A_1 P_2^2 + A_2 P_1^2 = 0$$

which gives imaginary solution for A_1/A_2 .

3. The assumption of constant velocities, or

$$V = V_1 = V_2$$

which suggests that for constant energy slope,

$$\frac{R^{2/3}}{n} = \frac{R_1^{2/3}}{n_1} = \frac{R_2^{2/3}}{n_2}$$

which is only valid for some cases. But as will be shown in a later chapter that as the difference between V_1 and V_2 is in many cases less than 10% this assumption is in general acceptable.

To illustrate the differences between all of these investigators a numerical example is used. For the sake of simplicity, Uzuner's data for wide channels with different n_1 and n_2 values are presented along with the predicted n_o/n_1 with n_2/n_1 values as shown in Table (2-1). A plot of these values is shown in Fig. (2.7).

As shown in Fig. (2.7) the scatter of the results indicate appreciable differences among the represented equations. The differences decreased as n_2/n_1 increased and with the exception of some equations (Chow, Hancu) the differences become small when $n_2/n_1 = 0.8$. The graph suggests that Bolokon and Sinotin predict very different results while Hancu and Chow give the upper range of values.

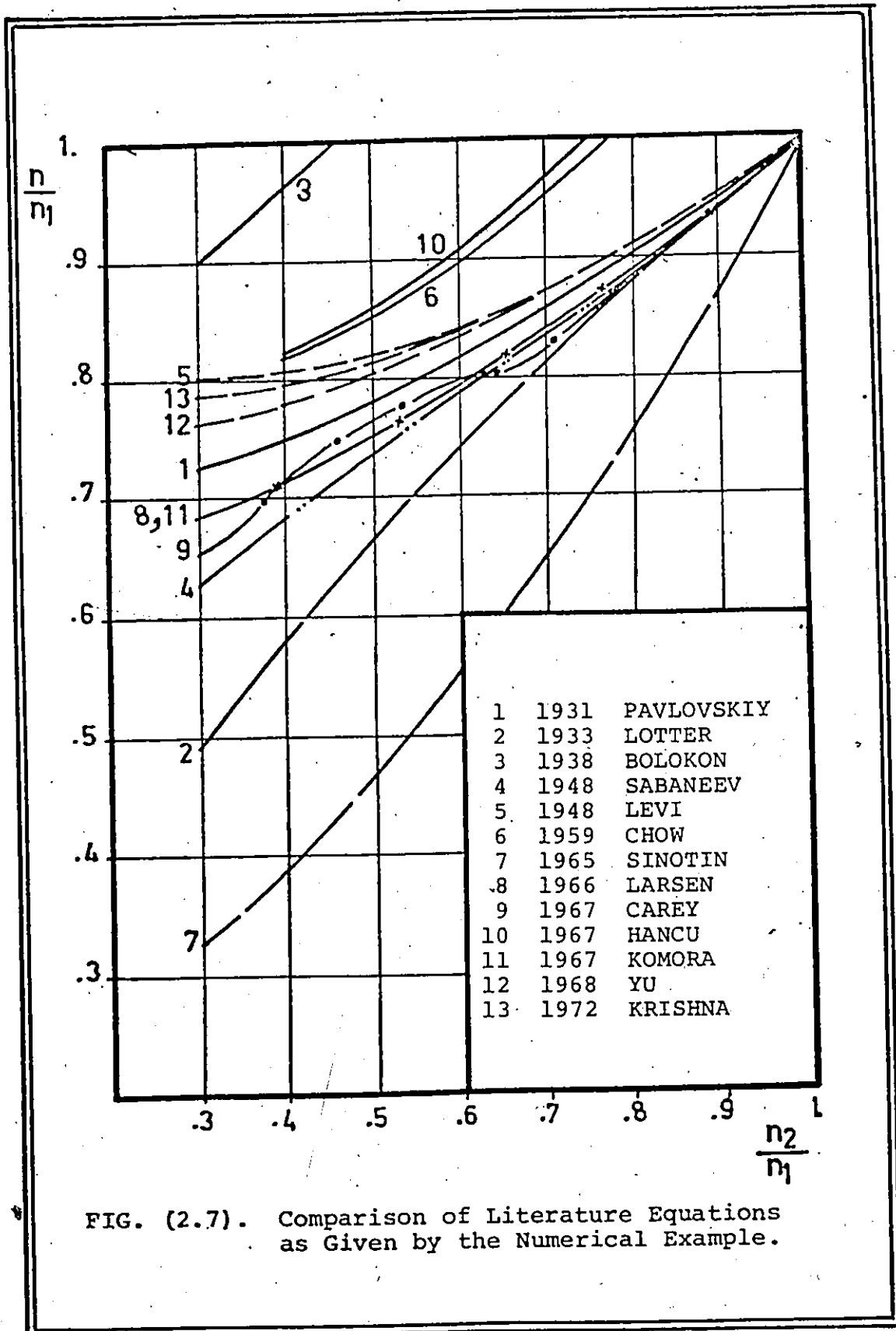
Illustrated Example:

All wide channels $a = P_1/P_2 = 1.0$

TABLE 2-7.

	(1)	(2)	(3)	(4)	(5)
Y	2.02	2.14	2.36	2.06	2.64
n_1	.0249	.0249	.0259	.0253	.0250
n_2	.0100	.0135	.0177	.0199	.0230
n_2/n_1	.402	.542	.68	.77	.92
PAVLOVSKIY (1931)	.76	.80	.86	.89	.96
LOTTER (1933)	.57	.70	.81	.87	.96
BOLOKON (1938)	1.16	1.25	1.35	1.41	1.52
SABANEEV (1948)	.69	.76	.83	.88	.96
LEVI (1948)	.81	.83	.86	.90	.96
CHOW (1959)	.82	.88	.95	.99	1.07
SINOTIN (1965)	.29	.44	.60	.70	.90
LARSEN (1966)	.73	.78	.85	.90	.96
KOMORA et al (1967)	.73	.78	.85	.89	.96
YU, GRAF et al (1968)	.78	.82	.87	.90	.97
KRISHNA, et al* (1972)	.79	.83	.86	.90	.96
CAREY (1967)	.73	.79	.83	.90	.96
HANCU (1967)	.82	.89	.95	1.01	1.11

*HANCU's curves for Y_1/Y_2 are used since Krishna et al gives no way to evaluate Y_1/Y_2 .



Larsen and Komora et al predict the same values with the advantage that Komora's equation is much simpler than Larsen's.

Pavlovskiy's equation seems to be the average of the known equations. It is also very simple in form and easy to apply.

In all the above it should be noticed that the comparison is for wide channels, since neither the effect of the channel geometry nor the flow conditions are taken into consideration.

CHAPTER 3
THEORETICAL ANALYSIS

3.1 Introduction

The purpose of this chapter is to develop a method to calculate the composite hydraulic roughness for an ice covered channel. When the discharge flows past a stationary cover Fig. (3.1) the front edge causes disturbance in the form of dead water zones and eddies, but after a certain distance downstream the flow establishes again the state of steady uniform flow. These two zones are the front zone and the steady uniform zone and are shown in Fig. (3.1).

3.2 Theoretical Assumptions

The following assumptions are utilized in this analysis:

1. The entire flow cross-section is considered to consist of two sub-sections, one exerting shear on and governed by the bed, and the other sub-section exerting shear on and influenced completely by the cover.
2. The boundary between the bed sub-section and the cover one is considered as the locus of no shear within the flow, which also is the locus of the maximum velocity surface.
3. The hydraulic equations such as the continuity, Chezy and Manning's equation can be applied to each sub-section separately.

4. The side wall effect is considered to be included in the bed sub-section which makes the division surface as shown in Fig. (3.2).

5. The fluid is homogeneous, incompressible and the flow is steady, uniform, and two-dimensional.

A separate correction may be applied at the front of the ice cover.

The main flow characteristics and notations are shown in Table (3-1) and explained in Fig. (3.2).

3.3 On The Flow Equations

Basically, the flow is governed by the Reynold's form of the Navier-Stokes equation which in two-dimensional flow becomes

$$\rho \left(\frac{\partial \bar{u}}{\partial t} + \bar{v} \frac{\partial \bar{u}}{\partial y} + \bar{u} \frac{\partial \bar{u}}{\partial x} \right) = - \frac{\partial \bar{P}}{\partial x} + \frac{\partial}{\partial y} \left(\mu \frac{\partial \bar{u}}{\partial y} \right) + \frac{\partial}{\partial y} \left(-\overline{\rho u' v'} \right) + F_{ix} \quad (3.1)$$

where \bar{u} and \bar{v} are average velocities in x and y directions, and the notations are given in Fig. (3.1), u' and v' are local velocity variation in the X and Y directions respectively, ρ and μ are the fluid density and viscosity \bar{P} is the average pressure and F_{ix} is defined as the body force.

Due to the assumption of steady flow the value $\partial \bar{u} / \partial t$ will equal zero while \bar{v} will vanish as it averages

TABLE 3.1. ASSIGNED NOTATIONS

Property	Flow Cross-Section	Channel Sub-Section	Cover Sub-Section
Flow Area	A	A ₁	A ₂
Wetted Perimeter	P	P ₁	P ₂
Hydraulic Radius	R	R ₁	R ₂
Flow Depth	Y	Y ₁	Y ₂
Relative Depth Ratio	ϵ	$\epsilon_1 = d_1/Y_1$	$\epsilon_2 = d_2/Y_2$
Local Velocity	U	U ₁	U ₂
Mean Velocity	V	V ₁	V ₂
Manning's Roughness	n	n ₁	n ₂
Shear Stress	τ	τ_1	τ_2
Shear Velocity	V*	V* ₁	V* ₂

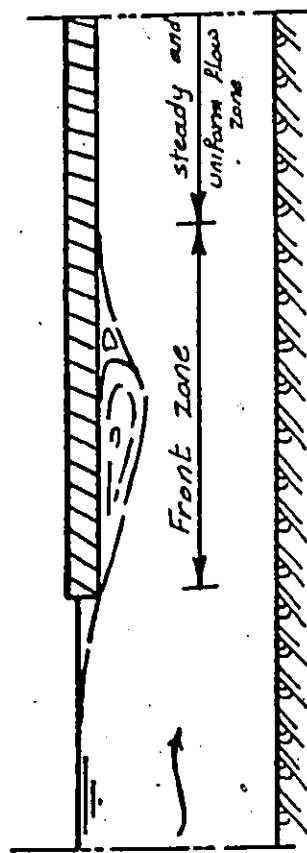


FIG. (3.1).

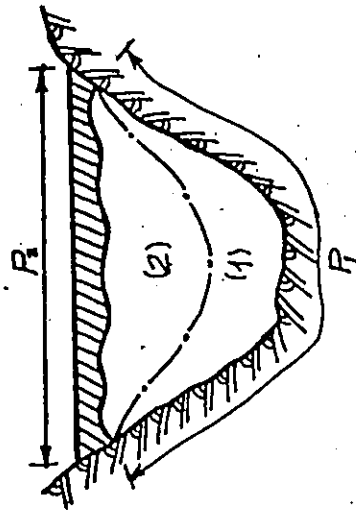


FIG. (3.2). Channel Cross-Section

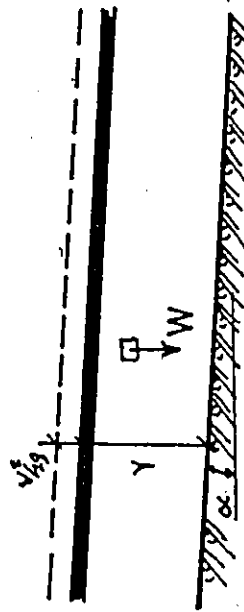


FIG. (3.3). Body Force.

a random variation. Also, as the flow is uniform with respect to the x direction, so both $\partial \bar{u} / \partial x$ and $\partial \bar{P} / \partial x$ will go to zero as they are averaging the uniformity functions.

Moreover, as shown in Fig. (3.3), the only body force applied to the flow is the gravity force represented by the weight component in the x direction. The unit body force (body force per unit volume) will be equal to

$$F_{ix} = \gamma \cdot \sin \alpha \quad (3.2)$$

But for practical values α is a small angle so its sin can be substituted by its tangent or just the bed slope S_0 . Replacing ρg as equal to γ , Eqn. (3.2) can be written as

$$F_{ix} = \rho g S_0 \quad (3.3)$$

where g is the acceleration due to gravity, and Reynolds Eqn. (3.1) can be simplified as

$$\frac{\partial}{\partial y} \left(\mu \frac{\partial \bar{u}}{\partial y} - \overline{\rho u' v'} \right) = -\rho g S_0 \quad (3.4)$$

where $\mu \frac{\partial \bar{u}}{\partial y}$ represents the laminar shear τ_L and $-\overline{\rho u' v'}$ represents the turbulent shear τ_t or

$$\frac{\partial}{\partial y} (\tau_L + \tau_t) = -\rho g S_0 \quad (3.5)$$

3.4 The Shear Distribution

Eqn. (3.5) can be integrated for each sub-section separately to develop the shear and velocity distributions.

For part (1) Eqn. (3.5) can be integrated to yield

$$\tau_{L_1} + \tau_{t_1} = -\rho g S_o Y_1 + C_1 \quad (3.6)$$

The upper boundary of sub-section (1) is the separation surface which is assumed to be the locus of zero shear and lies at a distance Y_1 above the bed. This fact implies the boundary condition that,

$$\tau_{L_1} = \tau_{t_1} = 0 \quad \text{at } Y_1 = Y_1 \quad (3.7)$$

Applying this boundary condition to Eqn. (3.6) results in

$$C_1 = \rho g S_o Y_1 \quad (3.8)$$

and so Eqn. (3.6) becomes

$$\tau_{L_1} + \tau_{t_1} = \rho g S_o (Y_1 - y_1) \quad (3.9)$$

Due to the existence of a laminar sublayer close to the bed at a very small distance of δ_1 only the laminar shear will exist in this boundary layer. Applying

such a condition at $y_1 = 0$ yields

$$\tau_{0_1} = \rho g S_0 y_1 \quad (3.10)$$

where τ_{0_1} is the shear on the bed.

In between the two forementioned boundary conditions that is $Y_1 > y_1 > \delta_1$ the laminar shear is very small and can be approximated by the turbulent shear such that

$$\tau_{t_1} = \rho g S_0 (Y_1 - y_1) \text{ for } y_1 > \delta_1 \quad (3.11)$$

Practically δ_1 can be considered as equal to zero since its value is very small in comparison with Y . The shear distribution, then, will be as shown in Fig. (3.4).

3.5.1 Velocity Distribution:

Employing Prandtl's mixing length theory for a mixing length L as

$$\tau_{t_1} = \rho L^2 \left(\frac{du_1}{dy_1} \right)^2 \quad (3.12)$$

and utilizing Von-Karman's definition for L ,

$$L = \kappa y_1 \quad (3.13)$$

where κ is Von-Karman's constant yields

$$\tau_{t_1} = \rho \cdot \kappa^2 \cdot y_1^2 \left(\frac{du_1}{dy_1} \right)^2 \quad (3.14)$$

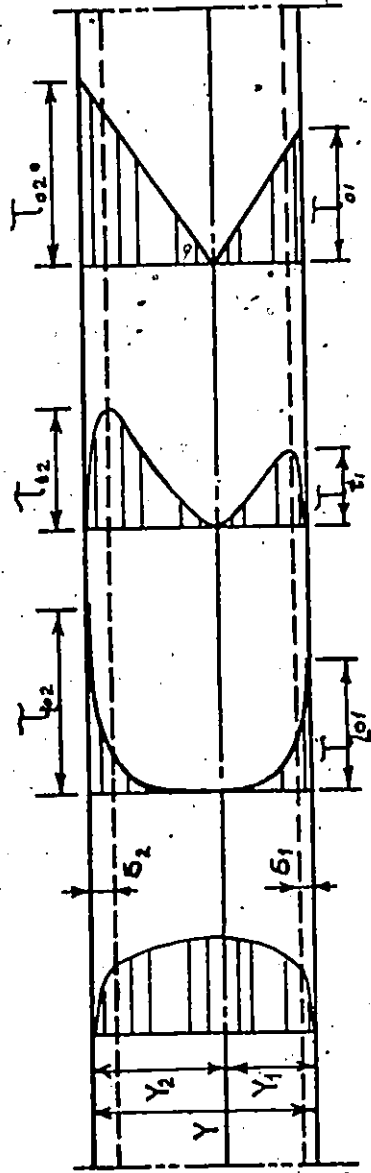
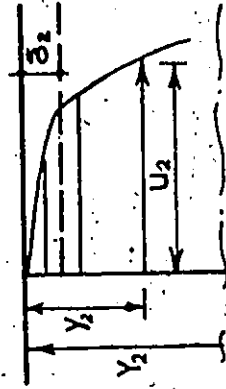
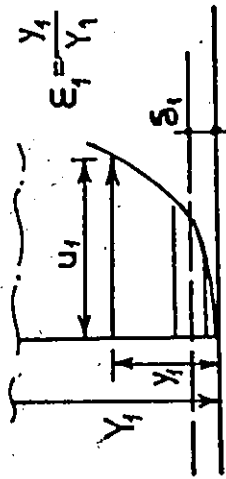


Fig.(3.4). Shear Distribution.



$$\frac{y_2}{E_2 y_2}$$



$$\frac{y_1}{E_1 y_1}$$

Fig.(3.5). Definition of ϵ_1/ϵ_2 .

Combining Eqns. (3.11) and (3.14) there results,

$$\frac{du_1}{dy_1} = \frac{1}{\kappa y_1} \sqrt{g S_0} \sqrt{Y_1 - y_1} \quad (3.15)$$

which in terms of the relative depth $\epsilon_1 = y_1/Y_1$, Fig. (3.5), becomes

$$\frac{du_1}{d\epsilon_1} = \frac{1}{\kappa} \sqrt{g Y_1 S_0} \frac{\sqrt{1 - \epsilon_1}}{\epsilon_1} \quad (3.16.1)$$

And since $\sqrt{g Y_1 S_0}$ is the shear velocity V_{*1}

$$\tau_{01} = \rho g Y_1 S_0 = \rho V_{*1}^2$$

the equation becomes

$$\frac{du_1}{d\epsilon_1} = \frac{V_{*1}}{\kappa} \frac{\sqrt{1 - \epsilon_1}}{\epsilon_1} \quad (3.16.2)$$

Integration of Eqn. (3.16.2) yields,

$$U_1(\epsilon_1) = \frac{V_{*1}}{\kappa} F_1(\epsilon_1) + C_1 \quad (3.17)$$

in which

$$F_1(\epsilon_1) = 2\sqrt{1 - \epsilon_1} - \ln \frac{1 + \sqrt{1 - \epsilon_1}}{1 - \sqrt{1 - \epsilon_1}} \quad (3.18)$$

$F_1(\epsilon_1)$ is the velocity function and given in Fig. (3.6).

Equating the mean velocity of the bed subsection V_1 with the value calculated from Eqn. (3.17) yields

$$C_1 = V_1 + \frac{1}{3} \cdot \frac{2V_{*1}}{\kappa} \quad (3.19)$$

or simplifying,

$$\frac{V_1 - u_1(\epsilon_1)}{(2V_{*1}/\kappa)} = F_2(\epsilon_1) \quad (3.20.1)$$

where

$$F_2(\epsilon_1) = \text{Ln} \frac{\sqrt{\epsilon_1}}{1 - \sqrt{1 - \epsilon_1}} - \sqrt{1 - \epsilon_1} - \frac{1}{3} \quad (3.20.2)$$

$F_2(\epsilon_1)$ is the dimensionless velocity function and is given both in Fig. (3.6).

A second boundary condition is applied when ϵ_1 equals unity where the computed local velocity becomes equal to the maximum velocity. But since $F_1(\epsilon_1=1)$ is zero, this results in,

$$C_1 = V_{\text{max}} \quad (3.21)$$

that is,

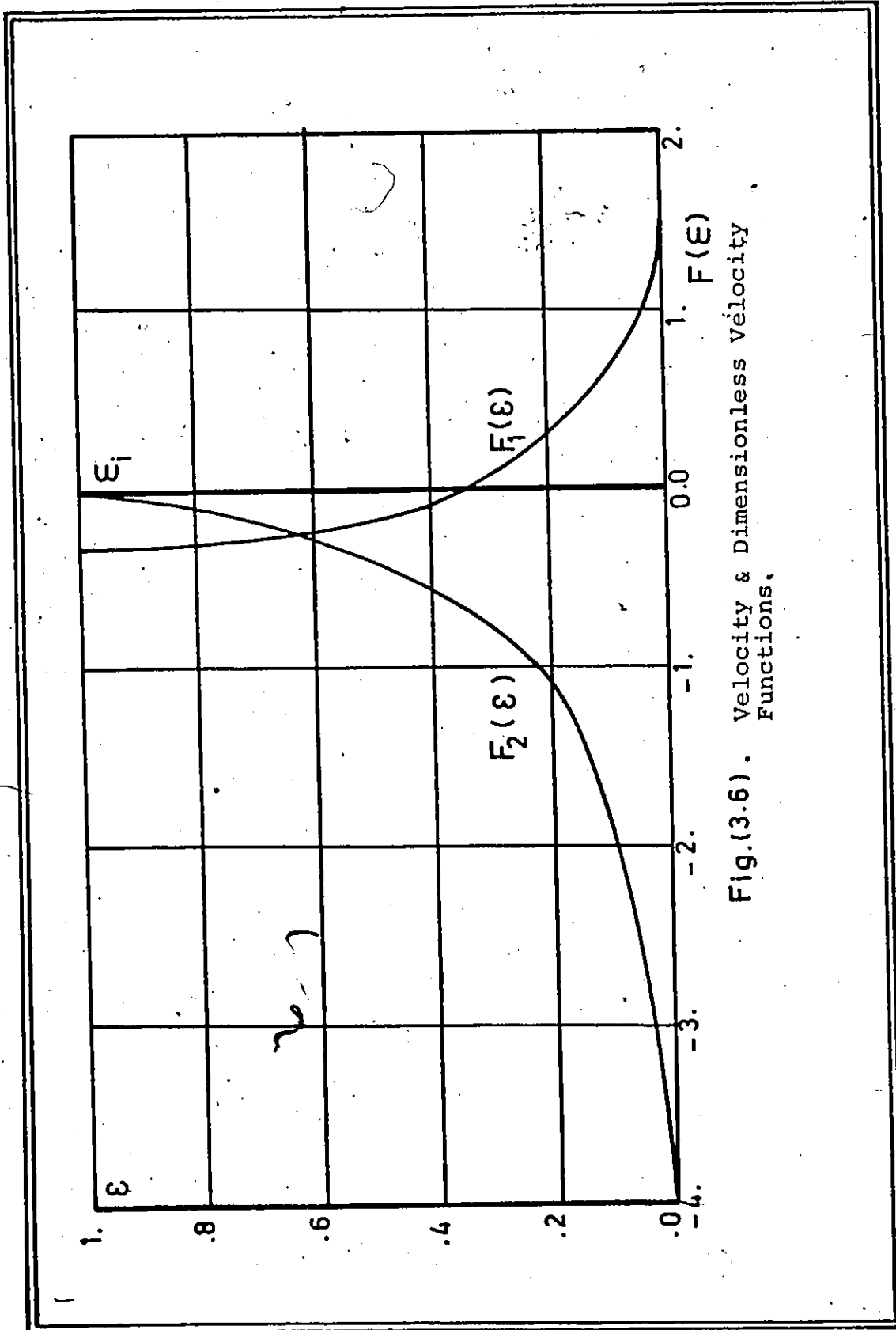


Fig.(3.6). Velocity & Dimensionless Velocity Functions.

$$u_1(\epsilon_1) = V_{\max} + \frac{V_{*1}}{\kappa} F_1(\epsilon_1) \quad (3.22)$$

Noticing that $F_1(\epsilon_1)$ is always a negative function and that at $\epsilon_1 = 1/3$, $F_1(t_1)$ is $-2/3$ while $F_2(\epsilon_1)$ vanishes which makes

$$u_1(\epsilon_1) = V_1 = V_{\max} - \frac{2}{3} \frac{V_{*1}}{\kappa} \quad (3.23)$$

Similarly, an identical set of equations can be derived for the ice cover sub-section in exactly the same way

$$u_2(\epsilon_2) = \frac{V_{*2}}{\kappa} F_1(\epsilon_2) + C_2 \quad (3.24)$$

$$\frac{V_2 - u_2(\epsilon_2)}{(2V_{*2}/\kappa)} = F_2(\epsilon_2) \quad (3.25)$$

$$u_2(\epsilon_2) = V_{\max} + \frac{V_{*2}}{\kappa} F_1(\epsilon_2) \quad (3.26)$$

and

$$u_2\left(\frac{1}{3}\right) = V_2 = V_{\max} - \frac{2}{3} \frac{V_{*2}}{\kappa} \quad (3.27)$$

With the above sets of equations the velocity distribution in an ice covered channel is completely defined.

3.5.2 Velocity Distribution Characteristics:

The difference between the sub-sections mean velocity can be obtained from Eqns. (3.23) and (3.27) to be

$$V_1 - V_2 = \frac{-2}{3\kappa} (V_{*1} - V_{*2}) \quad (3.28)$$

The mean velocities in the sub-sections become equal when the bed and ice cover has identical roughnesses. The velocity profile changes in the way shown in Fig. (3.7). The maximum velocity moves away from the rougher boundary.

Also, as the bed slope increases, the curvature of the velocity profile becomes more severe. The maximum velocity can be shown to be given by,

$$V_{\max} = \frac{1}{2}(V_1 + V_2) + \frac{1}{3\kappa} (V_{*1} - V_{*2}) \quad (3.29)$$

From the continuity equation and utilizing the previously derived relations, one can prove that

$$V = \frac{1}{2}(V_1 + V_2) + \frac{1}{3\kappa} (V_{*1} - V_{*2}) \left(\frac{A_1 - A_2}{A} \right) \quad (3.30)$$

which can be combined with Eqn. (3.29) to yield

$$\frac{V_{\max}}{V} = 1 + \frac{2}{3} \left(\frac{V_{*1}}{V} \frac{A_2}{A} + \frac{V_{*2}}{V} \frac{A_1}{A} \right) \quad (3.31)$$

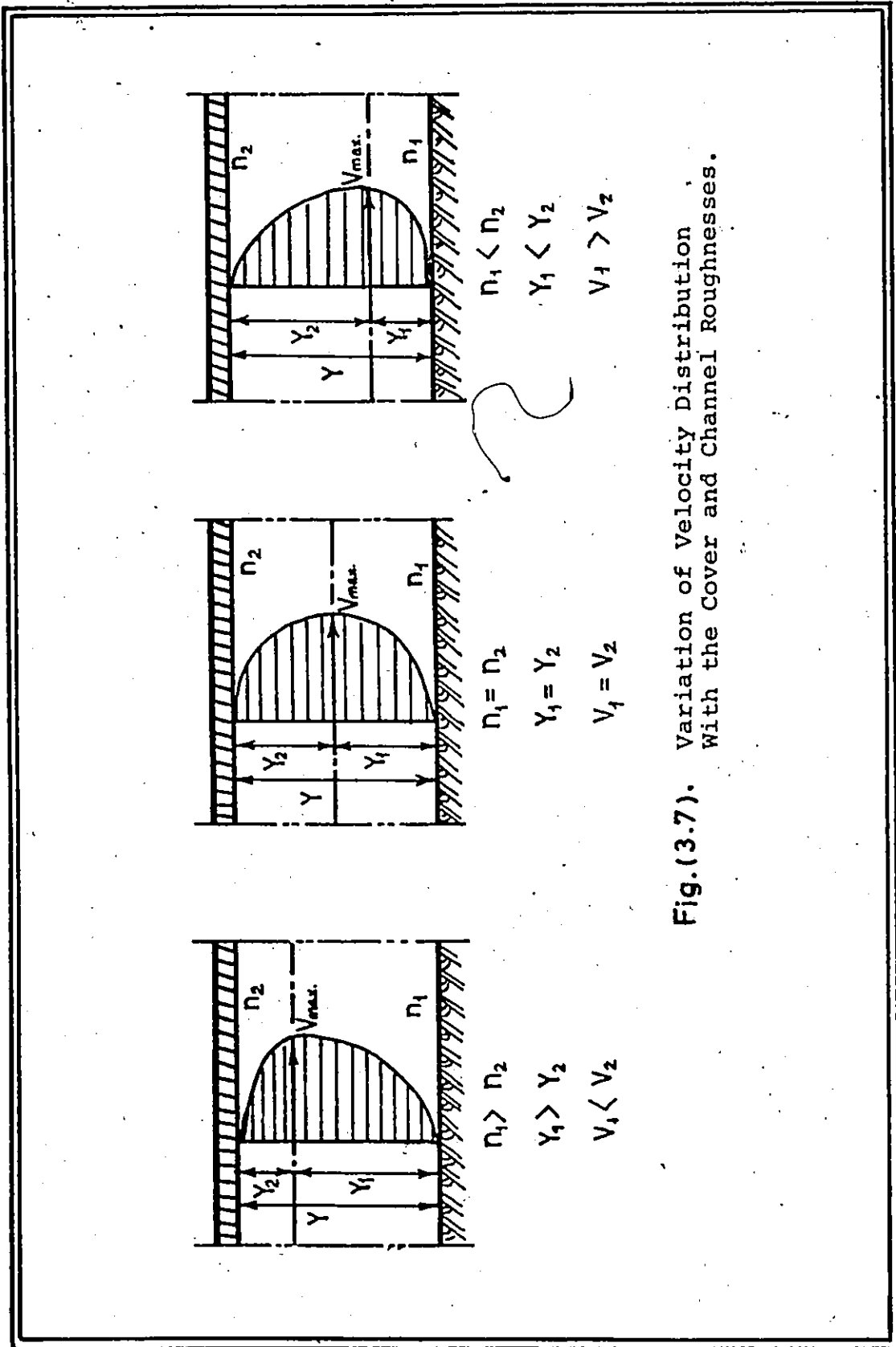


Fig.(3.7). Variation of Velocity Distribution With the Cover and Channel Roughnesses.

Eqn. (3.31) shows that the rougher the boundaries, the larger the relative maximum velocity ratio V_{\max}/V becomes.

3.5 The Dividing Surface Equation

As mentioned earlier, Manning's equation can be applied to each sub-section separately. Applying Manning's equation in the general form

$$V_i = \frac{1.49}{n_i} R_i^{2/3} S^{1/2} \quad (3.32)$$

with the values for the shear velocity as

$$V_{*i} = \sqrt{gR_i S} \quad i = 1, 2 \quad (3.33)$$

into Eqn. (3.28) to obtain,

$$\frac{R_1^{1/6}}{n_1 \sqrt{g}} = \frac{0.444}{\kappa} \frac{\sqrt{\lambda} - 1.}{1. - n_1/n_2 \lambda^{2/3}} \quad (3.34)$$

where n_1 and n_2 are Manning's roughness factors for the channel bed and sides, and cover respectively, λ is the hydraulic radius ratio and is given by the value

$$\lambda = \frac{R_2}{R_1} \quad (3.35)$$

The momentum equation can be applied to the problem noticing that the only contributing forces are the gravity forces and the boundary shears.

From Eqn. (3.8), the momentum equation is

$$\gamma A L S_0 = \tau_1 P_1 L + \tau_2 P_2 L$$

Substituting for τ_i as $\gamma R_i S$, $i = 1, 2$ and considering the slope to be constant, for uniform flow, results in,

$$R_1 = R/(\alpha + (1 - \alpha)\lambda) \quad (3.36)$$

$$R_2 = R\lambda/(\alpha + (1 - \alpha)\lambda) \quad (3.37)$$

in which α is the wetted perimeter ratio P_1/P .

Eqns. (3.34) and (3.36) can be combined to produce

$$\frac{R^{1/6}}{n_1 \sqrt{g}} = \frac{0.444}{R} \frac{\sqrt{\lambda} - 1}{1 - n_1/n_2 \lambda^{2/3}} (\alpha + (1-\alpha)\lambda)^{1/6} \quad (3.38)$$

Taking Von-Karmen's constant as equal to 0.4,

Eqn. (3.38) becomes

$$\frac{R^{1/6}}{n_1 \sqrt{g}} = 1.11 \frac{\sqrt{\lambda} - 1}{1 - n_1/n_2} \lambda^{2/3} (\alpha + (1-\alpha)\lambda)^{1/6} \quad (3.39)$$

The equation can be solved to determine the value of λ for a known cross-section to determine the division line.

3.6 The Composite Roughness Equation

From the cross-section geometry,

$$\frac{A_2}{A_1} = \lambda \frac{1-\alpha}{\alpha} \quad (3.40)$$

Introducing this relation into Eqn. (3.30) along with Eqns. (3.32) and (3.33) yields

$$\frac{n_1}{n} = \frac{1}{\alpha + (1-\alpha)\lambda} \left((1 + \frac{n_1}{n_2} \lambda)^{2/3} + \frac{n_1 \sqrt{g}}{R^{1/6}} \right) \cdot \frac{1}{4.47\kappa} \cdot \frac{\alpha - (1-\alpha)\lambda}{(\alpha - (1-\alpha)\lambda)^6} (1 + \sqrt{\lambda}) \quad (3.41)$$

Simplifying Eqn. (3.41) by means of Eqn. (3.39) to produce

$$\frac{n_1}{n} = \frac{1}{\alpha + (1-\alpha)\lambda} \left(1 + \frac{n_1}{n_2} \lambda^{2/3} \right) \left(1 + \frac{1-n_1/n_2}{1+n_1/n_2} \lambda^{2/3} \cdot \frac{\sqrt{\lambda} + 1}{\sqrt{\lambda} - 1} \cdot \frac{\alpha - (1-\alpha)\lambda}{\alpha + (1-\alpha)\lambda} \right) \quad (3.42)$$

from which the composite roughness n can be evaluated. Again using Von-Karman's constant as equal to 0.4, and substituting in Eqn. (3.42) yields

$$\frac{n_1}{n} = \frac{1}{\alpha + (1-\alpha)\lambda} \left(1 + \frac{n_1}{n_2} \lambda^{2/3} \right) \left(1 + \frac{1-n_1/n_2}{1+n_1/n_2} \lambda^{2/3} \cdot \frac{\sqrt{\lambda} + 1}{\sqrt{\lambda} - 1} \cdot \frac{\alpha - (1-\alpha)\lambda}{\alpha + (1-\alpha)\lambda} \right) \quad (3.43)$$

which will be referred to hereafter as the general equation for the estimation of the composite Manning hydraulic roughness factor n for an ice covered channel with any cross-sectional shape.

For the case of wide channels, the value of α becomes 0.5 and Eqns. (3.39) and (3.43) become

$$\frac{R^{1/6}}{n_1 \sqrt{g}} = \frac{\sqrt{\lambda} - 1}{1 - n_1/n_2 \lambda^{2/3}} \cdot (1 + \lambda)^{1/6} \quad (3.44)$$

and the composite roughness general equation is,

$$\frac{n_1}{n} = 0.8 \left(\frac{1}{1+\lambda} \right)^{2/3} \left(1 + n_1/n_2 \lambda^{2/3} \right) \left(1 - \frac{1 - n_1/n_2 \lambda^{2/3}}{1 + n_1/n_2 \lambda^{2/3}} \cdot \frac{(\sqrt{\lambda} + 1)^2}{\lambda + 1} \right) \quad (3.45)$$

where λ is given by

$$\lambda = \frac{Y_2}{Y_1} \quad (3.46)$$

for wide channels.

3.7 Methods of Solution

In the practical application of the proposed equations, it is somehow difficult to solve Eqn. (3.39) especially if a trial and error solution is to be applied, in designing an ice covered channel. Two methods can be used for such a solution.

The first method is by applying the numerical analysis methods, such as Newton-Rabson method, to Eqn. (3.39) to obtain the value of λ then Eqn. (3.43) can be directly used to estimate the composite roughness.

The second method is to use the solution charts developed for the composite solution of the two equations. Each chart is plotted to a fixed α value and is

illustrated in Fig. (3.9). It consists mainly of three graphs, the first one is the $R-\phi$ graph, where ϕ is a dimensionless parameter and equals $R^{1/6} n_1 \sqrt{g}$, for different n_1 values. The second graph relates ϕ for different n_1/n_2 ratios to λ value, and the third graph is used to evaluate the composite roughness n from the λ value for different n_1/n_2 ratios. An additional graph is added to indicate the different values of M where M is the Manning index value and equals $\frac{1.49}{n} R^{2/3}$.

The charts covered the practical ranges of

R from 0 to 100 ft.

n_1 from 0.01 to 0.04

n_1/n_2 from 0.30 to 0.90

α from 0.50 to 0.75

The charts are given in Appendix A with illustrations of its use.

3.8 Practical Applications

The two important applications are:

(1) the estimation of the composite discharges and stage curves for a known channel section, and,

(2) the design of ice covered channels.

Appendices B and C illustrate by means of numerical examples the use of this theoretical analysis in both of the two-applications.

CHAPTER 4

EXPERIMENTAL ARRANGEMENT AND RESULTS

4.1 Introduction

In this chapter the following subjects will be described:

- A. The test equipment, including the laboratory facilities, bedforms, simulated ice covers and ice traps.
- B. Measurement equipment: point gauges, pitot-tube, and shear apparatus.
- C. Experimental arrangement.
- D. Experimental results.

4.2 The Test Equipment

4.2.1 Laboratory Facilities:

(i) A centrifugal pump, capable of delivering up to a discharge of 3500 U.S.G.P.M. ($0.2267 \text{ m}^3/\text{sec}$), at a head of 22.0 ft. (6.71 m).

(ii) A magnetic flow meter which is calibrated directly to 10 U.S.G.P.M. ($0.0000648 \text{ m}^3/\text{sec}$) was used for the discharge measurements.

(iii) The test flume, Fig. (4.1), is 24 ft. (7.315 m.) long with a rectangular cross-section of 1.5 ft. (0.457 m.) width, and 2 ft. (0.61 m.) depth.

The bottom and right side of the flume is made of timber with ~~clear~~ plexiglass on the left wall. A gauze screen is provided at the upstream end to ensure suitable flow

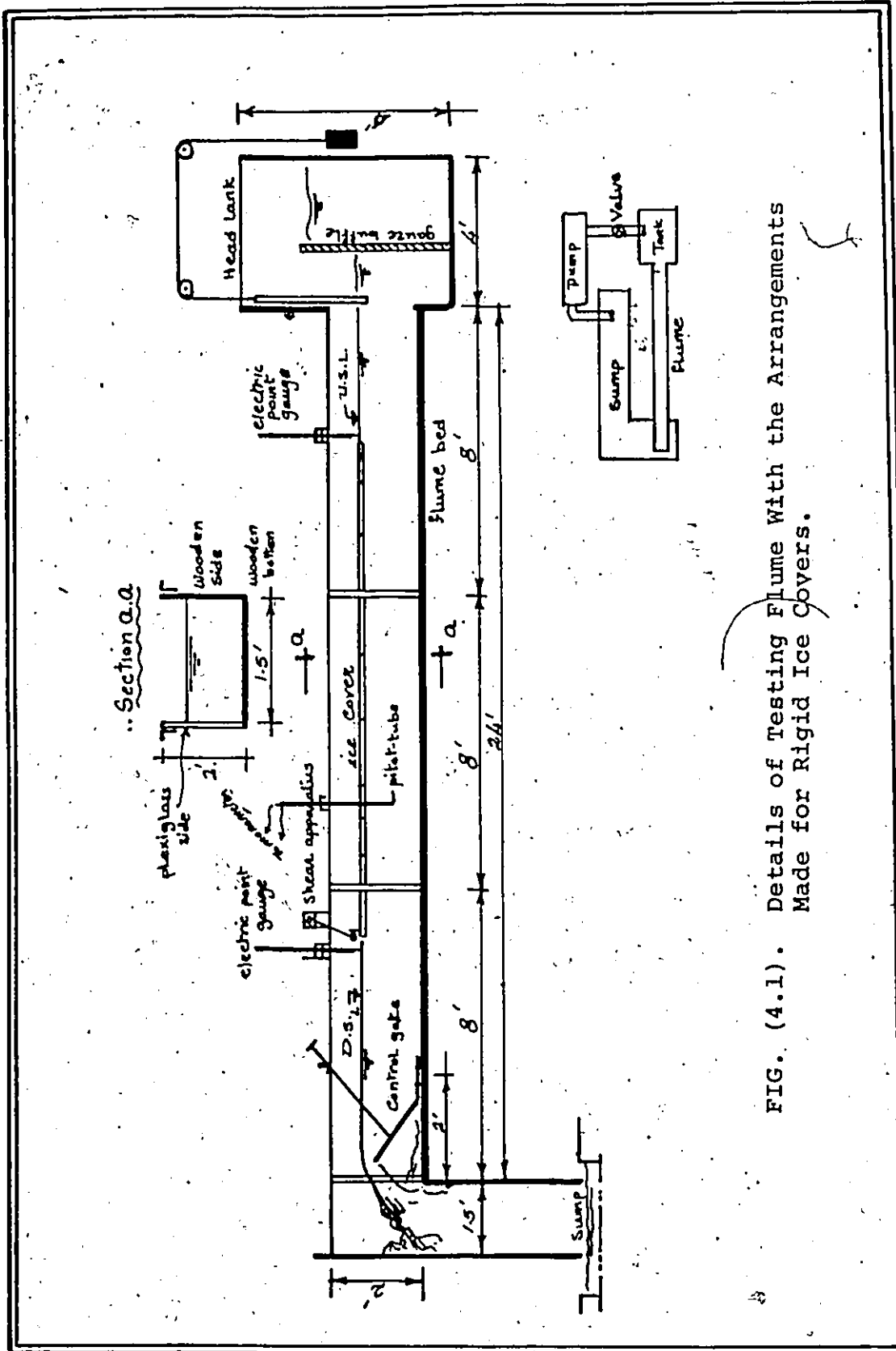


FIG. (4.1). Details of Testing Flume With the Arrangements Made for Rigid Ice Covers.

inlet conditions from the head tank. The head tank is 4 ft. (1.219 m.) high, and measures 4.25 ft. (1.219 m) by 3.66 ft. (1.118 m) in plan. An adjustable gate is fixed to the flume bed at the downstream end to control the flow depth. The flume system is shown in Plate (4.1).

4.2.2 Bedforms:

Two types of bedforms were used:

(i) A flat bed was used with the rigid cover. It consisted of the wooden floor of the flume.

(ii) Dune bedform was used with the loose cover to simulate a two-dimensional bed. The bed consisted of 10 adjacent identical concrete blocks arranged as shown in Fig. (4.2). A typical block is shown in Fig. (4.3). The wave length was 1.0 ft (0.305 m) with an amplitude of 1.2 in. (3.05 cm). The upstream face slope was steeper than the downstream face.

4.2.3 Simulated Ice Covers:

Two kinds of simulated ice covers were used:

(i) The rigid ice cover consisted of adjacent blocks of wooden frame, and polyethylene plastic pellets as a fill, held by two screens. The block was 17 in. (0.435 m) square. Two block thicknesses were used, namely 1 in. (0.025 m), and 2 in. (0.051 m). The 2 inch block was made by holding two 1-inch thickness blocks together with a sheet in between.

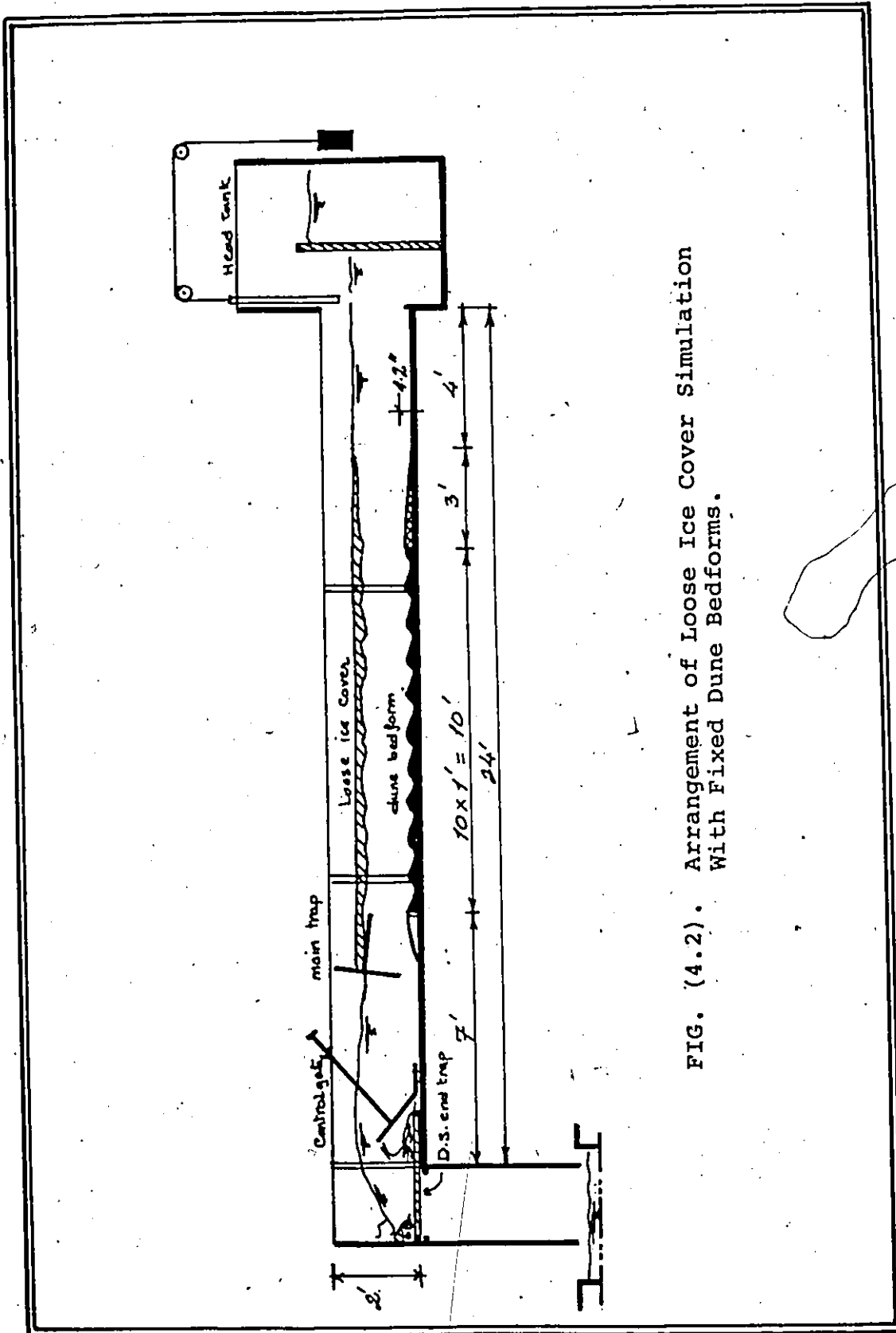


FIG. (4.2). Arrangement of Loose Ice Cover Simulation With Fixed Dune Bedforms.

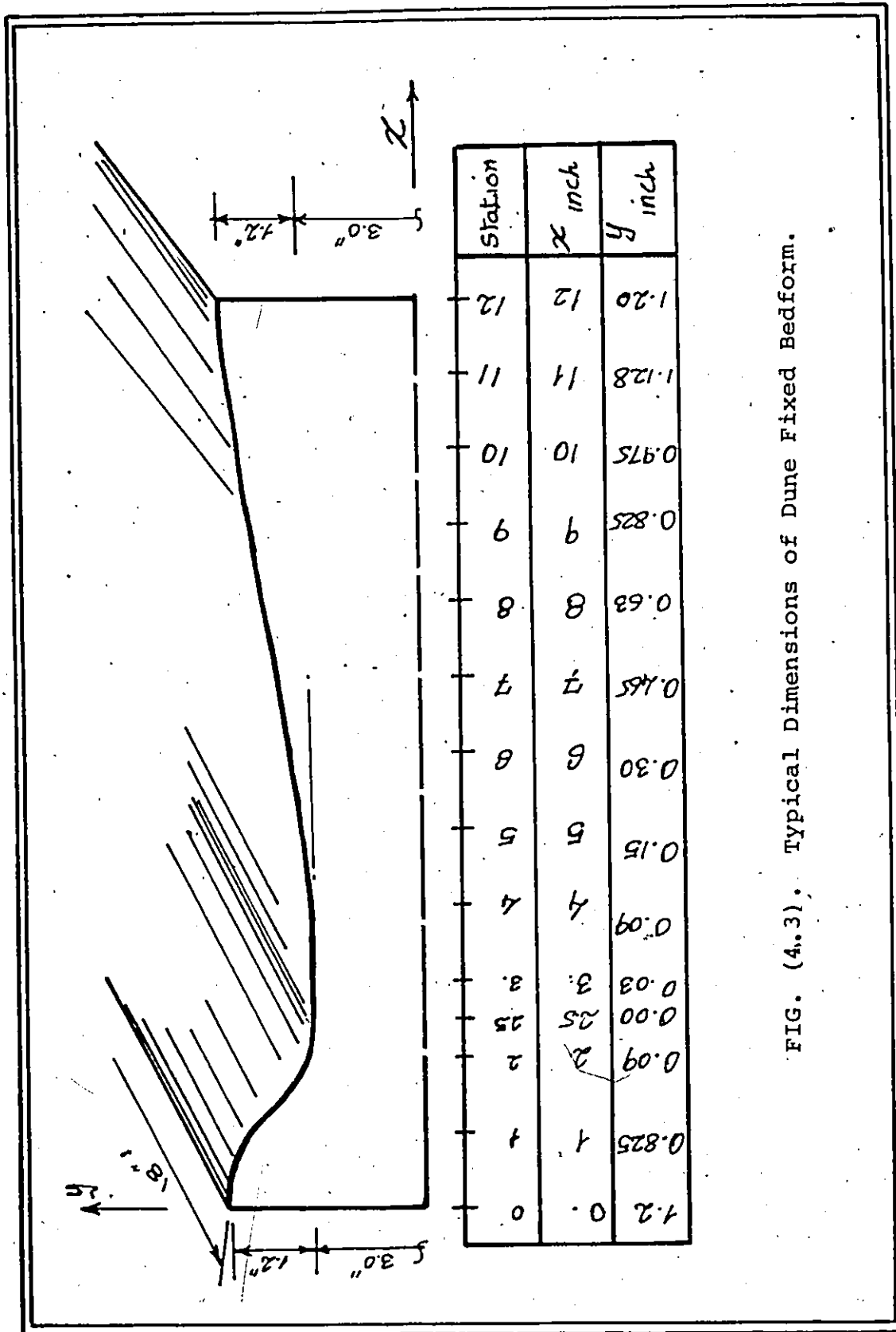


FIG. (4.3). Typical Dimensions of Dune Fixed Bedform.

The specific gravity of the cover was 0.8. Typical blocks are shown in Fig. (4.4).

(ii) Loose model ice covers were made of white polyethylene plastic pellets with a specific gravity of 0.92, and were used to simulate ice covers formed by drifting blocks. The pellets, Fig. (4.5), measured 0.2 in. (5 mm) in diameter with 0.08 in. (2 mm) core thickness, and 0.04 in. (1 mm) edge thickness.

4.2.4 Ice Traps:

A device for trapping the pellets was used with the loose cover to avoid too much loss into the pumping system. It consisted of:

(i) A downstream horizontal end trap with a wooden frame, covered with 0.08 in. (2 mm) opening square mesh.

(ii) A main control trap consisted of a vertical frame of 18 in. (0.457 m) square attached to a 17 in. (0.432 m) by 18 in. (0.457 m) rectangular horizontal frame. The frames were made of wood and covered by a standard screen.

Fig. (4.6) shows the details of the ice traps.

4.3 Measurement Equipment

4.3.1 Point gauges with electric bulb indicator were used to measure the water depths both upstream and downstream of the cover. The gauges were calibrated to

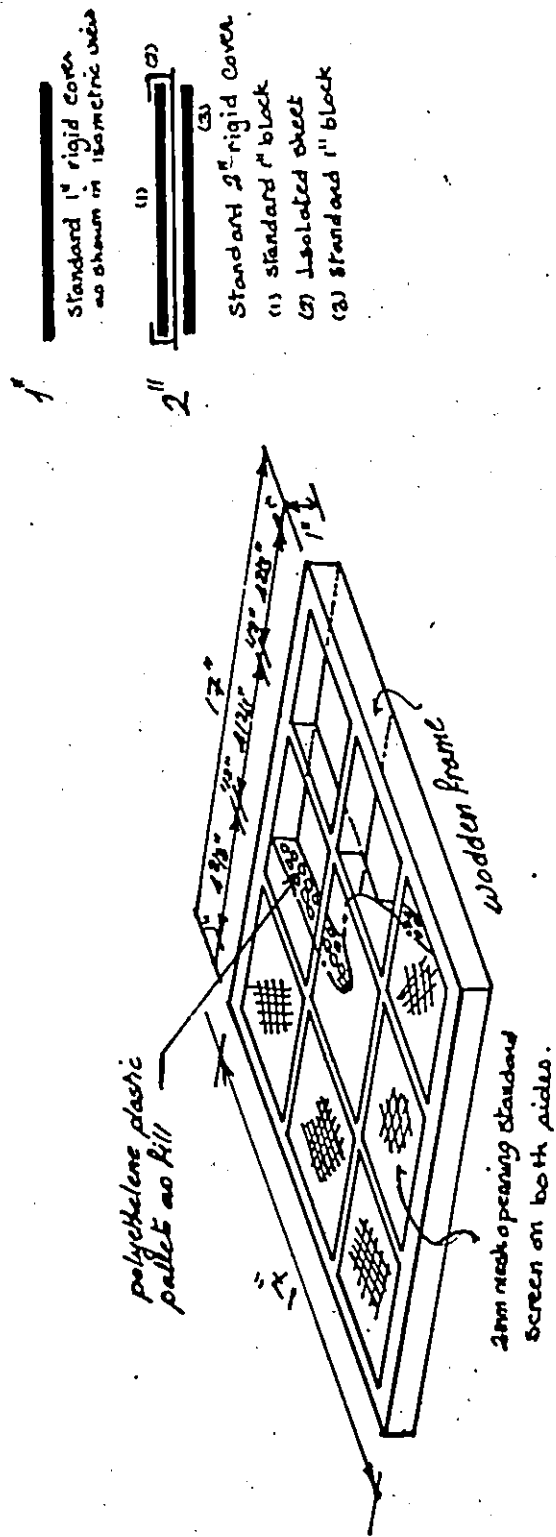


FIG. (4.4). Standard Rigid 1" and 2" Blocks Used to Simulate Rigid Ice Cover.

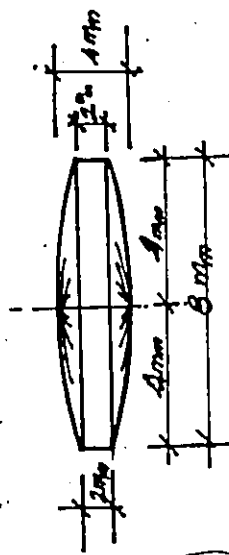


FIG. (4.5). Standard Polyethylene Plastic Pellet Used to Simulate Loose Ice Cover.

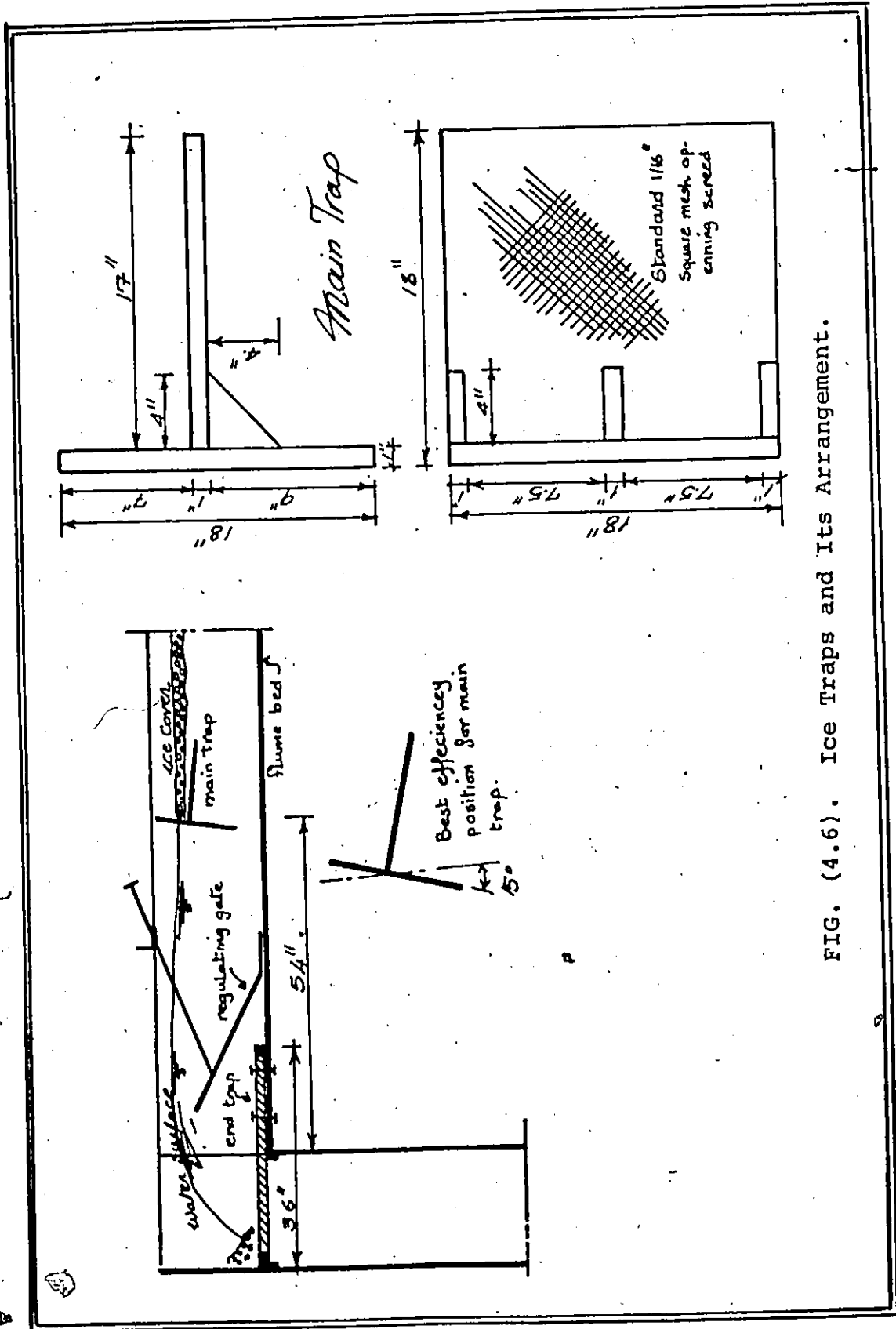


FIG. (4.6). Ice Traps and Its Arrangement.

read directly to $\pm .01$ in. (0.025 cm).

4.3.2 A Pitot-tube was used for the velocity measurements with a vertical manometer reading directly to $\pm .01$ in. (0.025 cm).

4.3.3 The loose cover underside configuration was photographed through the plexiglass side in a scale drawn on the side of the flume. Only the central profile was photographed.

4.3.4 The Shear Apparatus: A simple pendulum apparatus, Fig. (4.6), was designed to measure the shear which occurred in the interface of the flow between the water and the rigid cover. The pendulum consisted of a 1.71 lb. (0.765 kg) bar hinged to a bridge by means of two strings, which acted as an indicator to the attached balance scale. The exit end of the downstream block of the cover was provided with two vertical nails which transmitted the shear of the underside of the floating blocks to the weighted pendulum scale.

4.4 Experimental Arrangement, Procedure and Results

4.4.1 Seven different groups of experiments were carried out to study the flow of ice covered channels. The following is a summary of the arrangement of these groups and the conditions under which each run was performed, in addition to the reason of performing each experiment.

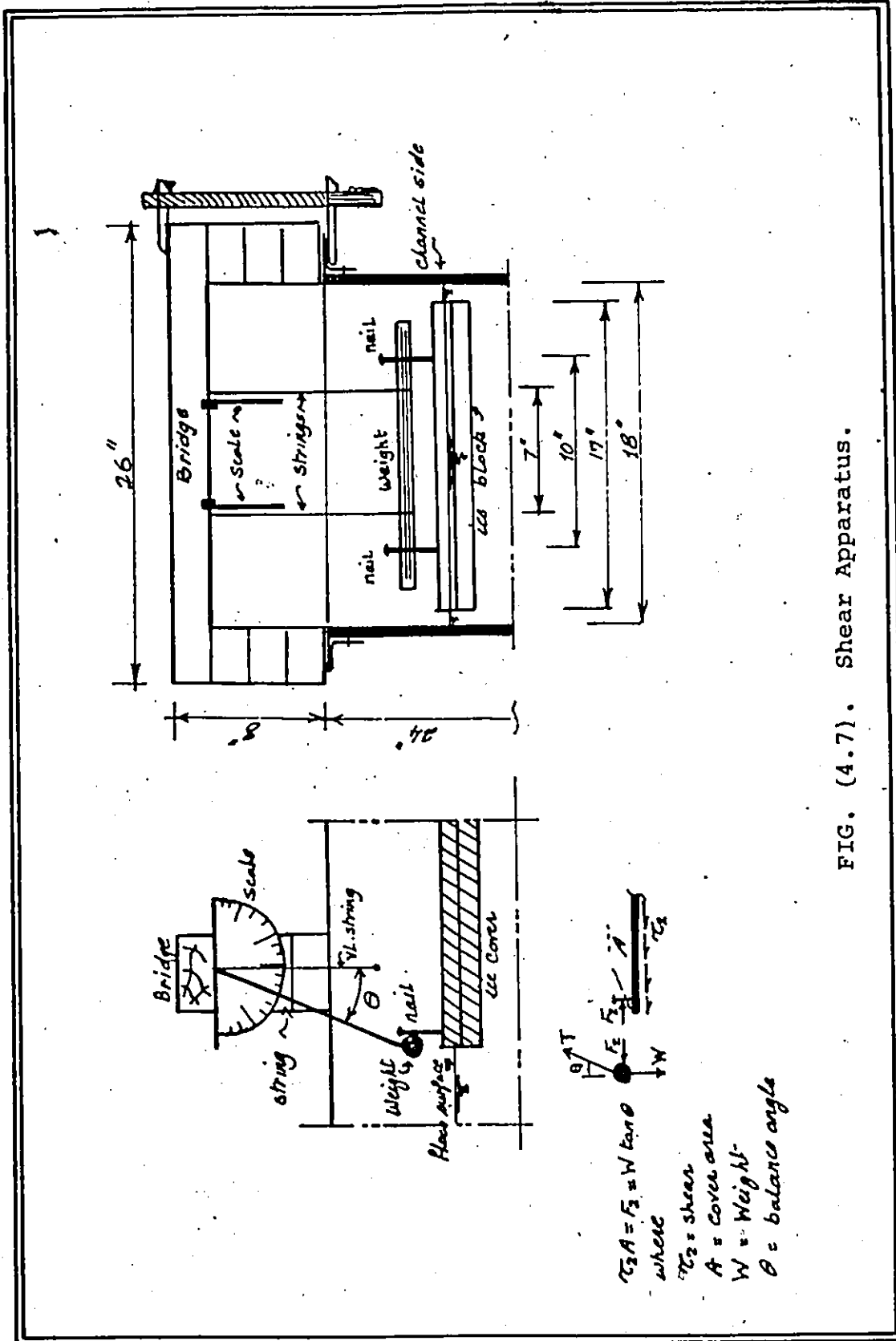


FIG. (4.7). Shear Apparatus.

4.4.2 Evaluation of the Channel Roughness: The first group of six experiments were performed under the conditions shown in Table (E-1) to estimate the channel Manning's roughness coefficient n_1 . The experimental results are shown in tests E1-1 to E1-6 in Appendix E. The average value of n_1 was found to be $0.01167 \text{ sec/ft}^{1/3}$.

4.4.3 Evaluation of the Cover Roughness: Four experiments were performed in the second group to estimate the roughness of the underside of the ice cover. The experiments were performed for a lined channel in the way shown by Fig. (4.8). The Manning's n_2 value was found to be $0.03589 \text{ sec/ft}^{1/3}$.

4.4.4 The front of the ice cover effect on the velocity profiles was performed by measuring different velocity profiles at different sections for the same flow conditions in the arrangement given in Table (E-2). The results are shown in tests (E3-1) to (E3-8).

The effect of the ice cover front on the shear profile indicated by group IV, was performed using the shear apparatus by measuring the shear along different sections of the cover downstream of the front edge.

4.4.5 The verification of the theoretically developed velocity profile and the division line equation, was performed through a different set of experiments, namely, group 5. The results are given in tests E5-1 to E5-9 of Appendix E.

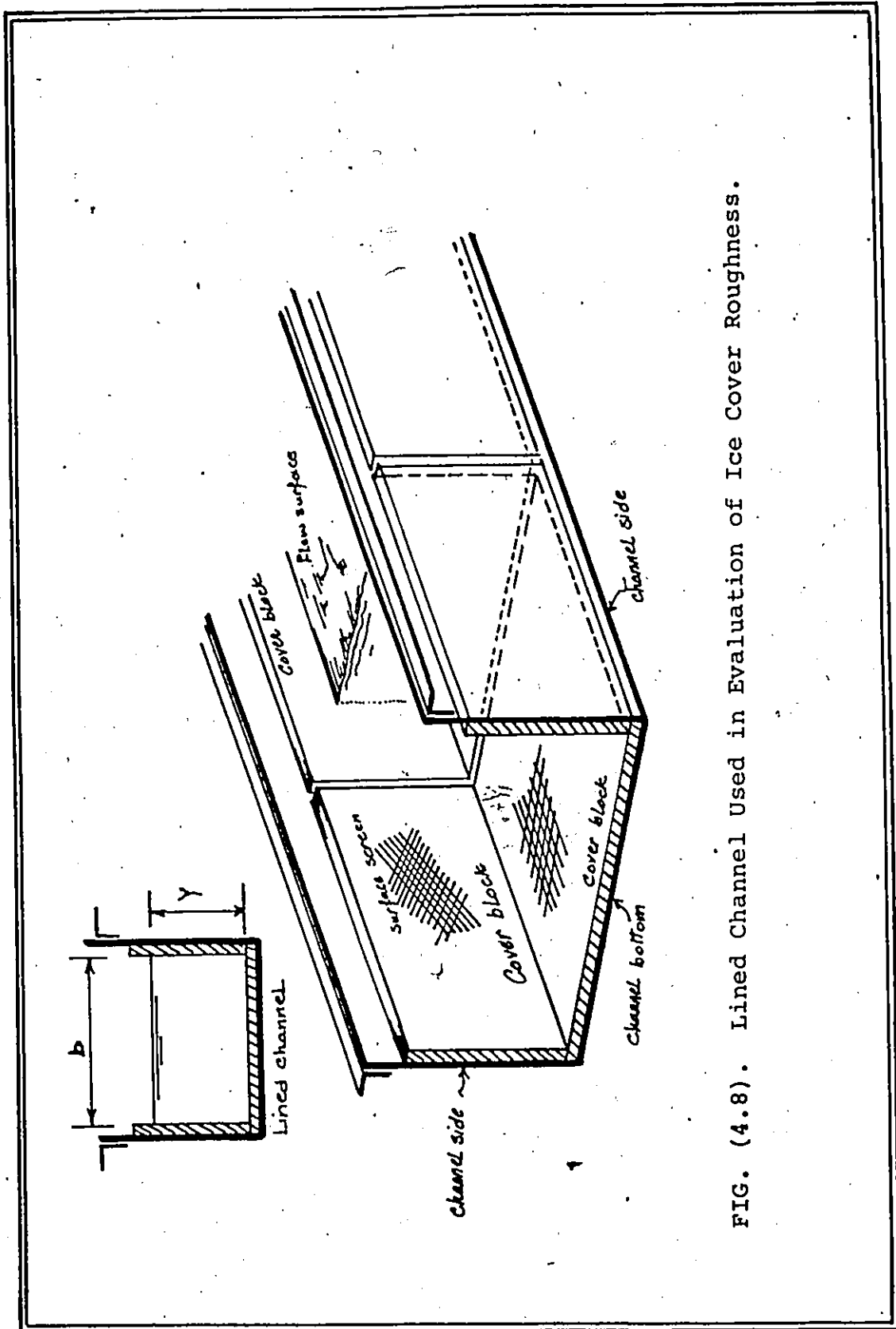


FIG. (4.8). Lined Channel Used in Evaluation of Ice Cover Roughness.

4.4.6 Composite Roughness:

The equation that was developed theoretically was performed for different flow conditions under two types of covers, one of 1 inch thickness as given by experimental runs (E6-1) to (E6-12) and the 24 remaining experiments were carried out using 2 inch cover thickness. The experimental results for the 2 inch cover are given in sheets E6-1 to E6-36 of Appendix E.

4.4.7 Loose Ice Cover Configuration:

In these experiments, the loose polyethylene plastic pellets were used to simulate the cover to study the underside configuration due only to hydraulic factors. The experiments were performed for a flow rate ranging from 0.6 cfs ($.017 \text{ m}^3/\text{sec}$) to 1.0 cfs ($.028 \text{ m}^3/\text{sec}$). Typical measured configurations are represented in Table (2) Appendix E, along with Figs. (E7-1) to (E7-5).

4.5 Experimental Errors

The sources of the experimental errors along with the expected errors are summarized in Appendix D.

CHAPTER 5

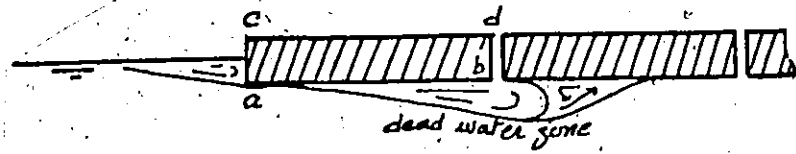
DISCUSSION OF THE EXPERIMENTAL RESULTS

5.1 The Effects of the Front Zone

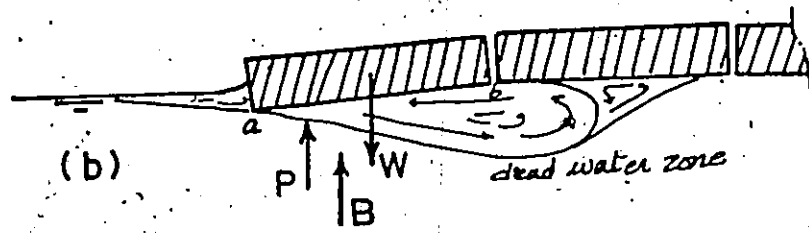
As the flow passes from the open water reach to the covered channel it experiences sudden disturbance resulting in the formation of the front zone. When the flow rotates around the corner (a), Fig. (5.1) it exerts a pressure reduction due to the streamline acceleration. This pressure reduction decreases in magnitude along the cover underside. The pressure drop causes the block to sink in order to gain more buoyancy forces to balance its weight. The more the flow increases the more severe the submergence until one point is reached when the water surface rides the upstream edge of the block. At this point the block will overturn, and sweep beneath the cover. The cover thickens in order to sustain its existence under this new condition, Fig. (5.2b). The forementioned description is based on actual laboratory observations and these effects were also reflected in the velocity profiles and shear distributions along the cover.

5.1.1 Cover Front Effect on Velocity Distribution

Fig. (5.3) shows the flow velocity profiles before reaching the cover and at different sections along it. An interpolation, as shown in Fig. (5.4), was used to predict the velocity profile at the front edge of the cover.



(a)



(b)

FIG. (5.1). Separation Zones and Stability Forces.

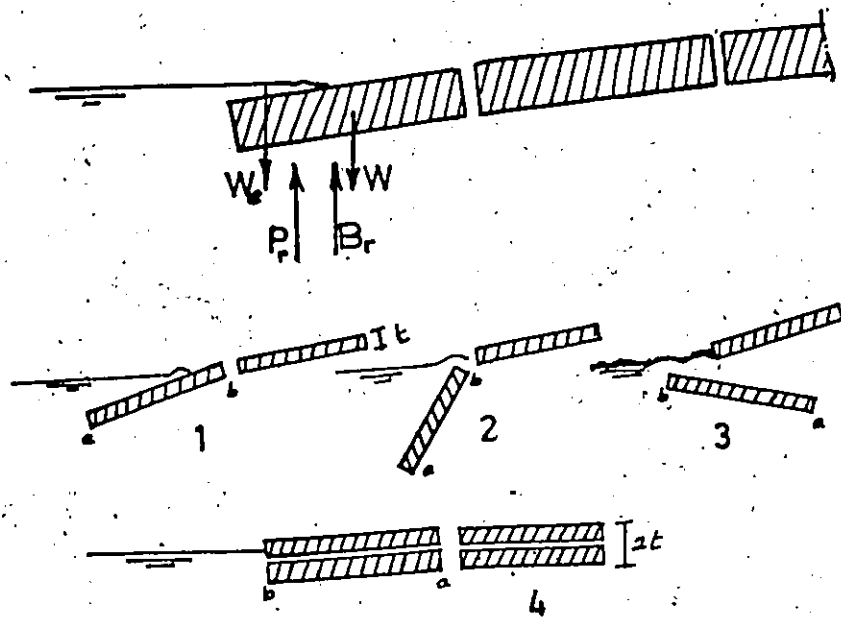


FIG. (5.2). Breakup of Ice Covers.

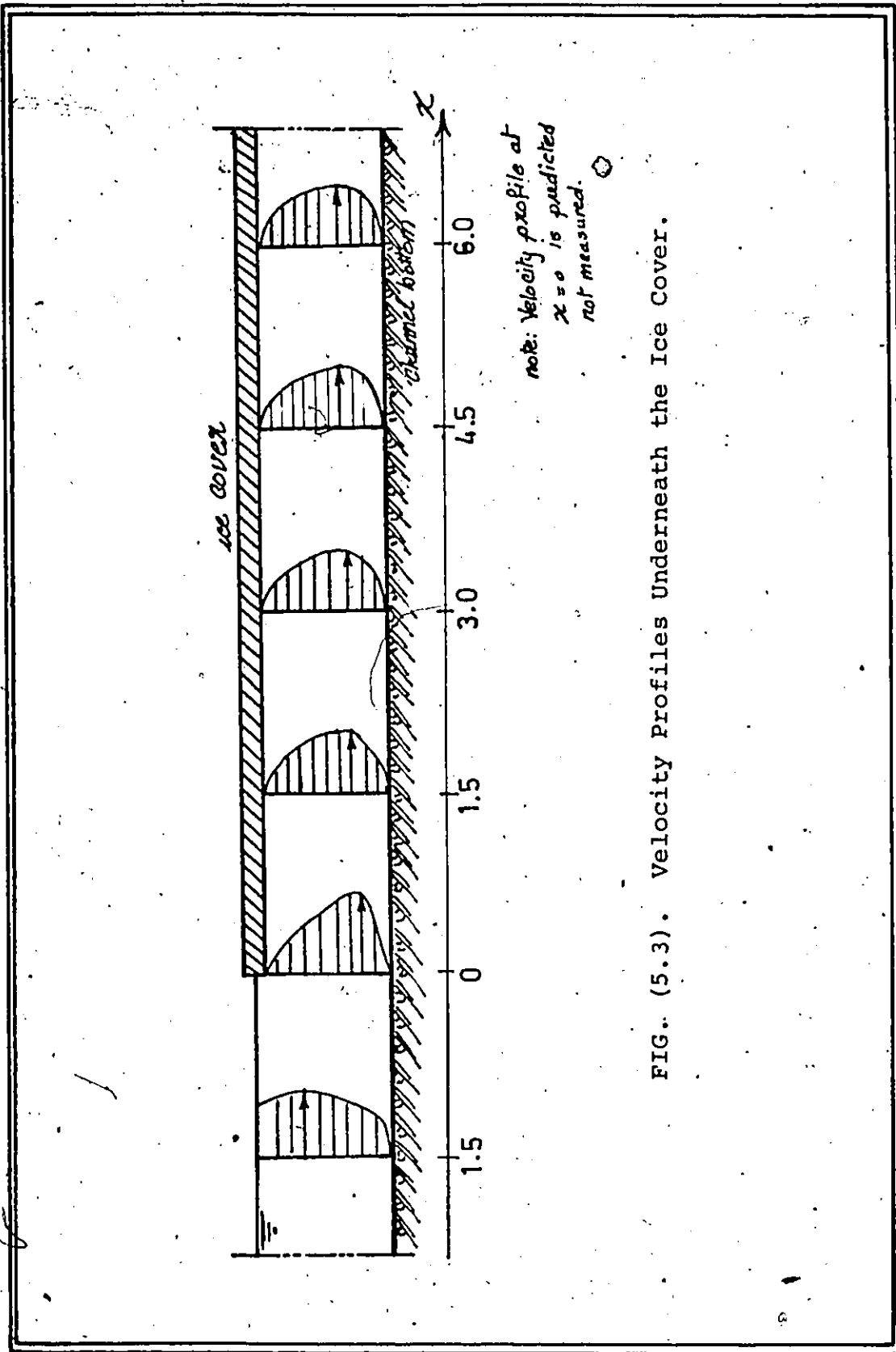


FIG. (5.3). Velocity Profiles Underneath the Ice Cover.

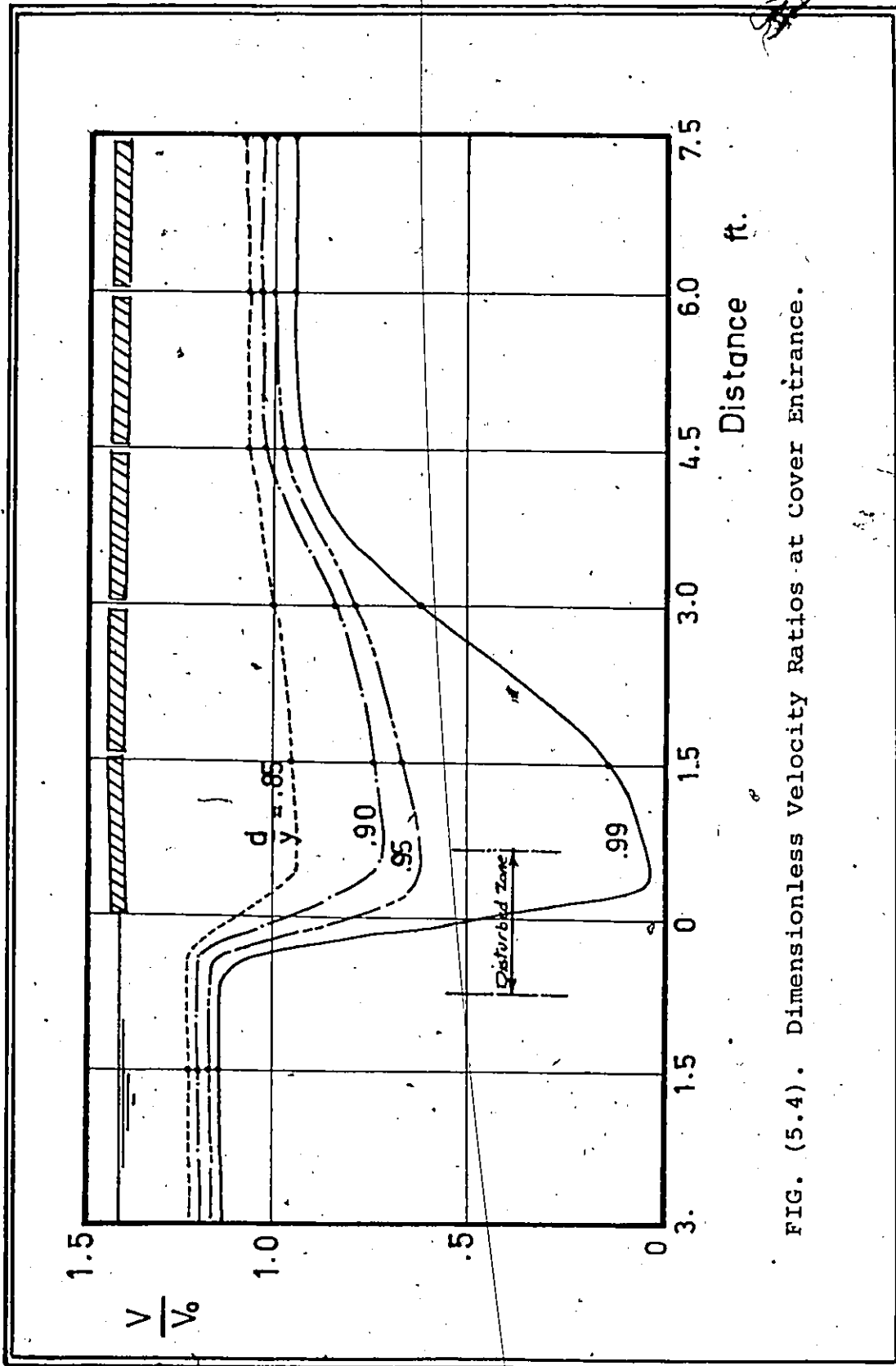


FIG. (5.4). Dimensionless Velocity Ratios at Cover Entrance.

From Fig. (5.3) it is clearly seen that the velocity is affected up to a distance of 6 ft.; beyond this distance the flow becomes steady and uniform. The fluctuations in the velocities under the edge were due to the fluctuations in the edge block. It is also noticed that the high reduction in the acceleration when the flow approaches the cover results in a very high initial cover resistance which forces the maximum velocity to move towards the channel bed before it rises gradually to its stable position in the steady flow zone. Also, the velocity near the cover boundary starts to increase and the velocity profile takes almost smooth patterns after it leaves the initial disturbed zone.

The importance of the study of the effect of cover front on the velocity profiles is to explain its effect on the shear distribution.

5.1.2 Effect of Cover Front on Shear Distribution:

The shear distribution along the ice cover was observed experimentally under different conditions. Fig. (5.5) shows the integrated shear distribution while the local shear distribution is represented in Fig. (5.6) and the dimensionless shear distribution is given in Fig. (5.7). From these curves it is shown that the shear starts with a very high initial value due to the sudden reduction in the flow acceleration around the submerged edge after which the shear decreases until around the

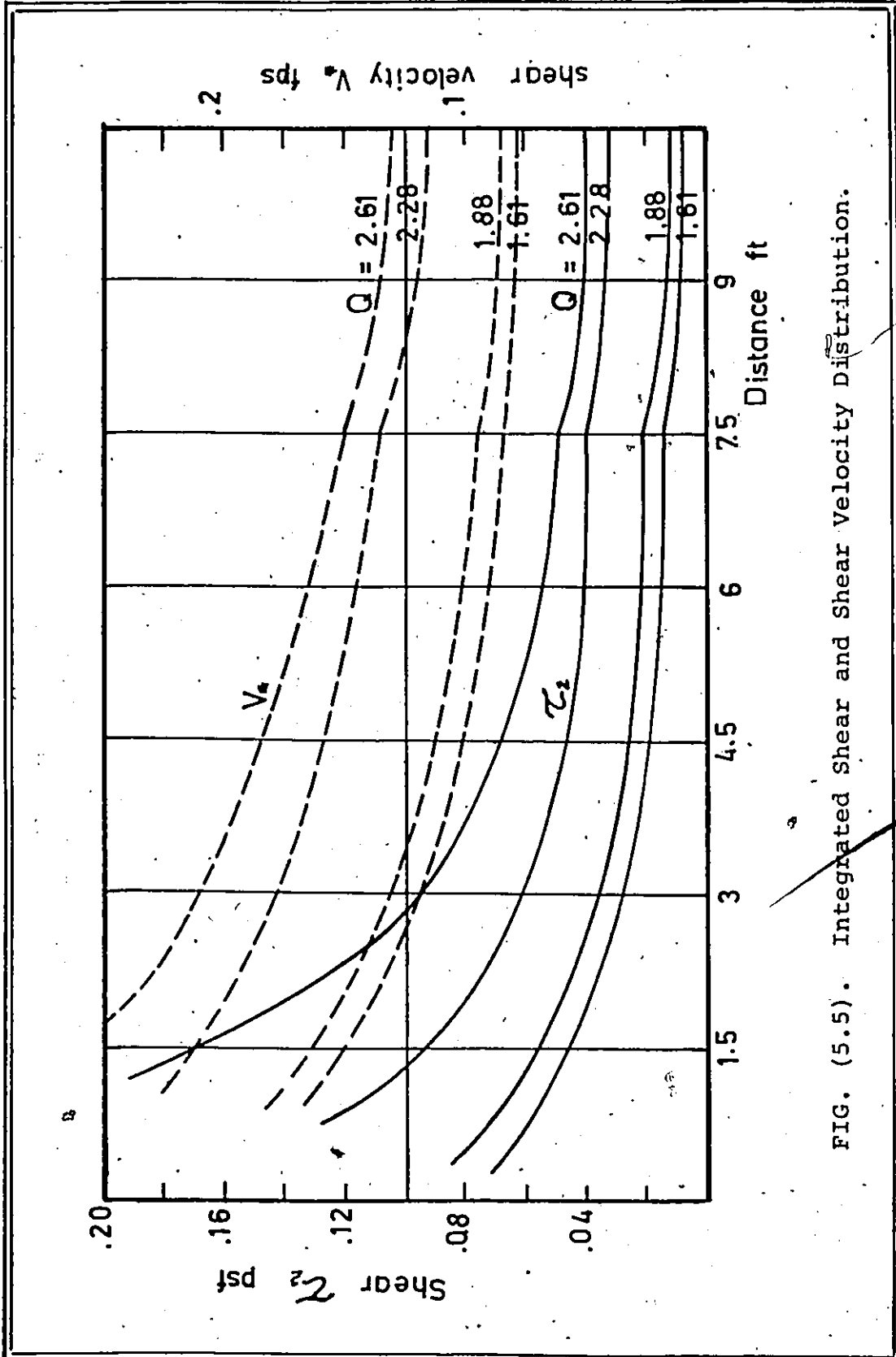


FIG. (5.5). Integrated Shear and Shear Velocity Distribution.

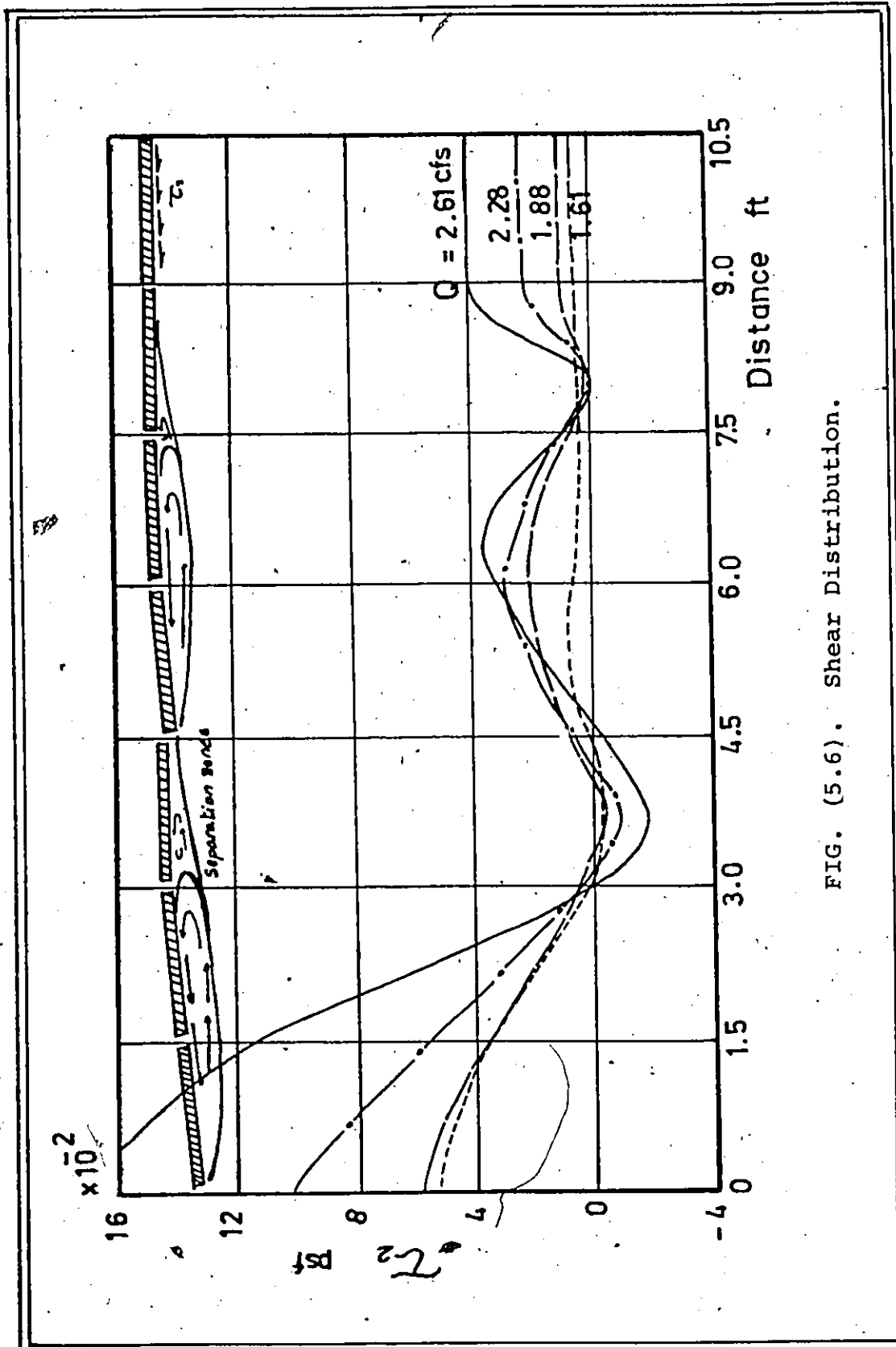


FIG. (5.6). Shear Distribution.

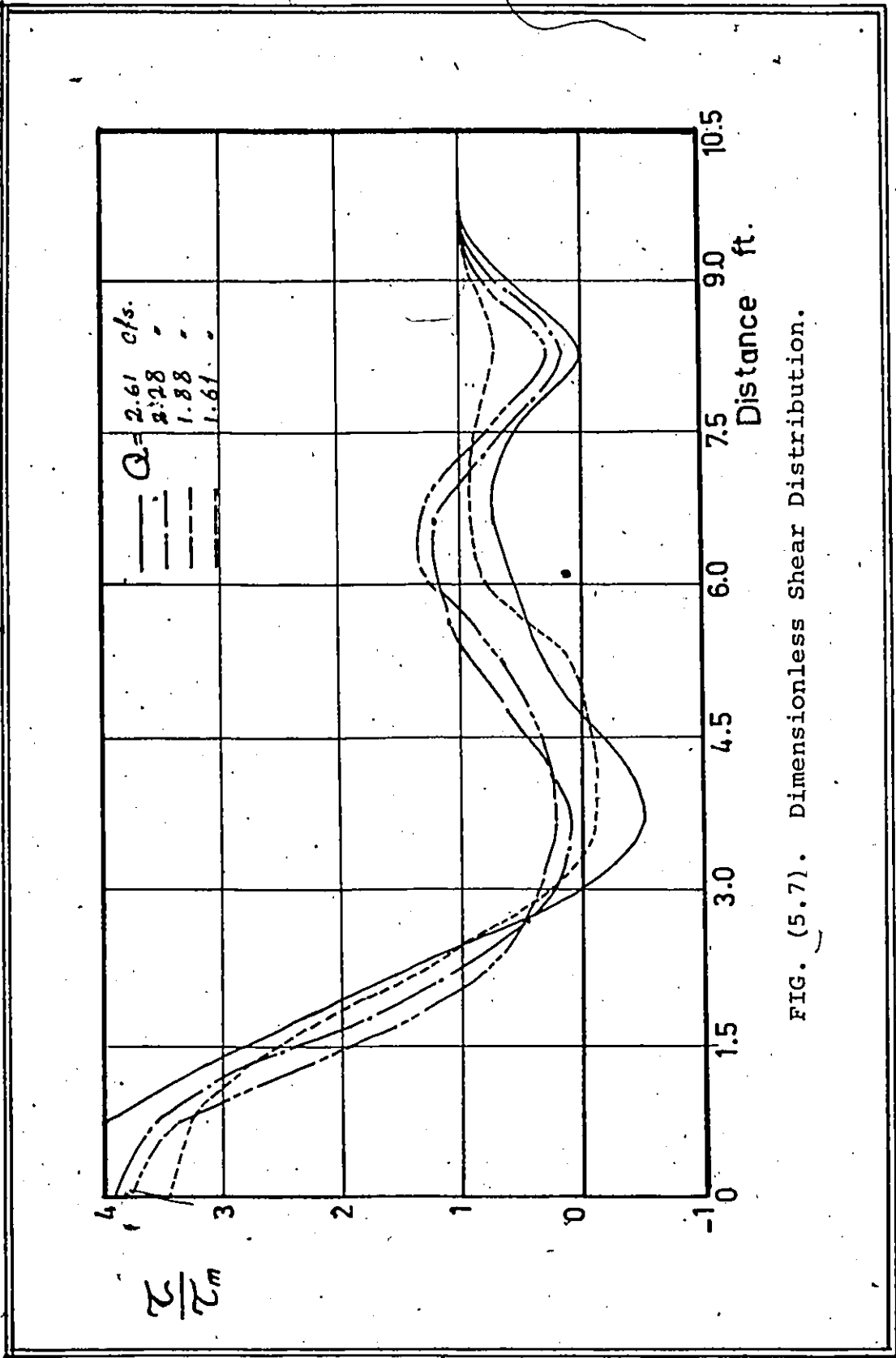


FIG. (5.7). Dimensionless Shear Distribution.

fourth block when another cycle starts. The reason for this can be attributed to the loss of the continuity due to the rigidity of the cover blocks and the free supporting system. The initial shear, along with the differences which appear in the shear distribution, increases with the discharge until it becomes too severe when the critical unstable conditions are reached. The relative shear distribution has almost a constant shape; the discharge effect is not significant in such a case.

Both the integrated shear and the local shear at a fixed point increases rapidly with the discharge as shown in Figs. (5.8) and (5.9). The pattern of the local shear changes is due to the effect of the second cycle shown before. The integrated shear seems to become almost constant just before the break up of the cover depending upon the length of that cover.

The integrated shear was found also to increase with the Reynolds number for the range of experiments as shown in Fig. (5.10).

5.1.3 General Conclusion:

A very high initial shear was noticed to exist due to the cover front edge effect which suggests a correction factor for the shear exerted by the cover underside for short covers. Short covers are estimated to be those covers in which the ratio L/t is less than 500. The cover front effect also depends upon the

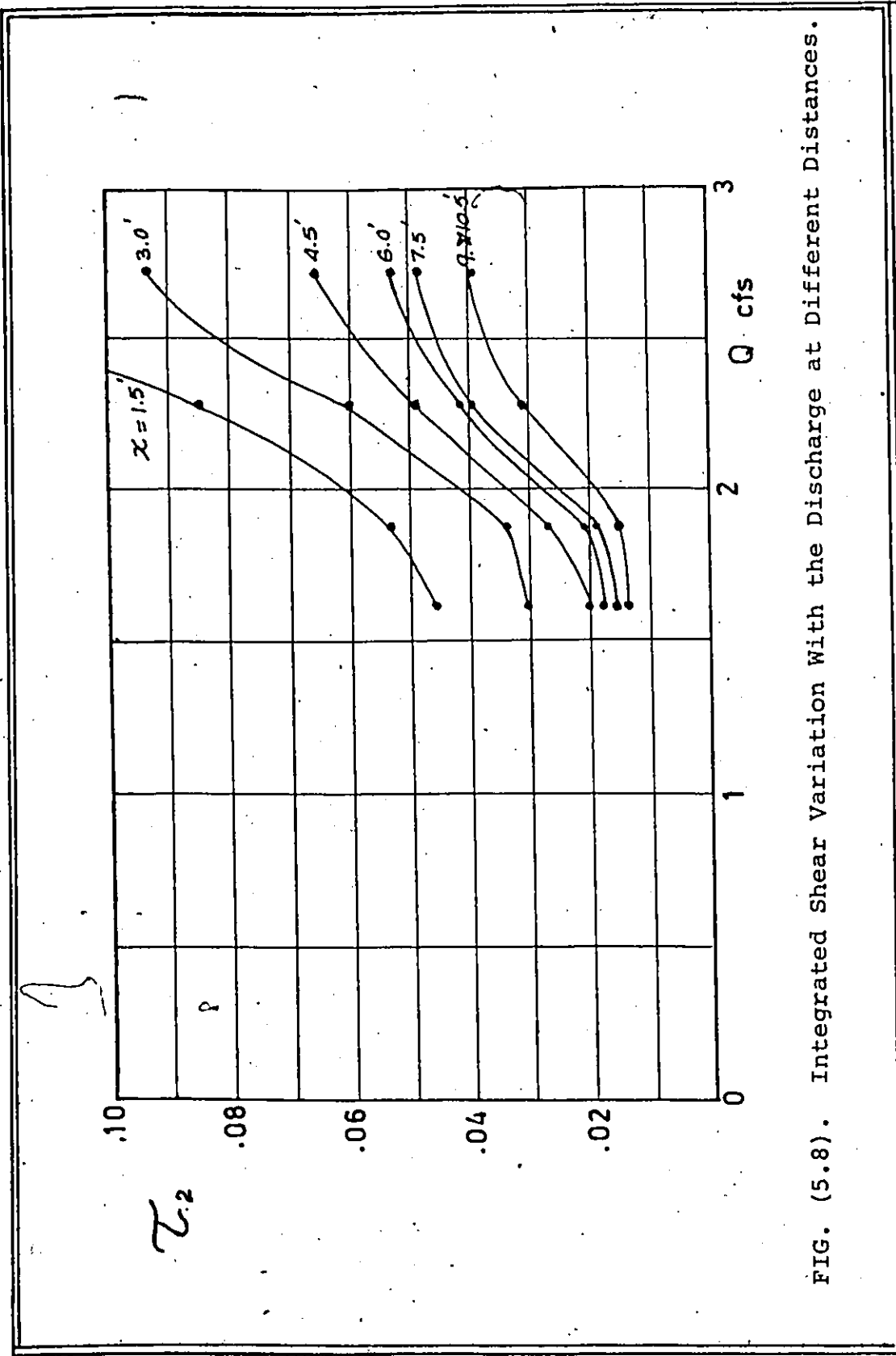


FIG. (5.8). Integrated Shear Variation With the Discharge at Different Distances.

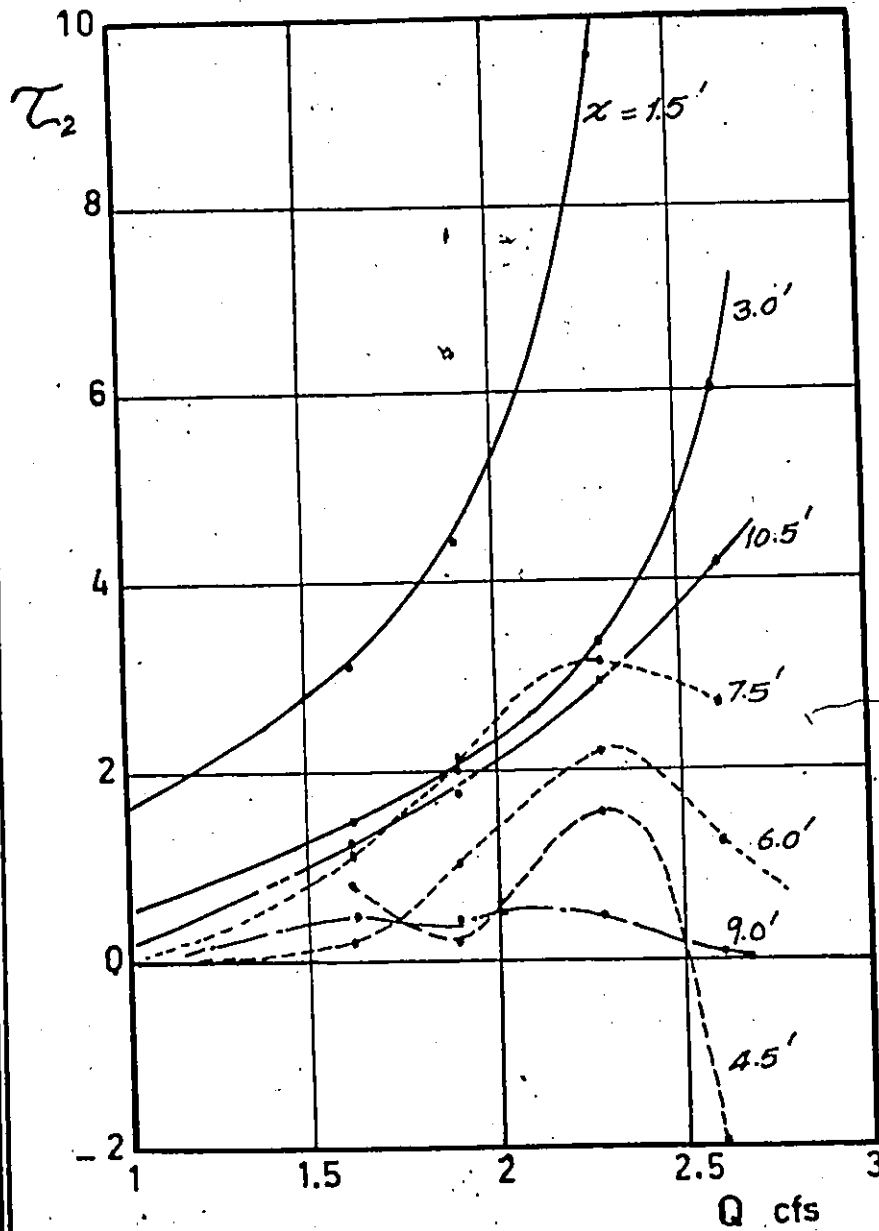


FIG. (5.9). Variations in Shear Stress With Discharge Along the Ice Cover Front.

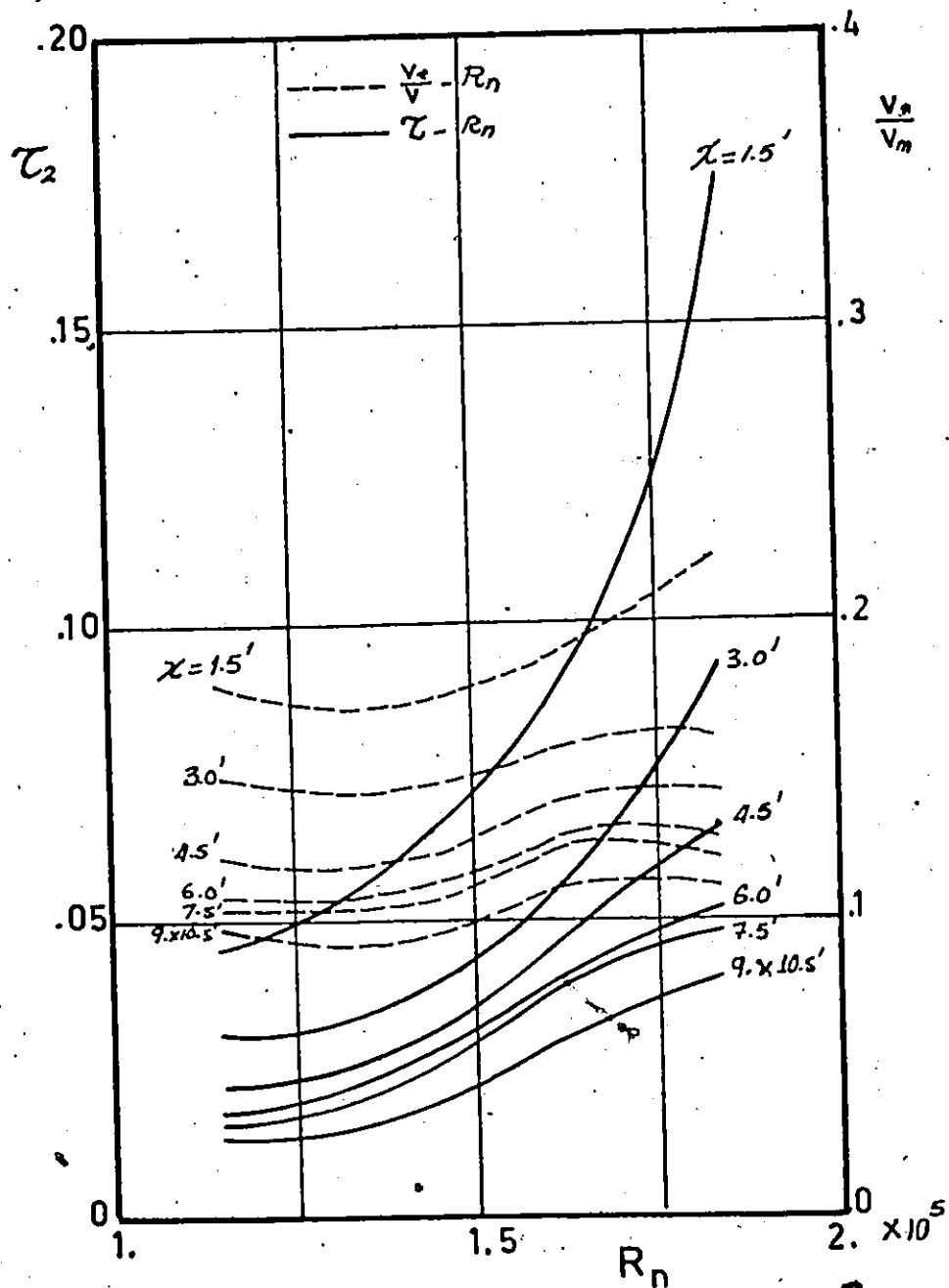


FIG. (5.10). The Variation of the Shear and the Dimensionless Shear Velocity with Reynolds number.

geometric shape of the cover edge which for loose covers will not be significant because of the streamlined edge.

5.2 The Velocity Distribution

As the discharge flows past the front zone, it becomes steady and uniform. Under this condition, the velocity takes the profile described in Chapter 3. Nine experiments were carried out to verify such a profile, and Fig. (5.11) shows both the measured and the theoretically predicted velocity distributions.

In developing the velocity distributions theoretically, Eqns. (3.22) and (3.26), namely

$$u_i/V_{\max} = 1. + \frac{1}{\kappa} \frac{V_{*i}}{V_{\max}} F_1(\epsilon_i), \quad i = 1, 2$$

were used, where V_{*i} equals $\sqrt{\tau_i/\rho}$, κ is Von Karmen's constant and V_{\max} is the maximum velocity. The measured maximum velocity was used in computing the theoretical profile. Also, the average sub-sections velocities V_1 and V_2 were predicted and plotted against the measured ones as shown in Fig. (5.12).

The agreement between the theoretical and measured velocity profiles is generally very good. In the channel sub-section the agreement is very close in all the runs. Except run 2, where high fluctuations in the velocity were measured, the differences were due to

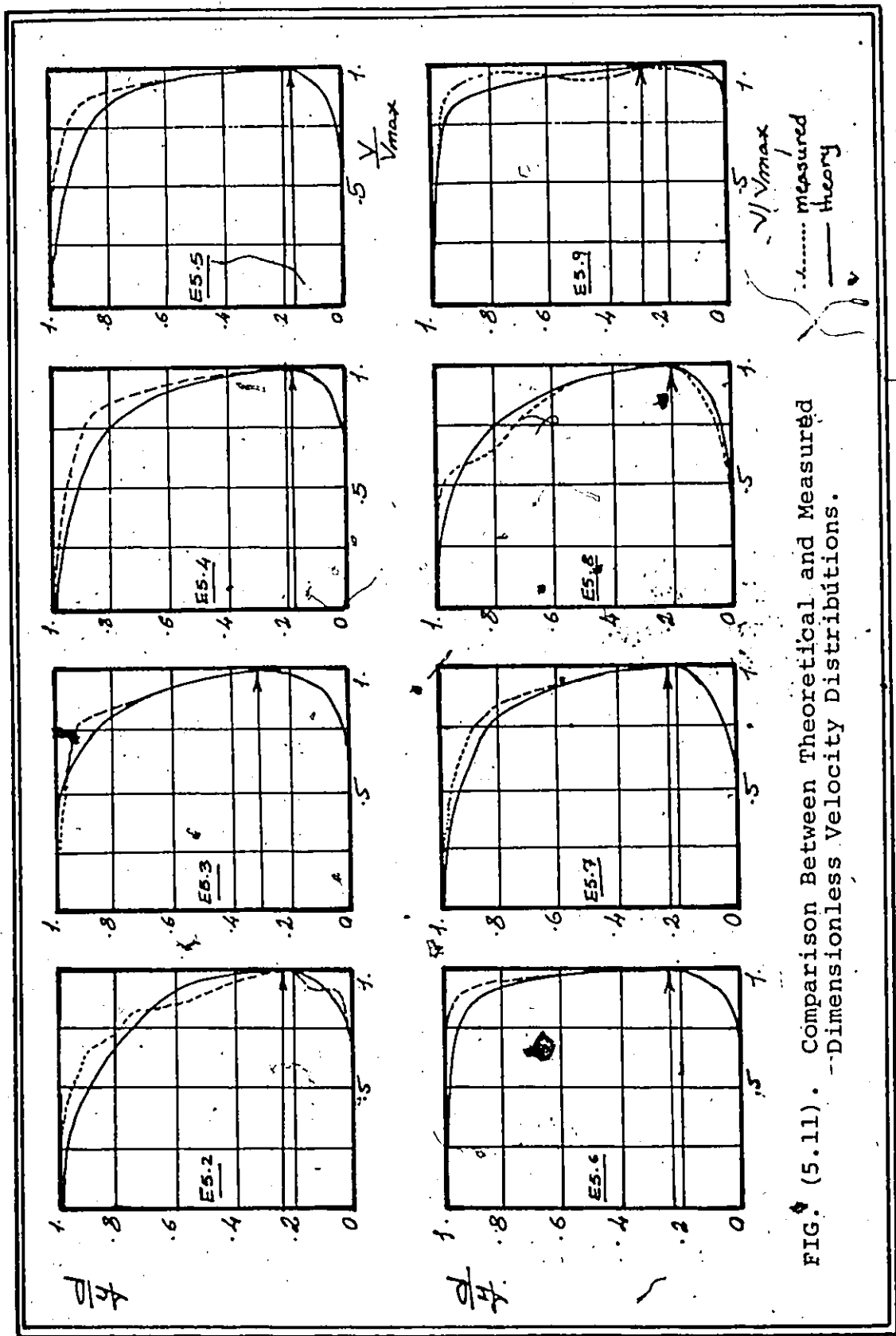


FIG. (5.11). Comparison Between Theoretical and Measured Dimensionless Velocity Distributions.

experimental errors. On the other hand, the differences between the predicted and measured velocities in the cover sub-section were noticed to be higher, especially in the boundary zone. The measured velocities were greater than the theoretical ones, which can be attributed to a technical difficulty in placing the pitot-tube. In order to introduce the pitot-tube used in the velocity measurements, a 6 inch gap was made in the cover, and a wooden substitution was used to replace the cover effect, a fact that produced a slight increase in the velocity due to the decrease of the cover roughness at the measured section. This effect appeared only near the boundary while the agreement in the flow core is satisfactory.

Also, as shown, the theory leads to very good agreement in computing the mean velocities and flow discharges as shown by Fig. (5.12).

In applying the theoretical velocity distribution, special care should be given for estimating the value of $F_1(\epsilon)$ near the boundary due to the rapid increase in its value at this zone.

5.3 Checking for λ Value

Near the side walls, the boundary roughness causes the maximum velocity to move away from the wall and the bed. This process affects the sub-sections

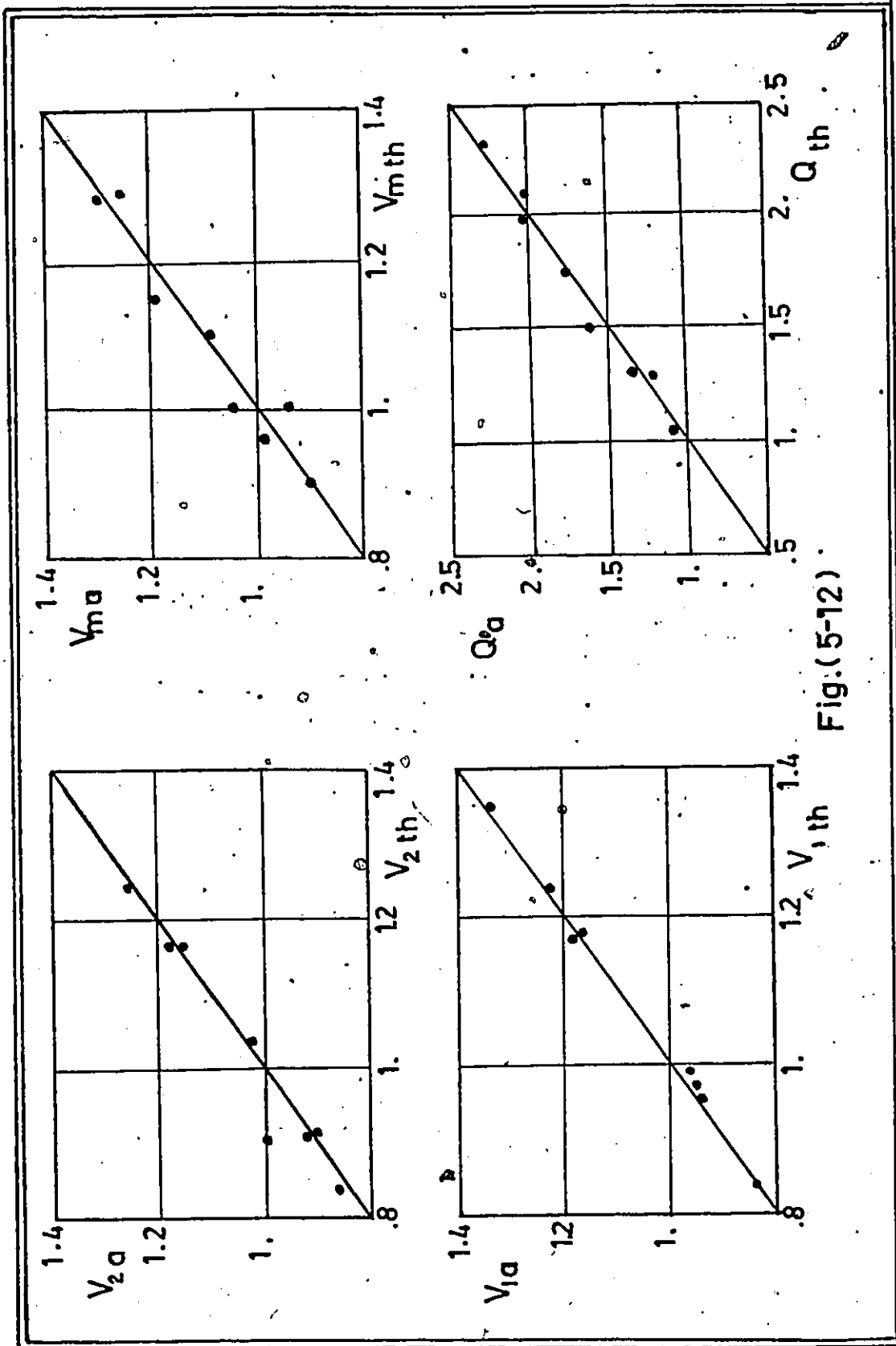


Fig.(5-12)

hydraulic radius ratio λ since the dividing line was defined as the locus of the maximum velocity point.

Theoretically, λ can be calculated by solving Eqn. (3.34), namely,

$$\frac{R^{1/6}}{n_1 \sqrt{g}} = \frac{0.444}{K} \frac{\sqrt{\lambda} - 1}{1 - n_1/n_2 \lambda^{2/3}} (\alpha + (1-\alpha)\lambda)^{1/6} \quad (3.34)$$

But experimentally, no direct way was available to measure this λ value due to the difficulty of measuring accurate velocity profiles near the side walls. So, in order to test the validity of Eqn. (3.34) an indirect method was proposed.

In a rectangular channel of width b , depth Y , if the division ratio at the center is Y_2/Y_1 , Fig. (5.13a) and approximating the separation surface to take the trapezoidal shape as shown, the value of λ will be given by,

$$\lambda = \frac{\alpha}{1-\alpha} / \left(\left(\frac{1}{1 - X/B} \frac{Y}{Y_2} - 1 \right) \right) \quad (5.1)$$

where α and the Y/Y_2 values can be measured.

First, considering the extreme values of X/B for $X/B = 0$, the case of Fig. (5.13b) and $X/B = \frac{1}{2}$, the case of Fig. (5.13c), a measured λ value can be estimated. In Fig. (5.14) these measured values are compared to the theoretical ones. It is clearly shown that the theory

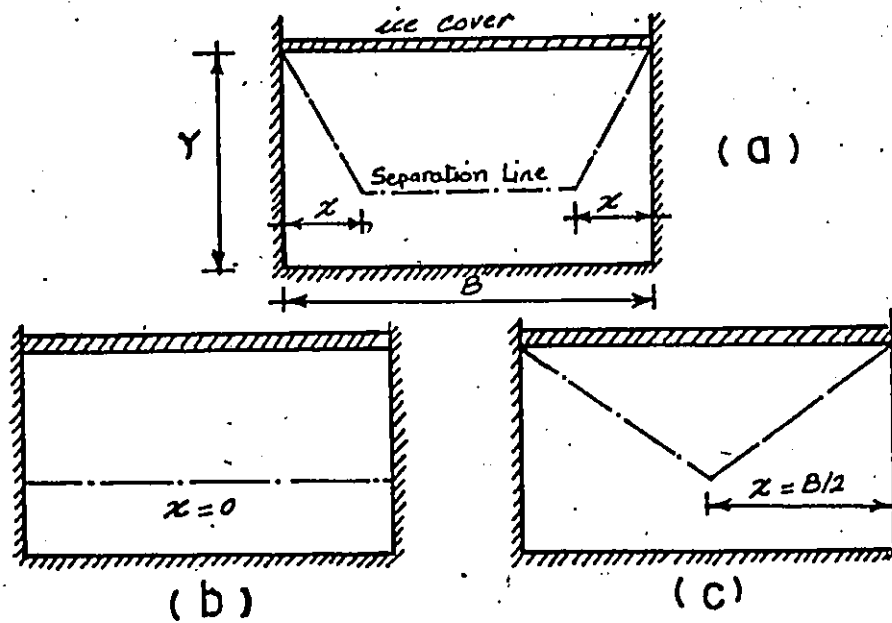
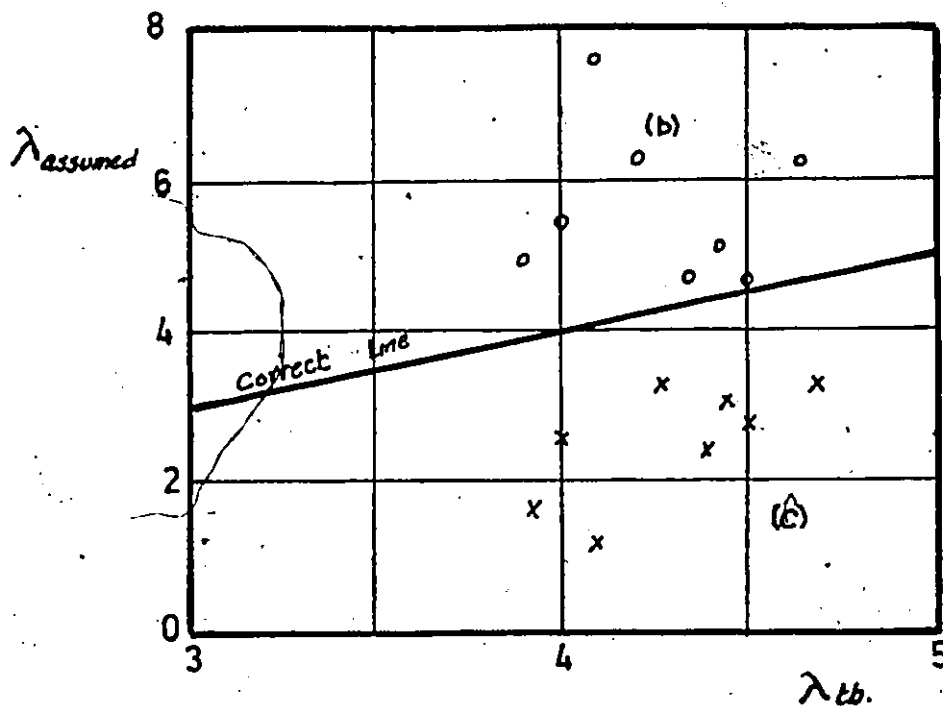


Fig.(5-13)

FIG. (5.14). Indirect Verification of λ Assumption.

gives intermediate values between cases (b) and (c) which indicates that the theory is in good agreement with the assumption of the separation line. Furthermore, the theoretically predicted λ value can be used to estimate X/B for different conditions by means of the equation

$$\frac{X}{B} = 1 - \frac{Y}{Y_2} \frac{(1-\alpha)\lambda}{\alpha + (1-\alpha)\lambda} \quad (5.2)$$

In Fig. (5.15) X/B is plotted against Q , and the relation shows that X/B increases as Q increases; the curve is plotted taking into account the limiting values of $X/B = 0$ and 0.5 . Also X/B is found to increase with the Reynolds number R_n as shown in Fig. (5.16). These two results can be explained by the fact that as the discharge increases the velocity increases at all points. The velocity gradient increases as the discharge increases and has the tendency to cause the separation line to move upwards and towards the center.

From the above discussion, it can be verified that the assumption for the separation line and the theoretical method for estimating the λ value are both meaningful and can be considered significantly correct.

In computing the λ value by numerical methods, a satisfactory initial solution was found to be

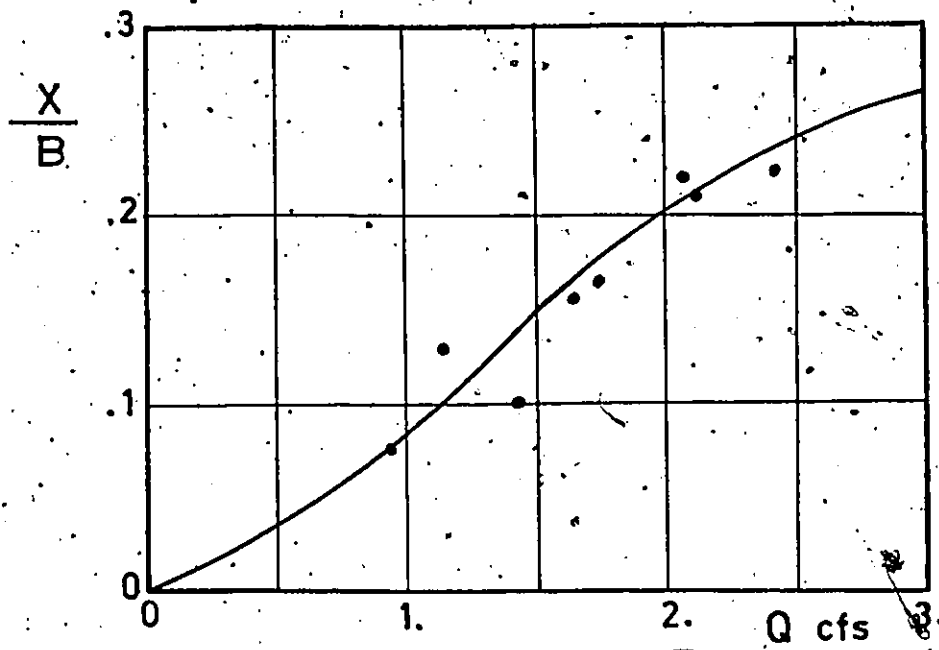


FIG. (5.15).

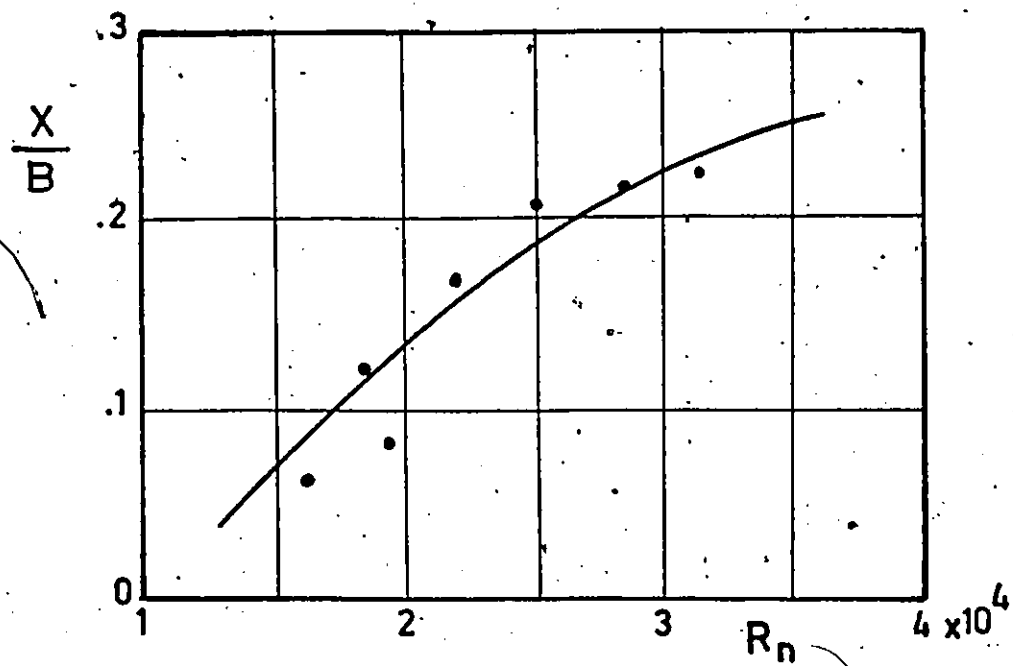


FIG. (5.16).

$$\lambda = 0.85 \left(\frac{n_2}{n_1} \right)^{1.5} \quad (5.3)$$

5.4 Composite Roughness: Experimental Data

As given in Chapter 3, once the λ value is determined the composite Manning's roughness coefficient n can be estimated theoretically using Eqn. (3.43),

$$\frac{n_1}{n} = \left(\frac{1}{\alpha + (1-\alpha)\lambda} \right)^{2/3} \left(1 + \frac{n_1}{n_2} \lambda^{2/3} \right) \left(1 + \frac{\sqrt{\lambda} + 1}{\sqrt{\lambda} - 1} \right)$$

$$\times \frac{\alpha - (1-\alpha)\lambda}{\alpha + (1-\alpha)\lambda} \left(\frac{1 - \frac{n_1}{n_2} \lambda^{2/3}}{1 + \frac{n_1}{n_2} \lambda^{2/3}} \right) \quad (3.43)$$

In order to verify this relation, 36 experiments, in the arrangement given in Chapter 4 were carried out. For each experiment the direct application of Manning's Equation gives the value of the composite roughness n as

$$n = \frac{1.49}{Q} A R^{2/3} S^{1/2} \quad (5.4)$$

where Q , A , R and S are the discharge, area, hydraulic radius and energy slope of the ice covered channel respectively.

Also, the experimental error was estimated, as given in Appendix D, and assumed to take the average maximum value of $\pm 33\%$.

In Fig. (5.17) a comparison between the theoretical and measured composite roughness is given. It is clear that the ratio between the actual and estimated roughnesses is accurate to within $\pm 10\%$ which falls within an average maximum experimental error of $\pm 33\%$. The 1 inch cover thickness shows a tendency of underestimating the theoretical values, although it is within the experimental error range. It can be attributed to the effect of the cover thickness on the underside roughness which was neglected in the theoretical calculations as the underside roughness n_2 used was that value measured for 2" thickness cover.

A rating curve was also theoretically developed and the results were plotted in Fig. (5.18) between the theoretical and measured discharges. The variation was found to be within $+12\%$ and -8% which can be explained by the forementioned reason and the inherent experimental errors. The theory therefore showed good agreement with the experimental observations.

The theoretically developed equations for the computation of the composite roughness proved to be very satisfactory in comparison with the experimental results.

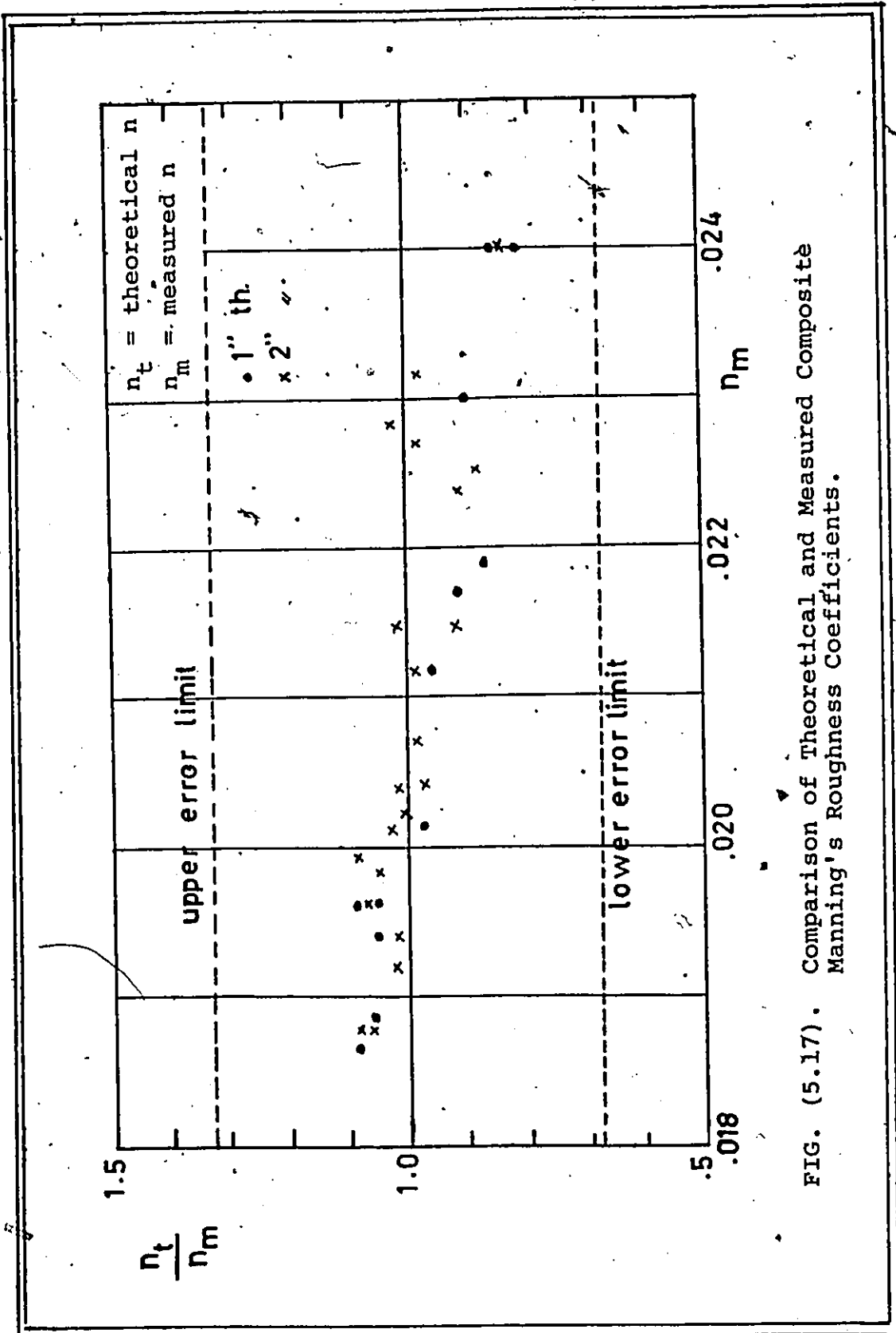


FIG. (5.17). Comparison of Theoretical and Measured Composite Manning's Roughness Coefficients.

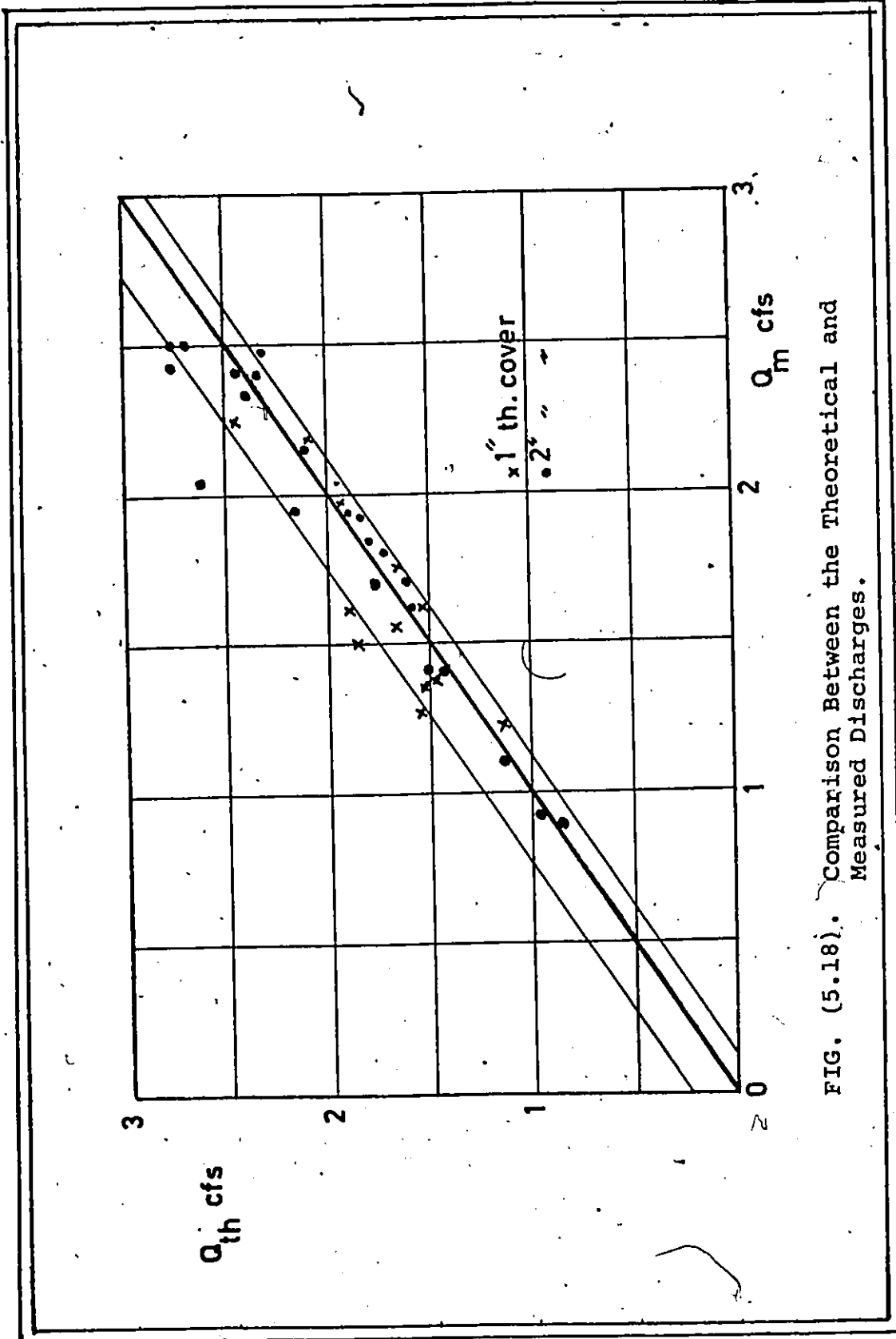


FIG. (5.18). Comparison Between the Theoretical and Measured Discharges.

5.5 Composite Roughness; Field Data Verification

The field data published by Uzuner, and Carey are used to further verify the theory.

5.5.1 Application to Uzuner's Data:

Uzuner reported field data of a wide range of $0.024 < n_1 < 0.026$; n_1 is the channel roughness and $0.010 < n_2 < 0.028$ where n_2 is the ice cover roughness.

He also reported the estimated composite roughness as obtained by the theories developed by Levi (1948), Carey (1966), Hancu (1967), and Larsen (1969) for this data which is summarized in Table (5.1), and also represented graphically in Fig. (5.19).

The proposed relation predicted intermediate values and hence proved its validity for practical application.

5.5.2 Comparison of Developed Theory with Carey's Equation

As the proposed equation takes into account all the common assumptions that were used before, it can be shown that the introduction of these assumptions used by Carey and other investigators, leads to the results obtained by their equations. An example is given to illustrate this point using data obtained by Carey.

The measured channel data are,

$$\begin{array}{ll} \alpha = 0.496 & \lambda = 0.434 \\ R = .1.350 & n_1 = 0.0247 \\ S = 3.79 \times 10^{-4} & \end{array}$$

TABLE 5-1

R	n ₁	n ₂	Levi 1948	Carey 1966	Hancu* 1967	Larsen 1969	Predicted Value
2.02	0.0249	0.0100	0.0201	0.0182	0.0203	0.0182	0.01917
2.12	0.0240	0.0122	0.0198	0.0191	0.0207	0.0184	0.01955
2.36	0.0259	0.0177	0.0223	0.0215	0.0246	0.0219	0.02292
2.10	0.0248	0.0154	0.0209	0.0204	0.0228	0.0203	0.02134
2.14	0.0249	0.0135	0.0206	0.0196	0.0222	0.0195	0.02066
2.12	0.0250	0.0161	0.0212	0.0208	0.0233	0.0207	0.02174
2.02	0.0250	0.0145	0.0208	0.0207	0.0224	0.0200	0.02113
2.06	0.0253	0.0199	0.0228	0.0227	0.0256	0.0227	0.02334
2.14	0.0253	0.0299	0.0277	0.0241	0.0328	0.0242	0.02832
2.40	0.0252	0.0245	0.0249	0.0248	0.0288	0.0248	0.02490
2.68	0.0252	0.0281	0.0267	0.0266	0.0312	0.0266	0.02700
2.48	0.0251	0.0240	0.0246	0.0246	0.0284	0.0245	0.02450
2.40	0.0252	0.0244	0.0248	0.0248	0.0287	0.0248	0.02470
2.64	0.0250	0.0230	0.0240	0.0240	0.0277	0.0240	0.02400

*for $\lambda_1 = 0.1$
 *from n/n_2

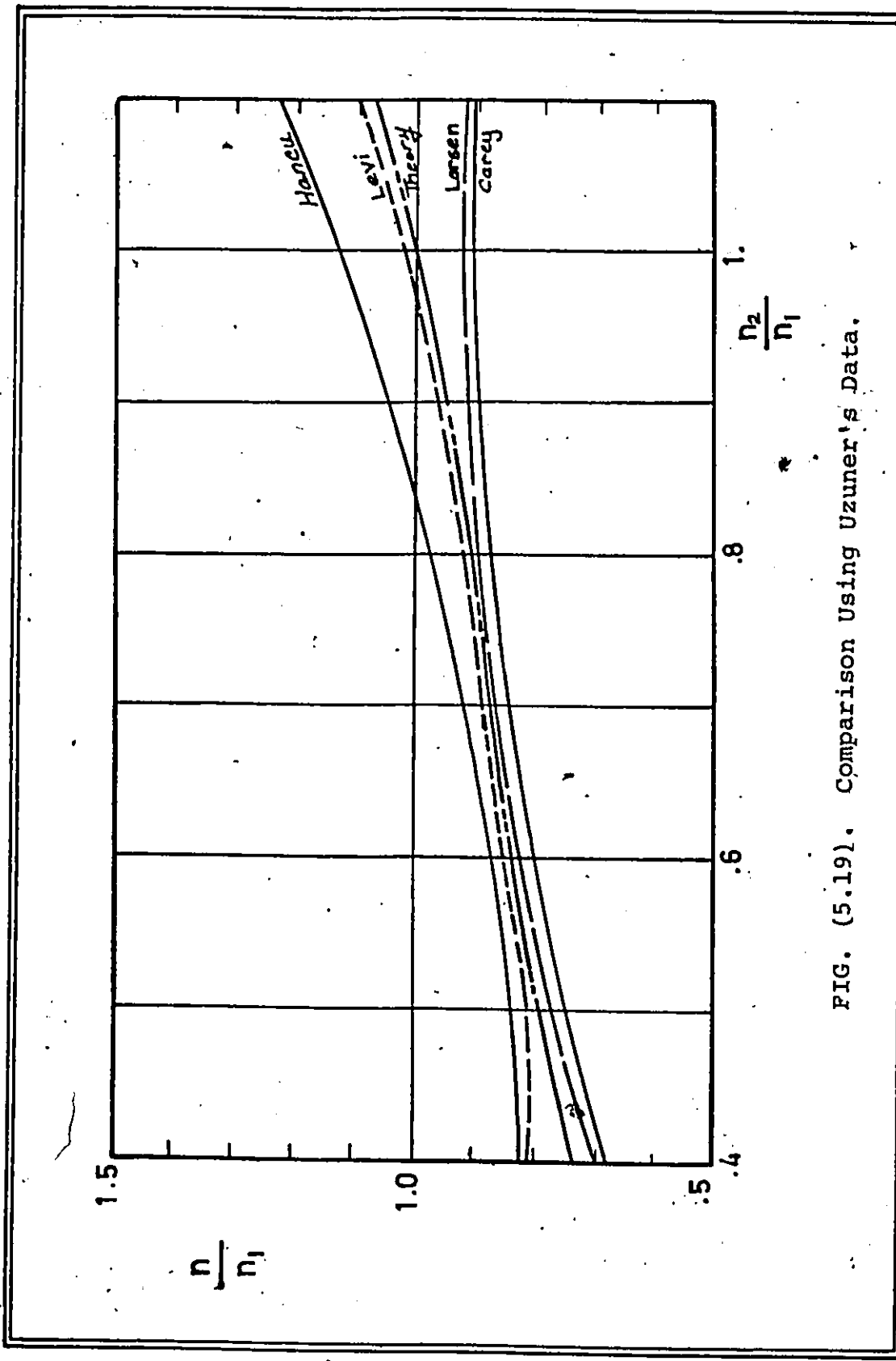


FIG. (5.19). Comparison Using Uzuner's Data.

Carey also predicted the value of

$$n_2 = 0.0142 \quad n = 0.0198$$

To estimate the n_2 value from the developed theory, Eqn. (3.39) gives

$$\frac{1}{n_2} = \frac{1}{n_1 \lambda^{2/3}} - \frac{0.444\sqrt{g}}{\kappa} \left(\frac{\alpha + (1-\alpha)\lambda}{R} \right)^{1/6} \frac{\sqrt{\lambda} - 1}{\lambda^{2/3}} \quad (5.5)$$

which gives $n_2 = 0.015$.

Introducing Carey's assumption and that of the other researchers on the equality of the two sub-sections mean velocity, or

$$\lambda = (n_1/n_2)^{1.5} \quad (5.6)$$

which is obtained from Eqn. (5.5) by omitting the second term yields n_2 value of 0.0142 which is the same as the value found by Carey.

Secondly, to compute the composite roughness, Eqn. (3.43) will be used, namely

$$\frac{n_1}{n} = \frac{1}{2} \left(\frac{1}{\alpha + (1-\alpha)\lambda} \right)^{2/3} \left(1 + \frac{n_1}{n_2} \lambda^{2/3} \right) \left(1 + \frac{\sqrt{\lambda} + 1}{\sqrt{\lambda} - 1} \right) \times \frac{\frac{\alpha - (1-\alpha)\lambda}{\alpha + (1-\alpha)\lambda} \left(1 - \frac{n_1}{n_2} \lambda^{2/3} \right)}{1 + \frac{n_1}{n_2} \lambda^{2/3}}$$

which yields $n_2 = 0.02$.

Introducing Carey's assumption as before gives n of 0.0198 which is the same value reported by him.

Experimental results, and Eqn. (3.43) support the conclusion that the mean velocities in the sub-sections are not identical except in the case when n_1 equals n_2 . It, therefore, appears that the assumption of equal mean velocities in the sub-section as used by Carey and others apply only when the roughness of the channel and ice cover are similar. Eqn. (5.5) gives the particular case for n_1 equals n_2 when the second term of the equation becomes zero in which case the results become similar to those predicted by Carey.

5.5.3 Comparison of Known Relations for Computation of Composite Roughness:

In order to compare the proposed equation with the known equations described in Chapter 2, the data of Uzuner and Carey were used, and the results are given in Fig. (5.20) in the form of a dimensionless plot. From Fig. (5.20), it can easily be seen that the proposed relation holds a central position among the known equations which have been used for many years. Among the known relations Pavlovskiy's one seems to be the closest to the proposed Eqn. (3.43), which is more comprehensive as it includes in addition more channel

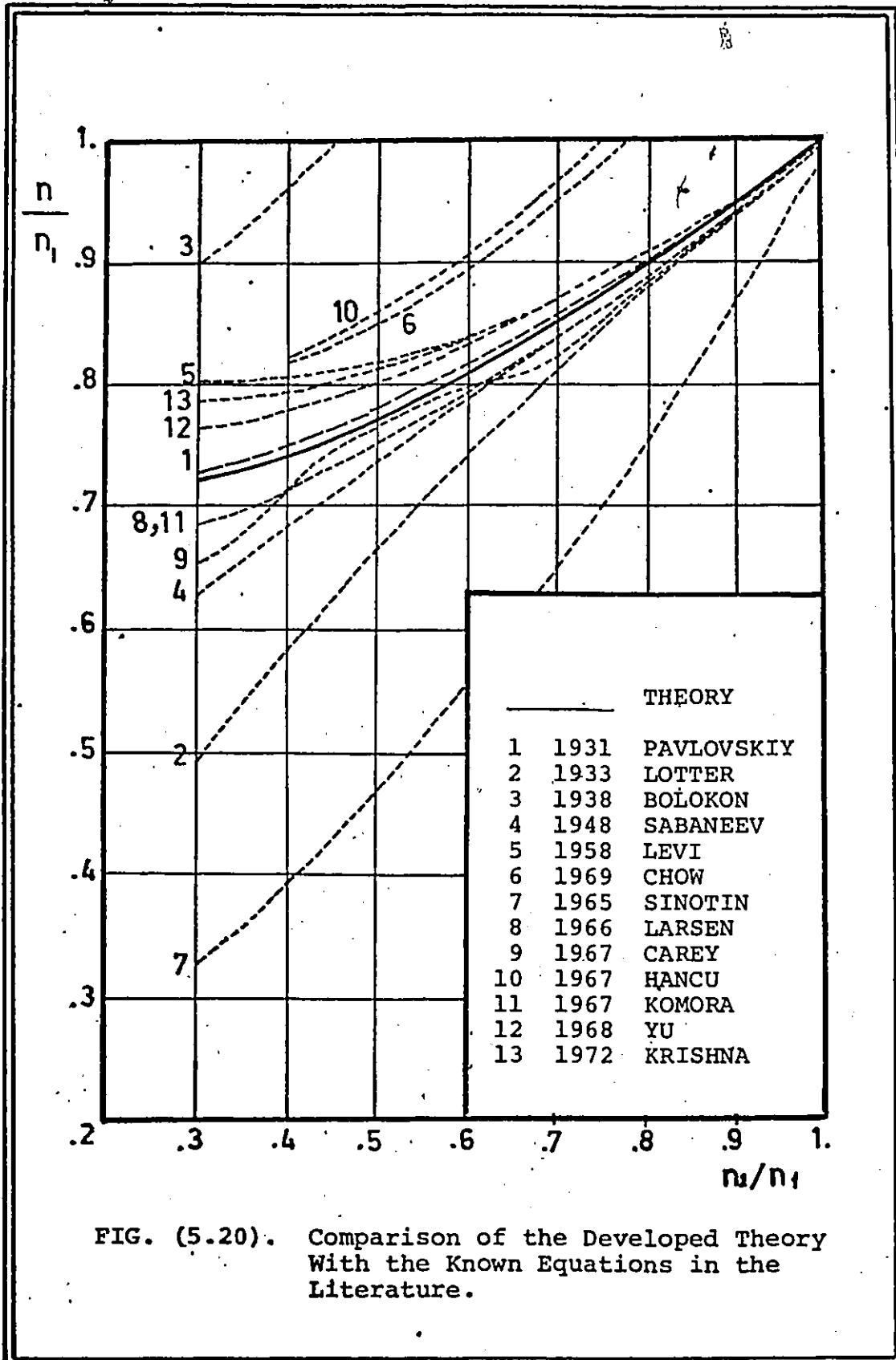


FIG. (5.20). Comparison of the Developed Theory With the Known Equations in the Literature.

geometry parameters. Eqn. (3.43) is, hence, recommended as more suitable for practical use.

5.6 Loose Cover Underside Configuration

The underside configuration of an ice cover is one of the most important factors in the problems of the flow in any ice covered channel, since it affects the cover roughness coefficient, and its stability in addition to the channel geometry parameters.

It was decided to study the hydraulic effects on such a configuration rather than the thermodynamic effects, since nothing was found in the literature with regard to this aspect. Polyethylene plastic pellets were used to simulate this loose ice cover and the arrangement is shown in Fig. (E-5) and the results are given in Appendix E.

A typical underside configuration is shown in Plate (5-1).

5.6.1 The Longitudinal Configuration:

From the figures it is generally noticed that:

1. A uniform regular wave configuration existed.
2. The cover thickness tends to increase as the discharge increased which can be explained by the stability requirements.
3. The wave length increased with the discharge in almost the same ratio. It varies from 2 ft. at 190 cfs to around 5 ft. at a discharge of 500 cfs.

4. The wave amplitude also was found to increase with the discharge but not in the same related way as the length. It ranged from 0.5 in. to 1.5 in. for a discharge of 200 cfs to about 2.5 in. for a flow of 500 cfs.

5. The waves are steeper in the downstream face than the upstream following the bed forms in the general shape.

6. The wave crests almost formed above the gentle, sloping upstream face of the bed waves while the trough always formed above the troughs of the bed waves.

7. No definite relation was found between the underside of the ice cover wave amplitude or length and the bedforms. This can be explained by the fact that only one value of the discharge will form the fixed bedform, and any change in the discharge from this value would result in similar changes in the shapes of both the cover underside and bed formations; only the cover underside could change because of the fixed bed shape.

8. An ice load was noticed to move in a similar way to the sediment load. The ice particles moved only by intermittent leaps and/or by a creeping process. Neither saltation or any kind of suspended load movements were noticed.

5.6.2 The Lateral Configuration:

As shown in Plate (5-2) and Fig. (5.21) the lateral underside configuration has the following features.

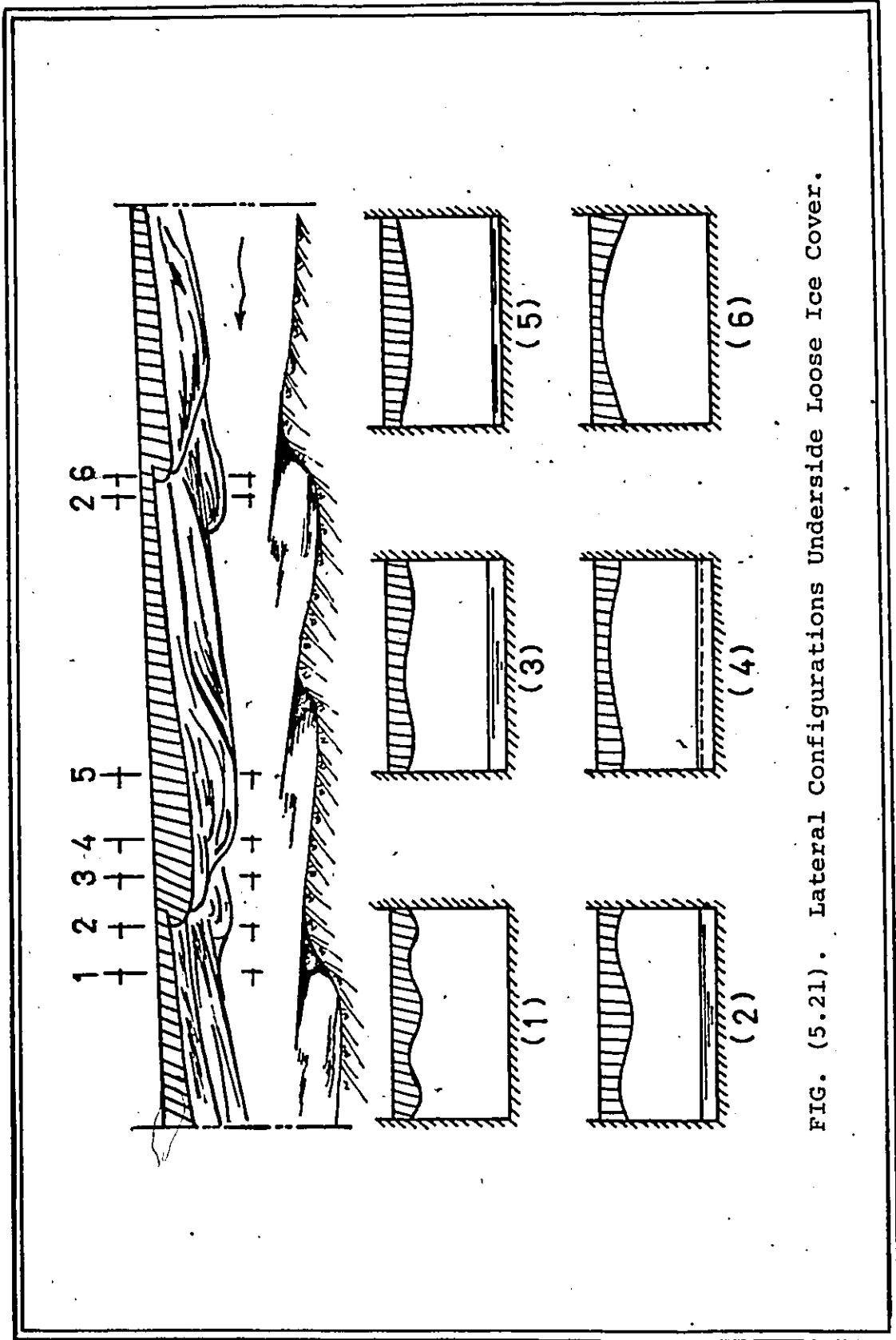


FIG. (5.21). Lateral Configurations Underside Loose Ice Cover.

1. There is a change in phase between the longitudinal configuration between the central and the side sections. The central configuration is leading by about $1/5$ of the wave length. This is due to the high resistance caused by the side boundary roughness.

2. Different cross-sectional shapes of the cover can be seen according to the position at which the cross-section is taken, as shown in Fig. (5.21), Cases (1) to (6). The cover may be thicker at the central part, Case (5), or at the sides, Case (4); it may consist of one wave as is shown by Cases (4) and (5), or more than one wave, such as Cases (1), (2) and (3). The reason for these differences is the change of phase explained before.

3. The central longitudinal configuration is found to be in good agreement with the bed formations for almost all the discharges.

4. Although the bedforms were two dimensional, the cover underside wave formation is three dimensional, in spite of the limited width of the flume.

Further studies are required towards reaching definite quantitative results with regard to the underside configuration of the loose covers.

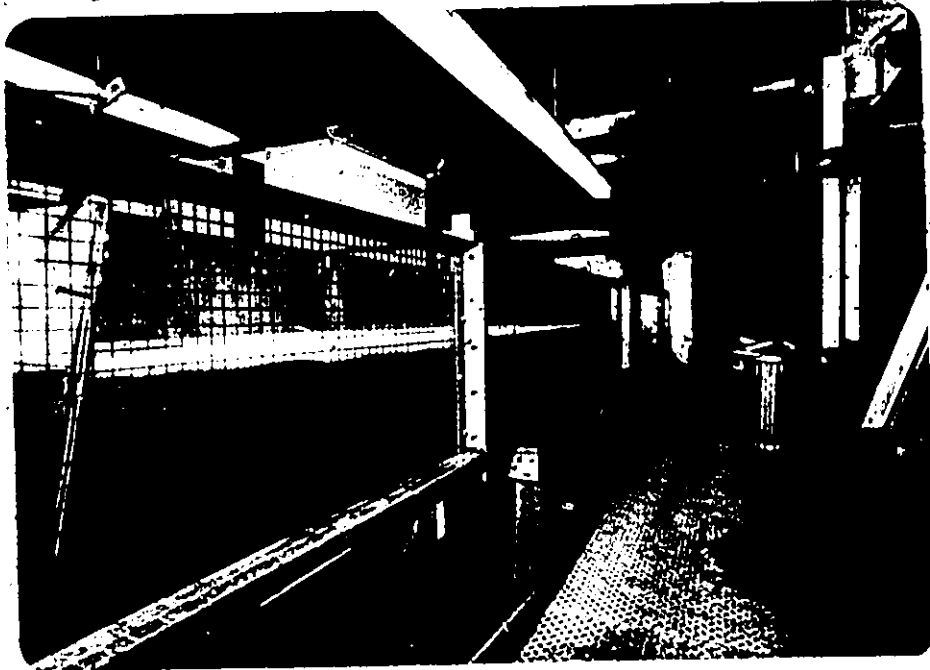


Plate 5.1

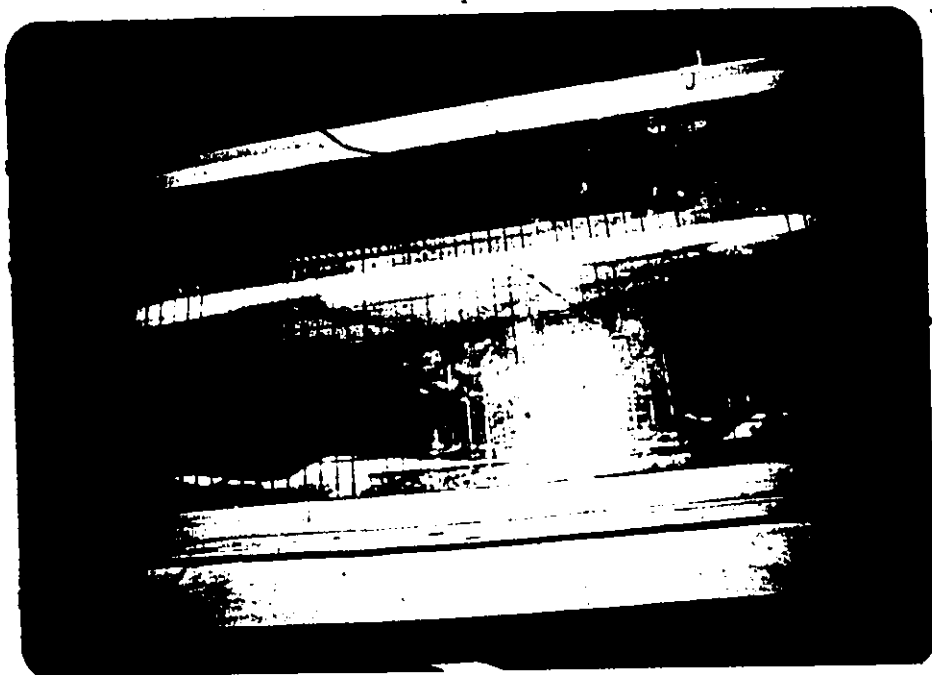


Plate 5.2

CHAPTER 6
DIMENSIONAL ANALYSIS

6.1 Introduction

Besides the theoretical analysis of composite roughness estimation, the dimensional analysis approach is very important to review the problem.

6.2 The Factors Affecting the Problem

In the general case of an ice covered channel, there are definite Manning's roughness coefficients, for the ice cover and the channel boundaries. Other parameters that affect the problem are summarized, with reference to Fig. (6.1), as

A. Geometric:

Flow cross-sectional wetted parameters

ice cover wetted parameter	P_2
channel wetted parameter	P_1
and composite wetted parameter	P

which are geometrically related by

$$P = P_1 + P_2 \quad (6.1)$$

*Flow cross-sectional area:

ice sub-section area	A_2
channel sub-section area	A_1
total cross-sectional area	A

with the geometric relation of

$$A = A_1 + A_2 \quad (6.2)$$

*Flow hydraulic radii:

ice sub-section	R_2
channel sub-section	R_1
and composite hydraulic radius	R

and the hydraulic radius is defined as

$$R = A/P \quad (6.3)$$

*Ice cover average thickness t

B. Kinematic:

*The average velocity of flow in

ice sub-section	V_2
channel sub-section	V_1
and channel mean velocity	V

related to the continuity equation

$$VA = V_1 A_1 + V_2 A_2 \quad (6.4)$$

*Manning's roughness coefficients for

ice cover	n_2
channel boundaries	n_1
and the composite roughness	n

*The acceleration due to gravity or g .

C. Dynamic:

*The average flow resistance shear as

ice cover	τ_2
channel boundaries	τ_1
and the mean shear	τ

*The fluid properties:

fluid density	ρ
fluid dynamic viscosity	μ

The dimensions of each of the above variables are given in the dimensional matrix shown in Table (6.1).

TABLE 6.1. THE DIMENSIONAL MATRIX

	P_1	P	R_1	A_1-A_2	μ	R_2	t	v	n_1	n_2	g	ρ	R	
	K_1	K_2	K_3	K_4	K_5	K_6	K_7	K_8	K_9	K_{10}	K_{11}	K_{12}	K_{13}	K_{14}
M	0	0	0	0	1	0	0	0	0	0	0	0	1	0
L	1	1	1	2	-1	1	1	1	$-\frac{1}{3}$	$-\frac{1}{3}$	$-\frac{1}{3}$	1	-3	1
T	0	0	0	0	1	0	0	-1	1	1	1	-2	0	0

TABLE 6.2. THE MATRIX OF SOLUTION

π TERM	P_1	P	R_1	A_1-A_2	μ	R_2	t	V	n_1	n_2	n	g	p	R
	K_1	K_2	K_3	K_4	K_5	K_6	K_7	K_8	K_9	K_{10}	K_{11}	K_{12}	K_{13}	K_{14}
π_1	1	-1	0	0	0	0	0	0	0	0	0	0	0	0
π_2	-1	2	0	0	0	0	0	0	0	0	0	0	0	-1
π_3	0	0	1	0	0	0	0	0	0	0	0	0	0	-1
π_4	0	-1	0	1	0	0	0	0	0	0	0	0	0	-1
π_5	0	0	0	0	-1	0	0	1	0	0	0	0	1	1
π_6	0	0	-1	0	0	+1	0	0	0	0	0	0	0	0
π_7	0	0	0	0	0	0	1	0	0	0	0	0	0	-1
π_8	0	0	0	0	0	0	0	1	0	0	0	0	0	0
π_9	0	0	0	0	0	0	0	0	-1	0	0	-0.5	0	$-\frac{1}{6}$
π_{10}	0	0	$\frac{2}{3}$	0	0	$-\frac{2}{3}$	0	0	1	-1	0	0	0	0
π_{11}	0	0	0	0	0	0	0	0	1	0	-1	0	0	0

6.3 Dimensional Analysis

A general dimensionless π term is defined as

$$\pi = P_1^{K_1} \cdot P_2^{K_2} \cdot R_1^{K_3} \cdot (A_1 - A_2)^{K_4} \cdot \mu^{K_5} \cdot R_2^{K_6} \cdot t^{K_7} \cdot V^{K_8} \cdot n_1^{K_9} \cdot n_2^{K_{10}} \cdot n^{K_{11}} \cdot g^{K_{12}} \cdot \rho^{K_{13}} \cdot R^{K_{14}} \quad (6.5)$$

in which the quantities R , g , ρ are chosen as the three repeating variables. A complete set of dimensionless products is given in the matrix of solution Table (6.2)

The π terms are as follows:

- π_1 : $\pi_1 = P_1/P$, or wetted perimeter ratio α
- π_2 : $\pi_2 = P^2/PR_1$
- π_3 : $\pi_3 = R_1/R$, hydraulic radius ratio
- π_4 : $\pi_4 = (A_1 - A_2)/A_1$ excess area ratio
- π_5 : $\pi_5 = \pi VR/\mu$, Reynolds number R_n
- π_6 : $\pi_6 = R_2/R_1$, subsections hydraulic radius ratio λ
- π_7 : $\pi_7 = t/R$, cover thickness ratio
- π_8 : $\pi_8 = V/\sqrt{gR}$, Froude number F_n
- π_9 : $\pi_9 = R^{1/6}/n_1\sqrt{g}$
- π_{10} : $\pi_{10} = (n_1/n_2) \lambda^{2/3}$
- π_{11} : $\pi_{11} = n_1/n$

Channel roughness is not a function of the Froude number and becomes independent of the Reynolds number when the latter exceeds a critical value. Under these conditions the Froude and Reynolds numbers can be

omitted from the dimensional analysis which is the case considered here. π_2 can also be excluded as it is a geometric property that can be derived through π_1 , π_3 and π_4 .

6.4 General Solution

The general solution is carried out in two steps, namely the solution for λ , then the solution for the composite roughness.

6.4.1 Solution for :

The general solution is

$$\phi\left(\alpha_1 \frac{R_1}{R} \lambda_1 \frac{R_1^{1/6}}{n_1 \sqrt{g}}, \frac{A_1 - A_2}{A}, \frac{n_1}{n_2} \lambda^{2/3}\right) = 0 \quad (6.6)$$

From the geometric relations,

$$\frac{R_1}{R} = \alpha + (1-\alpha)\lambda$$

So the π terms $\alpha_1 \frac{R_1}{R} \lambda_1 \frac{R_1^{1/6}}{n_1 \sqrt{g}}, \frac{A_1 - A_2}{A}$ can be considered as one term, namely,

$$\pi^1 = \frac{R_1^{1/6}}{n_1 \sqrt{g}} / (\alpha + (1-\alpha)\lambda)^{1/6} \quad (6.7)$$

In the limiting case when n_1 equals n_2 and P_1 equals P_2 , λ equals unity and to obtain consistency with this condition the π_E term is used relative to this limiting value and given by the relationship,

$$\pi_E = |\pi - \pi_L| \quad (6.8)$$

can be applied to make

$$\pi_{6E} = \sqrt{\lambda} - 1$$

and

$$\pi_{10E} = 1 - \frac{n_1}{n_2} \lambda^{2/3}$$

Substituting into Eqn. (6.6) yields,

$$\phi\left(\frac{\left(\frac{R}{\alpha + (1-\alpha)\lambda}\right)^{1/6}}{n_1 \sqrt{g}}, (\sqrt{\lambda} - 1), \left(1 - \frac{n_1}{n_2} \lambda^{2/3}\right)\right) = 0 \quad (6.9)$$

The relation given in Eqn. (6.9) can be used in the general form,

$$\frac{\left(\frac{R}{\alpha + (1-\alpha)\lambda}\right)^{1/6}}{n_1 \sqrt{g}} = C_1 (\sqrt{\lambda} - 1)^a \left(1 - \frac{n_1}{n_2} \lambda^{2/3}\right)^b \quad (6.10)$$

which is the same relation developed theoretically in Chapter 3, namely Eqn. (3.39). The theoretical development results in the values of

$$C_1 = \frac{0.444}{\kappa}$$

$$a = + 1.0$$

$$b = - 1.0$$

where κ is von Karmen's constant.

The experimental data was used to check the forementioned relations as will be shown later.

6.4.2 Solution for Composite Roughness:

The general solution is

$$\phi\left(\alpha, \frac{R_1}{R}, \frac{A_1 - A_2}{A}, \lambda, \frac{R_1^{1/6}}{n_1 \sqrt{g}}, \frac{n_1}{n_2} \lambda^{2/3}, \frac{n_1}{n}\right) = 0 \quad (6.11)$$

Applying the development used in (6.4.1) a general excess term of,

$$\bar{\pi} = \left(1 - \frac{\alpha - (1-\alpha)\lambda}{\alpha + (1-\alpha)\lambda} \cdot \frac{1 + \sqrt{\lambda}}{1 - \sqrt{\lambda}} \cdot \frac{1 - \frac{n_1}{n_2} \lambda^{2/3}}{1 + \frac{n_1}{n_2} \lambda^{2/3}}\right) \left(1 + \frac{n_1}{n_2} \lambda^{2/3}\right)$$

can be used to replace $\alpha, \frac{A_1 - A_2}{A}, \lambda, \frac{R_1}{n_1 \sqrt{g}}$ terms.

Also substituting the R_1/R value as

$$\frac{R_1}{R} = \alpha + (1-\alpha)\lambda$$

Putting these relations into Eqn. (6.11) results in the function

$$\phi'(\bar{\pi}, (\alpha + (1-\alpha)\lambda), \frac{n_1}{n}) = 0 \quad (6.12)$$

or in the general form

$$\frac{n_1}{n} = C_2 (\alpha + (1-\alpha)\lambda)^A \bar{\pi}^{-B}$$

ie.

$$\frac{n_1}{n} = C_2 (\alpha + (1-\alpha)\lambda)^A \left(1 + \frac{n_1}{n_2} \lambda^{2/3}\right)^B \left(1 - \frac{\alpha - (1-\alpha)\lambda}{\alpha + (1-\alpha)\lambda}\right)$$

$$\times \frac{1 + \sqrt{\lambda}}{1 - \sqrt{\lambda}} \cdot \frac{1 - \frac{n_1}{n_2} \lambda^{2/3}}{1 + \frac{n_1}{n_2} \lambda^{2/3}} \quad (6.13)$$

Eqn. (6.13) is identical to the theoretical equation, Eqn. (3.43), with the constants having the values,

$$C_2 = 0.5$$

$$A = -2/3$$

$$B = 1.0$$

A regression procedure was applied to this relation using the experimental data.

6.5 Experimental Data Fitting

The experimental data have been fitted to the previously developed dimensionless equations to yield:

(i) For the solution of λ : the values of the exponents in the equation was found by multiregression analysis to be

$$a = 1. , b = 00.85 , \text{ and}$$

$$\text{Constant} = C_1 = 1.0$$

which compares favourably to the theoretical values of 1.0, -1.0 and 1.11.

(ii) For the composite roughness solution, another multiregression analysis was applied to the dimensionless terms of Eqn. (6.28) to give the values of

$$A = -0.54 , B = 2.0 , \text{ and the}$$

$$\text{Constant } C_2 = 0.8$$

In comparison to the theoretical values of -0.66, 1.0, and 0.5 respectively, it showed good agreement. The reason for the deviation is mainly due to the high experimental errors in computing the composite roughness n.

CHAPTER 7
CONCLUSIONS

From the forementioned studies and discussion the following conclusions can be drawn.

1. A velocity distribution for flow in an ice covered channel can be represented by the equation

$$u_i(\epsilon) = V_{\max} + \frac{V_{*i}}{\kappa} F_1(\epsilon_i) = V_i - \frac{2V_{*i}}{\kappa} F_2(\epsilon_i) \quad (3.20,23)$$

2. A relation for the separation line was developed from the solution of the equation,

$$\frac{R^{1/6}}{n_1 \sqrt{g}} = \frac{0.444}{\kappa} \frac{\sqrt{\lambda} - 1}{1 - \frac{n_1}{n_2} \lambda^{2/3}} (\alpha + (1-\alpha)\lambda)^{1/6} \quad (3.39)$$

for which λ is considered the independent variable.

3. The composite Manning's roughness coefficient n can be determined by the relation,

$$\frac{n_1}{n} = \frac{1}{\alpha + (1-\alpha)\lambda} \left(1 + \frac{n_1}{n_2} \lambda^{2/3} \right) \left(1 + \frac{\sqrt{\lambda} + 1}{\sqrt{\lambda} - 1} \right)$$

$$\frac{\alpha - (1-\alpha)\lambda}{\alpha + (1-\alpha)\lambda} \left(\frac{1 - \frac{n_1}{n_2} \lambda^{2/3}}{1 + \frac{n_1}{n_2} \lambda^{2/3}} \right) \quad (3.43)$$

4. Dimensionless curves have been introduced to help in the solution of the forementioned relations.

5. The developed equations showed good agreement with both experimental and field data.

6. For short covers, that is, where the L/T ratio is less than 500, it is recommended to introduce correction factors, to take into account the disturbance at the entrance to the upstream end of the cover.

7. The study of the loose ice cover underside configurations showed a tendency to form ripple or dune type of ice waves which depended on the bedform and the flow conditions. Further work is needed to, quantitatively, study this configuration.

APPENDIX A

GRAPHICAL SOLUTION OF
THE COMPOSITE ROUGHNESS PROBLEM

In this appendix, the graphical solution of Eqns. (3.39) and (3.43) is given. The solution is given by three groups of curves, namely:

Group 1:

Given in Fig. (A-1), consists of three families of curves:

1. R - ϕ curves for different n_1 values where R is the channel hydraulic radius, and ϕ is given by

$$\phi = R^{1/6} / n_1 \sqrt{g} \quad (\text{A.1})$$

2. $n_{\text{ratio}}-n_1$ curves for different n values where the n_{ratio} is n_1/n and n_1 and n are Manning's roughness coefficients for the channel, and the composite section respectively.

3. R - M curves for different n values where M is the Manning index value and given by

$$M = \frac{1.49}{n} R^{2/3} \quad (\text{A.2})$$

Group 2:

Shown in Figs. (A.2) to (A.5) each figure for different α values ranging from 0.5, which is the case of wide channel, to 0.65, which is representative of a deep channel.

In each figure, two families of curves are given:

1. ϕ - λ curves for different n_1/n_2 values, marked by a solid line, where λ is given as

$$\lambda = R_2/R_1 \quad (A.3)$$

2. $\lambda - \frac{n_1}{n_2}$ curves for different n_1/n_2 values.

The intermediate values of α or n_1/n_2 , can be obtained by interpolation.

Group 3:

Fig. (A.6) gives a family of curves between the discharge ratio and n_1/n for different α values. The discharge ratio is given as

$$\text{discharge ratio} = Q/Q_0$$

where Q is the discharge with an ice cover, Q_0 is the discharge without an ice cover for the same cross-section at fixed flow depth.

The use of the curves is illustrated in Appendices B and C.

It is noticed from the curves that α has no practical effect in estimating the value of λ . It affects the composite roughness but in a practically negligible manner for value of n_1/n_2 less than 0.6.

On the other hand, α affects the discharge more than λ or the discharge ratio.

The accuracy of the curves is up to $\pm 5\%$ depending upon the user. For more accurate results, numerical solutions should be applied

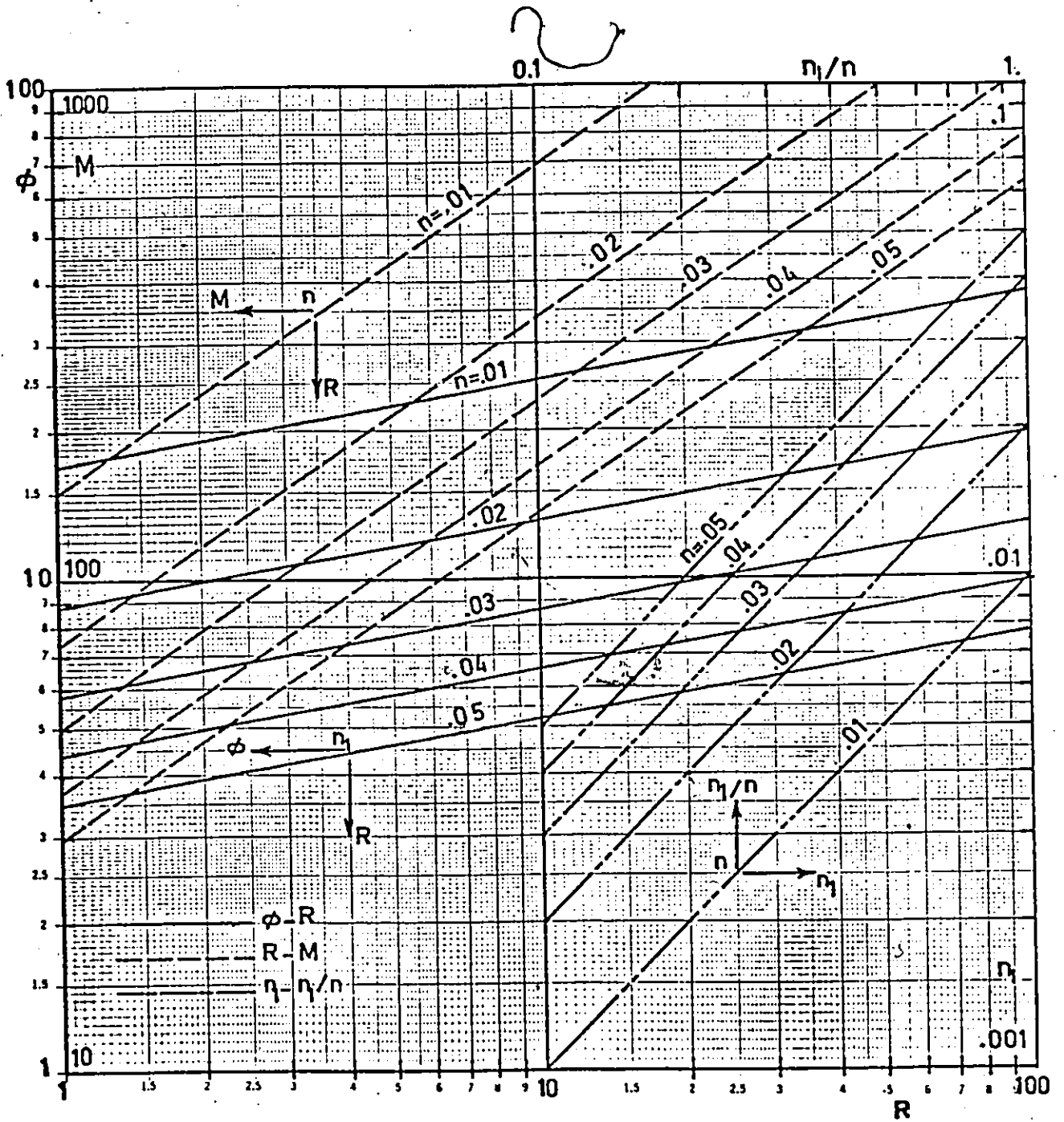


Fig. (A-1)

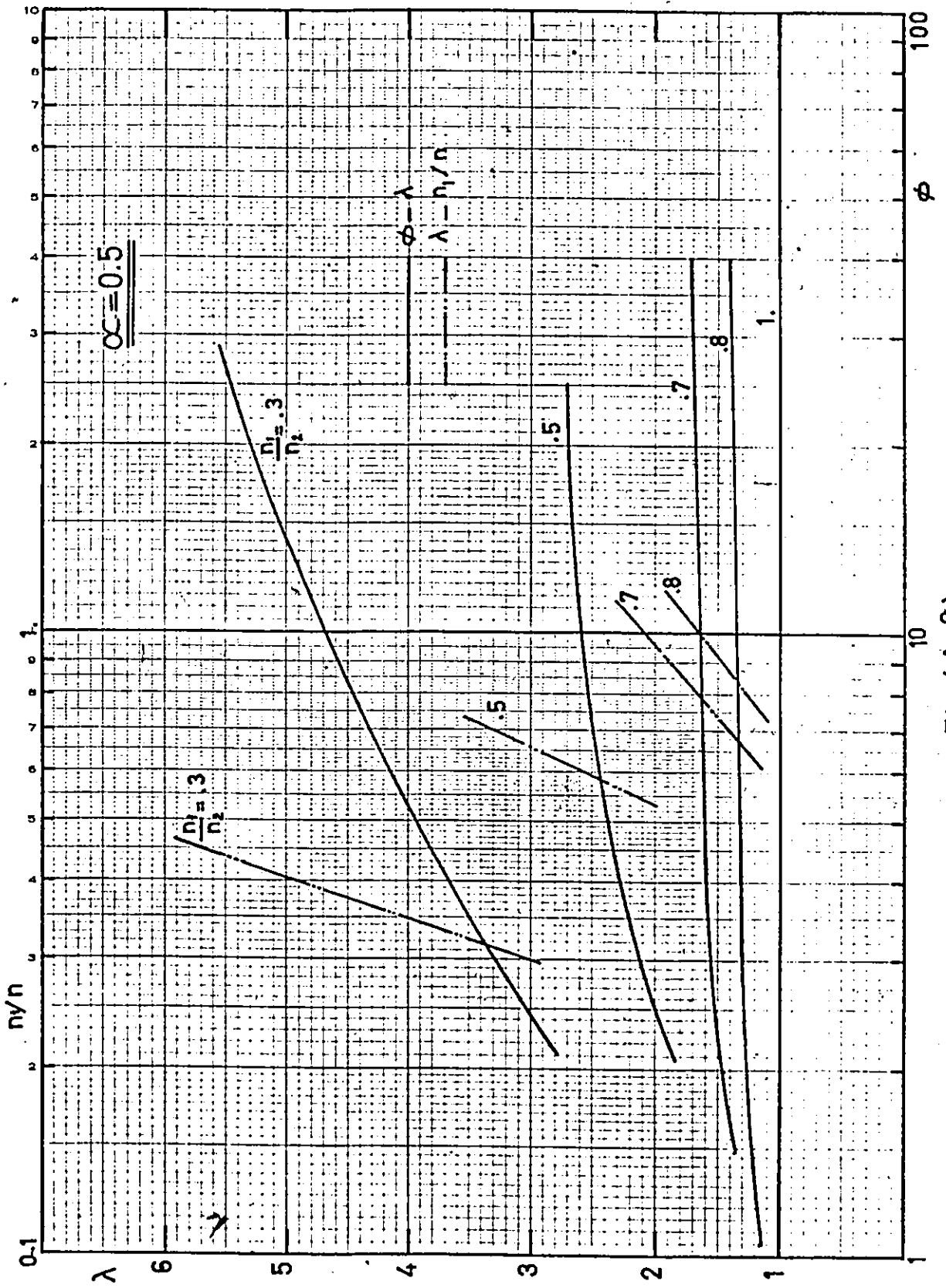


Fig. (A-2)

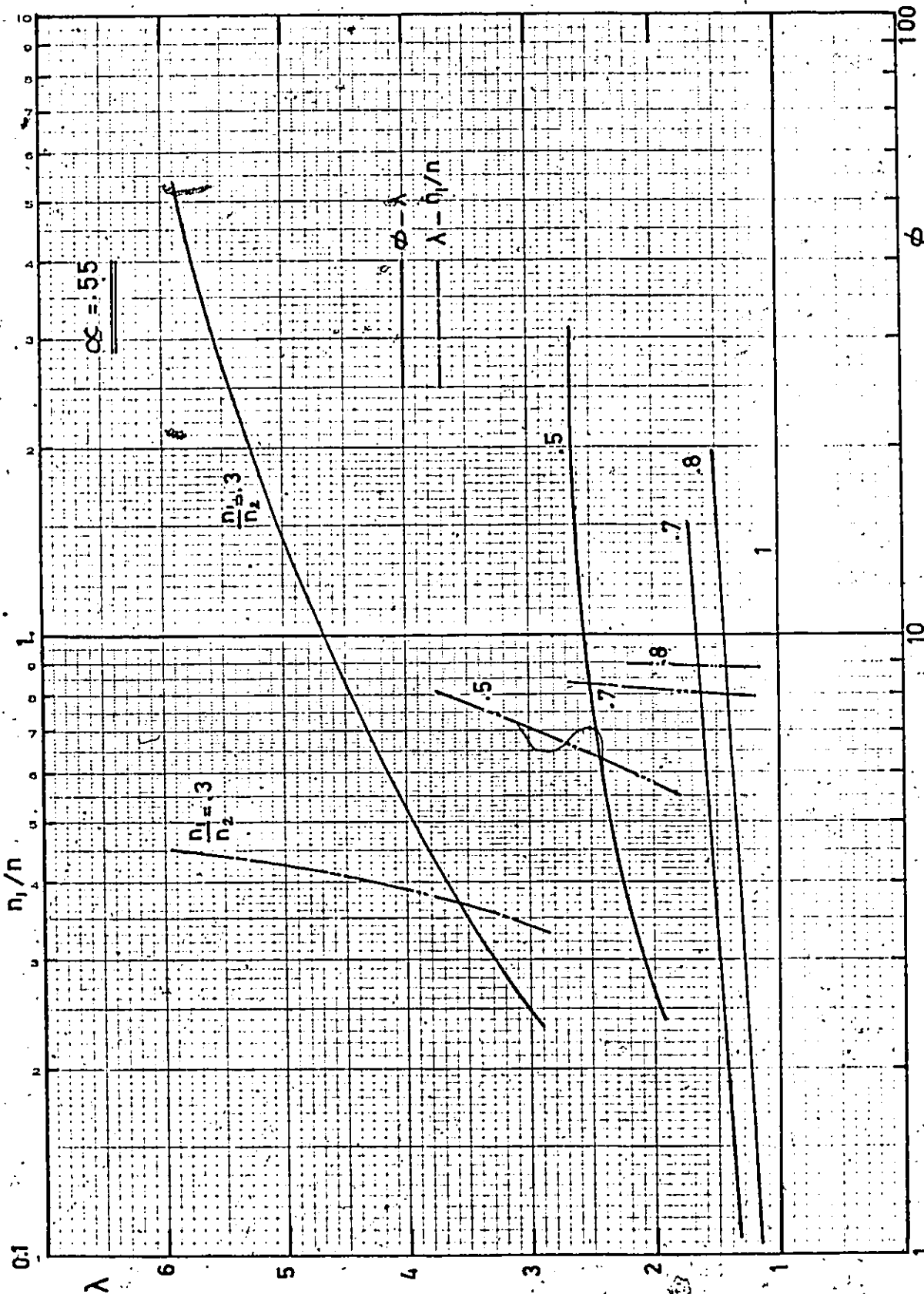


Fig. (A-3)

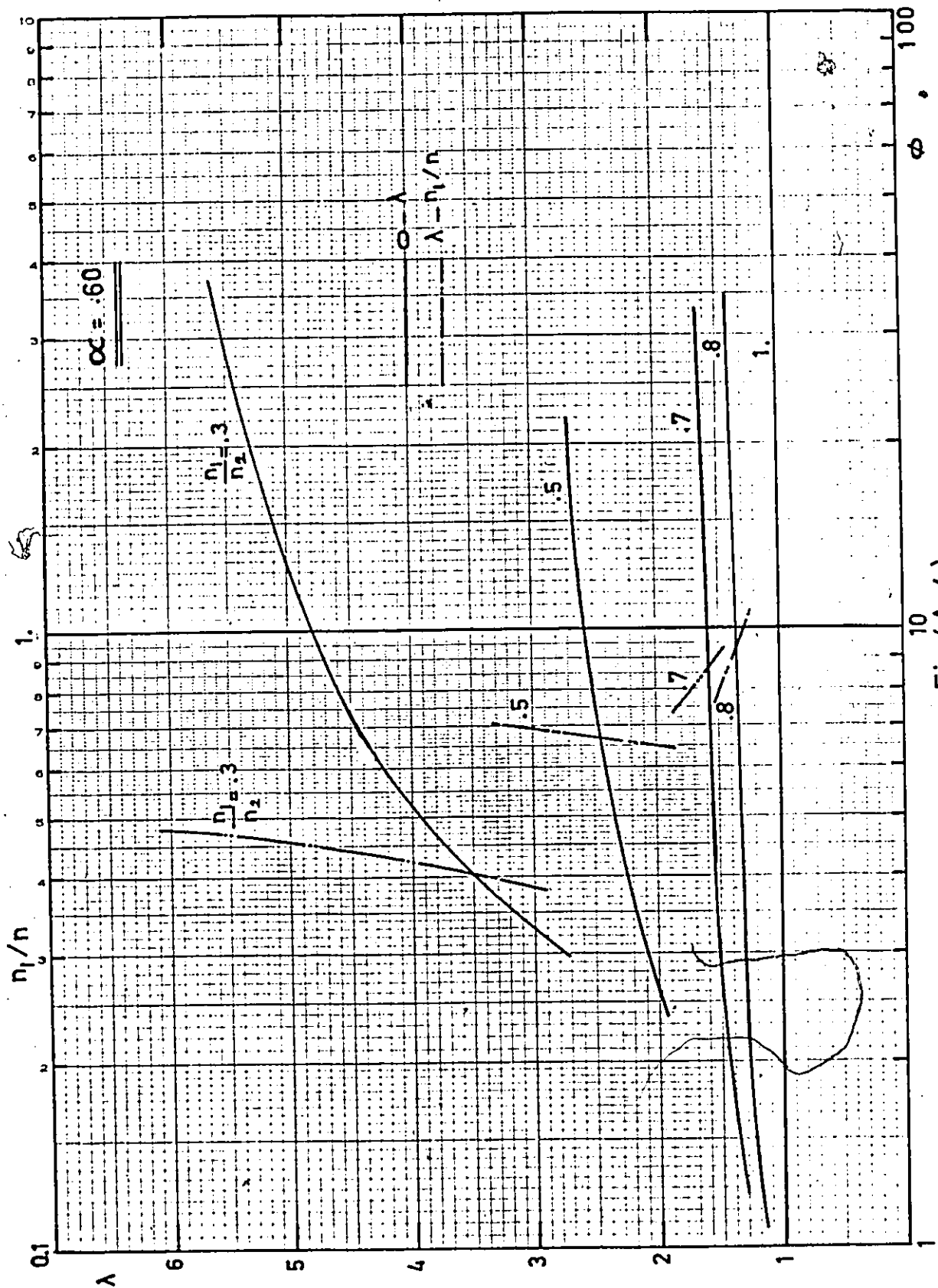


Fig.(A-4)

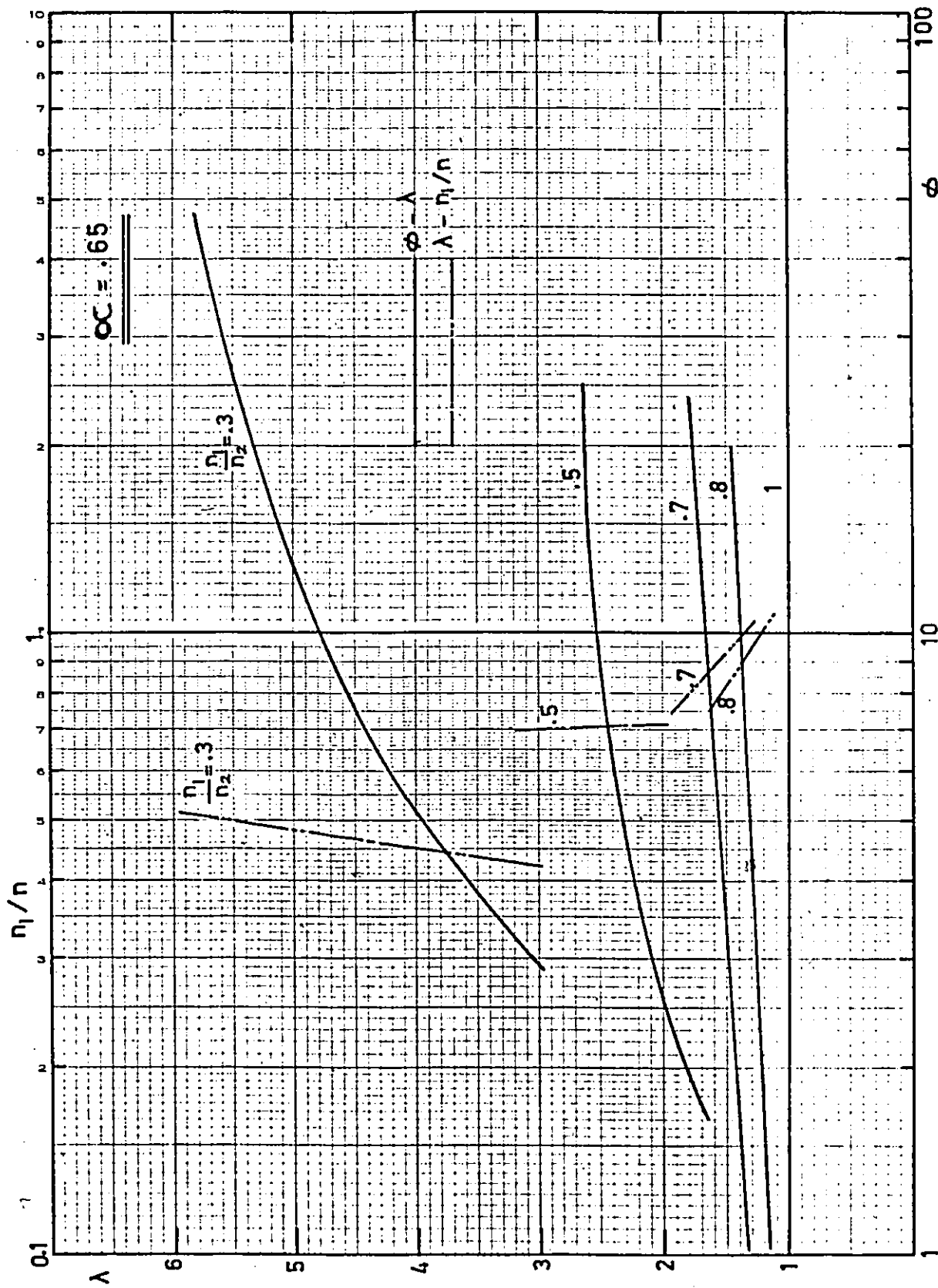


Fig. (A-5)

100-100000-1000

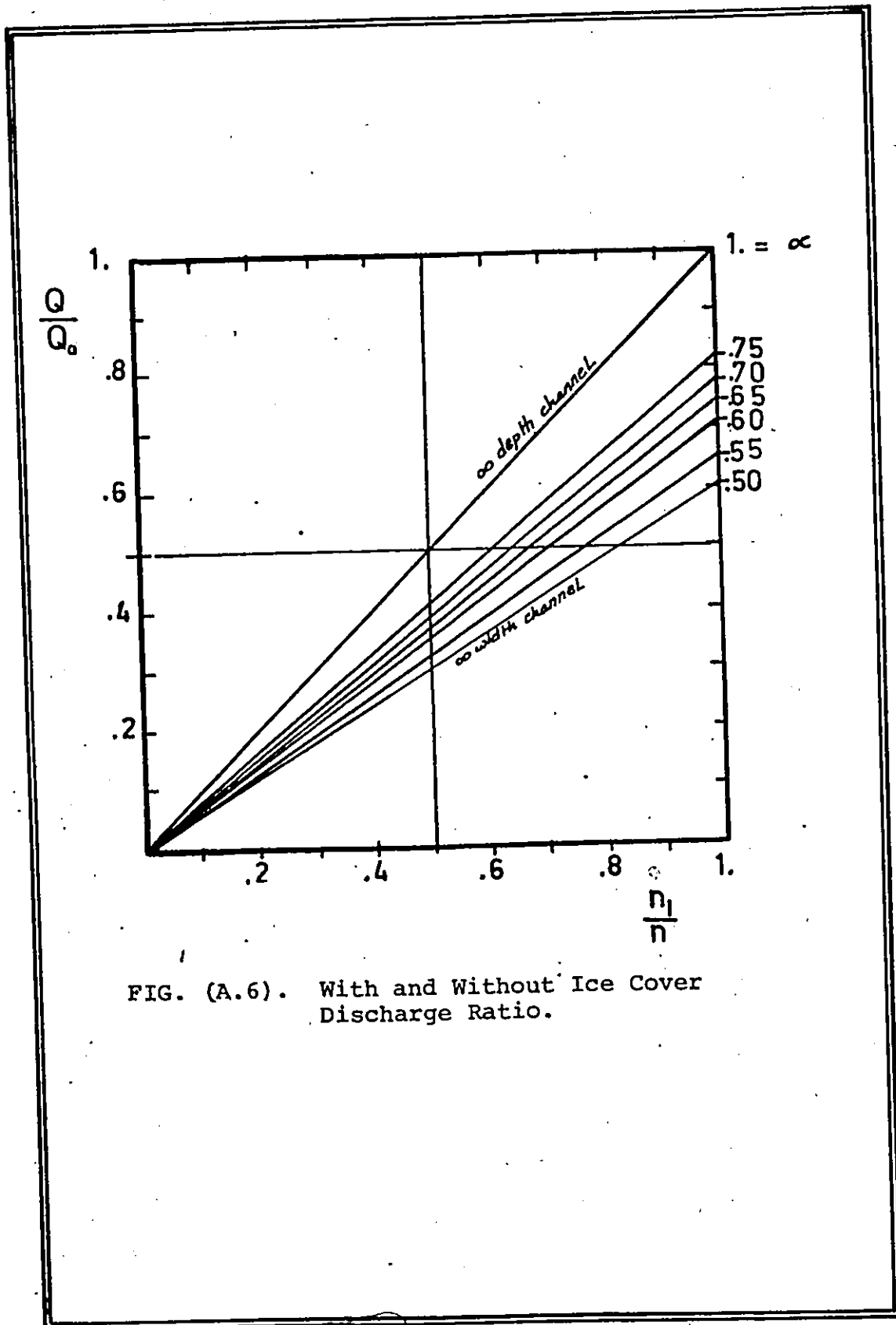


FIG. (A.6). With and Without Ice Cover Discharge Ratio.

APPENDIX B
COMPUTATION OF RATING CURVES
NUMERICAL EXAMPLE

In this appendix, a numerical example is given to illustrate the use of the proposed curves to estimate the composite roughness and hence the discharge.

Given: An ice covered channel having a trapezoidal cross-section of the dimensions shown in Fig. (B.1). The following information is available.

Manning's roughness coefficients $n_1 = 0.2$, $n_2 = 0.03$ and bed slope $S = 1.2 \times 10^{-5}$.

Required: Estimation of the rating curve with and without ice cover.

Solution: For this example, the detailed calculations at a flow depth of 10' is used.

*Channel data

$$P_1 = b + 4.47Y = 74.70 \text{ ft.}$$

$$P_2 = b + 4Y = 70.00 \text{ ft.}$$

$$P = P_1 + P_2 = 144.70 \text{ ft.}$$

$$A = Y(b+2Y) = 500.00 \text{ ft.}$$

$$R = A/P = 3.46 \text{ ft.}$$

$$\alpha = P_1/P = 0.52$$

$$n_{\text{ratio}} = n_1/n_2 = 0.66$$

*Curves solution

1. Fig. (A-1), for $n_1 = 0.02$, $R = 3.46$

$$\phi = 10.84$$

2. Fig. (A-2), for $\alpha = 0.5$ (approximate),
 $n_1/n_2 = 0.66$

$$\lambda = 1.77, \frac{n_1}{n} = 0.74$$

3. Fig. (A-1), $n = 0.026$, $M = 131$

4. The composite discharge Q

$$Q = M \times S^{\frac{1}{2}} \times A = 226.9 \text{ cfs}$$

5. Without ice cover, the discharge

$$Q = \frac{1.49}{0.02} R^{2/3} S^{\frac{1}{2}} A = 458.25 \text{ cfs}$$

where $R = A/P_1 = 6.69$.

*Rating curves

Following the same procedure, the discharge is computed for different depths of flow. The results are given in Table (B.1), and the rating curves, discharge-depth relationship is given in Fig. (B.2).

Flow Depth	Discharges	
	With Cover	Without Cover
0.0	0	0
2.5	27	59
5.00	62	126
7.50	129	270
10.00	227	458
12.50	360	740
15.00	529	1025

The same resulting curves can be obtained by using Fig. (A.6) which gives directly for n_1/n values the corresponding ratio of the discharge with ice cover to the discharge without any cover. The use of the curves in Fig. (A.6) is recommended as it is easier to use and theoretically gives the same result.

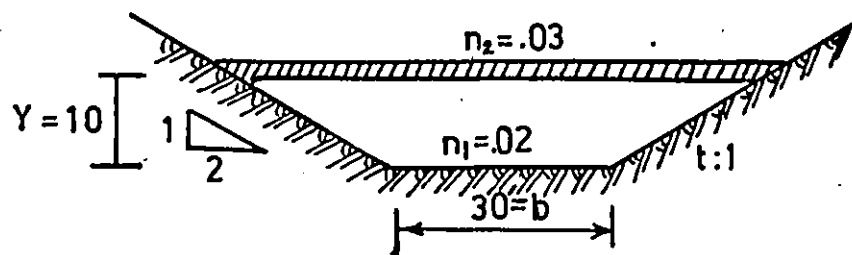


FIG. (B.1). Channel Cross-section.

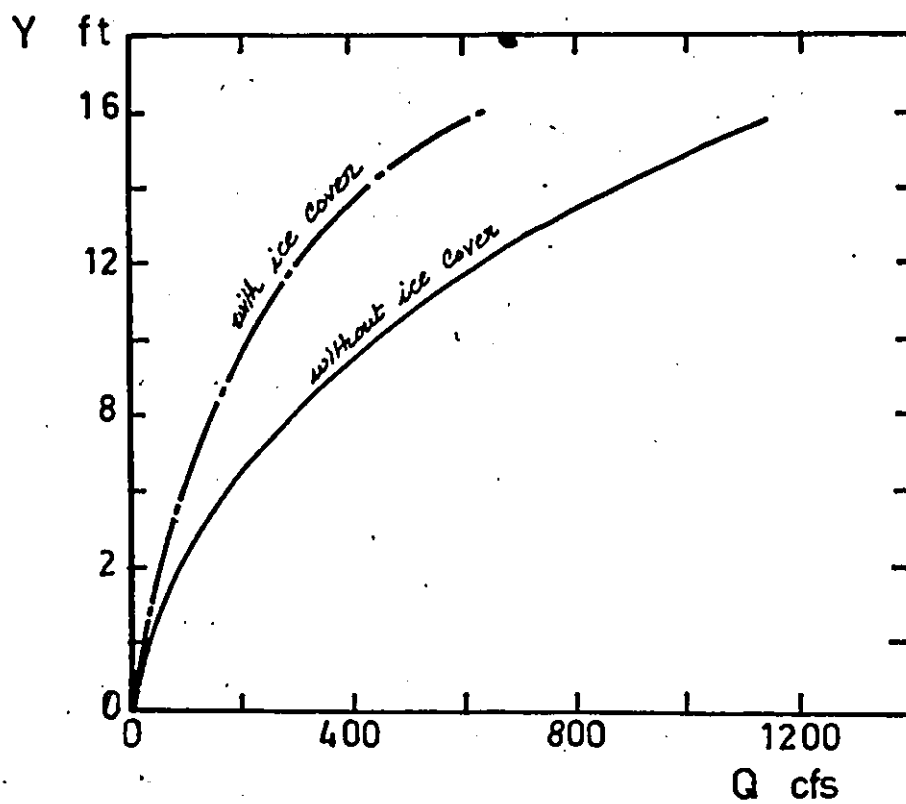
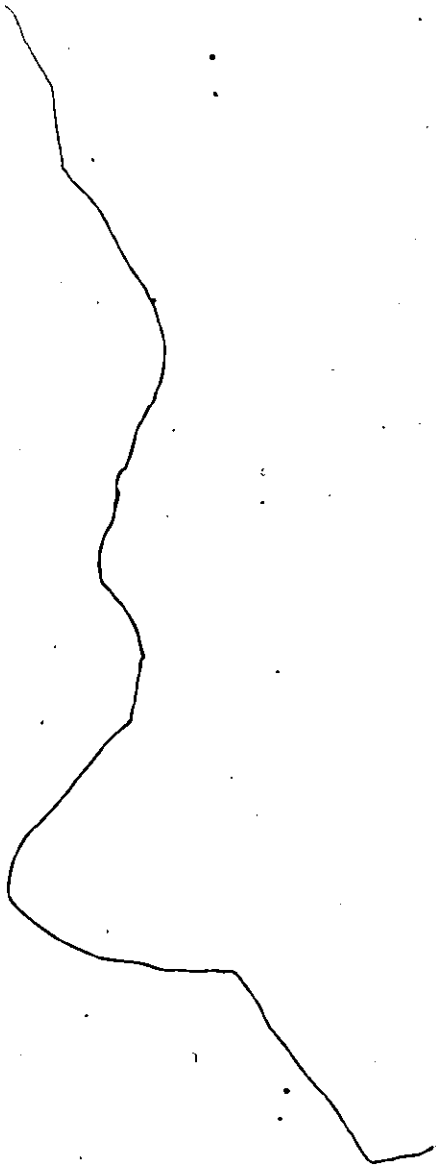


FIG. (B.2). Rating Curves.

APPENDIX C
DESIGN OF ICE COVERED
CHANNELS
NUMERICAL EXAMPLE



In this appendix a numerical example is illustrated to explain the use of the developed equations, along with the graphical solution shown in Appendix A in the design of ice covered channels.

Given: A trapezoidal channel with the following data is known:

*cover has a 5 inch thickness

*cover underside Manning's roughness is expected to equal 0.03, while the channel one is 0.02

*bed slope 1.2×10^{-5}

*channel is designed to carry a discharge of 250 cfs

*side slopes not to exceed 2:1

Required: Design the channel and check its capacity without the ice cover.

Solution:

(A) Design of channel

1. Applying Ernest's equation to estimate the approximate velocity for a stable cover

$$V = \sqrt{\frac{1}{2} g \frac{\rho - \bar{\rho}}{\rho} t} \quad (C.1)$$

putting the ice specific gravity of 0.92 gives

$$V = 0.7, \text{ fps}$$

2. M value

$$M = \frac{1.49}{n} R^{2/3} = \frac{V}{S^{1/2}} = 200$$

3. Estimation of n

.Assume $n = 0.025$

.Fig. (A.1) yields $R = 6$, $\phi = 10$

.Assume $\alpha = 0.50$

.Fig. (A.2) yields $\lambda = 1.9$, $\frac{n_1}{n} = 0.73$

.Fig. (A.1) gives $n = 0.0275$, $M = 179$

.n is not equal to the assumed one, repeat the trial with the average value

.After successive iterations,

$$R = 0.34, \phi = 10.7, \lambda = 1.8,$$

$$n = 0.026, M = 130$$

4. The continuity equation

$$Q = A \times V = A \times M S^{1/2} \quad (C.2)$$

gives with Fig. (C.1)

$$A = Y(b + 2Y) = 510 \text{ ft}^2$$

And the geometric relation

$$P = 2b + 8.47Y = \frac{A}{R} = 150. \text{ ft.}$$

5. Solving,

$$b = 35' \quad Y = 9.35'$$

6. Check $\alpha = 0.51$ so that the assumption of $\alpha = 0.55$ is valid.

7. The channel designed cross-section is given in Fig. (C.2).

(B) Check Discharge Under Free Water Conditions

1. Under the maximum depth of flow namely 9.35' the discharge in the channel with an ice cover was 230 cfs.

2. For $\alpha = 0.51$, from Fig. (A.6) for n_1/n value of 0.77 the discharge ratio is 0.48.

3. The discharge without ice cover is Q_0

where

$$Q_0 = Q / (Q/Q_0) \quad (C.3)$$

or

$$Q_0 = 480 \text{ cfs}$$

which is the required discharge.

$$\begin{aligned}
 P_1 &= 2y\sqrt{P_1} + b \\
 P_2 &= D + 2ty \\
 P &= P_1 + P_2 \\
 A &= (b + ty) y \\
 R &= A/P
 \end{aligned}$$

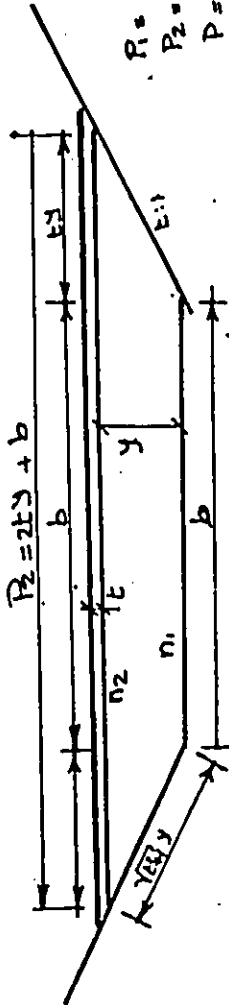


FIG. (C.1). Definition Sketch

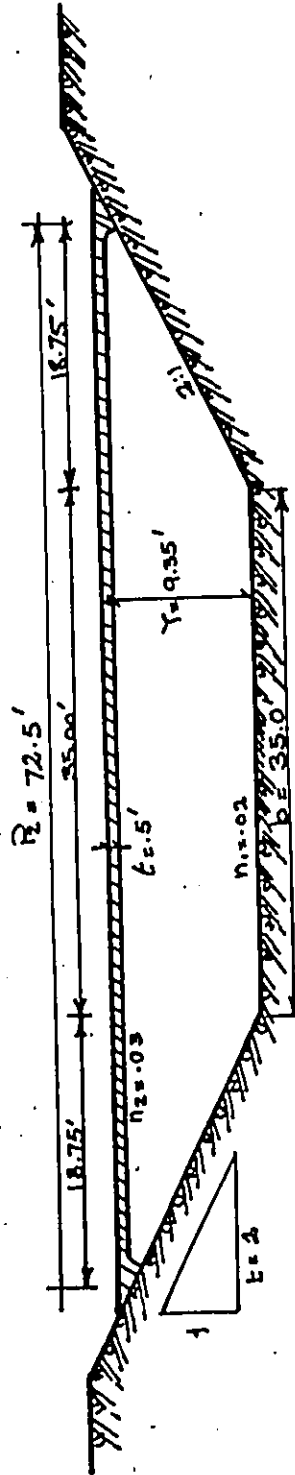


FIG. (C.2). Dimensions of the Design. Cross-Section.

APPENDIX D
EXPERIMENTAL ERRORS

EXPERIMENTAL ERRORS

The sources of the experimental errors in performing the laboratory tests in this study can be summarized as follows:

1. The errors in measuring the upstream and downstream depths of flow:

- a. Variation of the floor ± 0.090 inch.
- b. Upstream reference reading ± 0.040 inch.
- c. Downstream reference reading ± 0.040 inch.
- d. Electric point gauge reading ± 0.010 inch.
- e. The water-surface fluctuations:
 - Upstream ± 0.12 inch
 - Downstream ± 0.08 inch
- f. Distance between upstream and downstream positions ± 0.10 inch.

2. The errors that might occur in the velocity measurements by the pitot-tube:

- a. A common instrument precision of $\pm 1\%$ was assumed.
- b. Manometer reading of ± 0.05 inch which caused a possible error in the observed velocity of about $\pm 1.2\%$ at low velocities and $\pm 1.0\%$ at high velocities.
- c. Vertical distance, measured by the attached point gauge of ± 0.060 inch.

3. The shear measurements are subject to an error of $\pm 5\%$ in measuring the balance angle due to the common errors of reading, and the errors due to the fluctuations in the shear value caused by the unsteadiness in the flow was $\pm 10\%$.

Composite Error:

Applying the general equation of the theory of errors

$$(\delta Q)^2 = \left(\frac{\partial Q}{\partial x_1}\right)^2 \overline{x_1^2} + \left(\frac{\partial Q}{\partial x_2}\right)^2 \overline{x_2^2} + \dots$$

where

$$Q = Q(x_1, x_2, \dots)$$

and Q is a defined relation leads to the combined expected experimental error in estimating the combined roughness by

$$E_n/n = \left(\frac{E_V}{V}\right)^2 + \frac{4}{9}\left(\frac{E_R}{R}\right)^2 + \frac{1}{4}\left(\frac{E_S}{S}\right)^2$$

where

E_V/V = relative error in V .

E_R/R = relative error in R .

E_S/S = relative error in S .

and are given by

$$E_V/V = \pm 2.0\%$$

$$E_R/R = 2R (E_Y/Y)^2$$

$$E_S/S = (E_Y/L) \sqrt{2 + S^2} \quad (E_Y/L) \times \sqrt{2} \quad \text{as } S \text{ is}$$

very small compared to the value of 2.

And, E_y is the error in the water depth measurement, assumed constant in both upstream and downstream ends.

The value of the experimental error in the composite roughness differs from one run to another, a fact that should be taken into consideration.

An average error in estimating the composite Manning's roughness coefficient was found to be $\pm 33\%$.

APPENDIX E
EXPERIMENTAL RESULTS

In this appendix the experimental results of all the runs mentioned in Chapter (4) are given.

TABLE E-1

EVALUATION OF CHANNEL MANNING'S ROUGHNESS n_1

Run No.	Q	Y	S	n_1
E1-1	2.14	1.113	2×10^{-4}	0.01
E1-2	1.84	1.063	3	0.0112
E1-3	1.30	0.965	2.5	0.0146
E1-4	2.56	1.340	2.5	0.0115
E1-5	1.82	1.220	1.7	0.0115
E1-6	1.37	1.440	1	0.0120

Average $n_1 = 0.01167$

TABLE E-2

EVALUATION OF COVER MANNING'S ROUGHNESS n_2

Run No.	Q	Y	S	n_2
E2-1	2.14	1.04	4×10^{-3}	0.034
E2-2	1.72	0.97	3	0.035
E2-3	1.20	0.88	3	0.039
E2-4	0.92	0.80	1.9	0.038

Average $n_2 = 0.03589$

Q in cfs

Y in ft

TABLE E-3

EFFECT OF COVER FRONT ON VELOCITY PROFILES

Run No.	Cover	Cover Thick	x	Q	Y
E3-1	Out	-	-1.5	2.5	1.49
E3-2	In	2"	1.5	2.5	1.39
E3-3	In	2"	3.0	2.5	1.39
E3-4	In	2"	4.5	2.5	1.39
E3-5	In	2"	6.0	2.5	1.39
E3-6	In	2"	7.5	2.5	1.39

TABLE E-4

EFFECT OF COVER FRONT ON SHEAR DISTRIBUTION

Run No.	1	2	3	4
Q	2.61	2.28	1.88	1.61
Y	1.33	1.353	1.287	1.237
R_n	1.857×10^5	1.63×10^5	1.413×10^5	1.143×10^5
x	Total shear values			
1.5	0.379	0.21	0.12	0.104
3.	0.418	0.262	0.15	0.14
4.5	0.451	0.232	0.155	0.171
6	0.474	0.34	0.182	0.20
7.5	0.531	0.45	0.218	0.165
9	0.53	0.35	0.22	0.2
10.5	0.63	0.41	0.263	0.225

x in ft

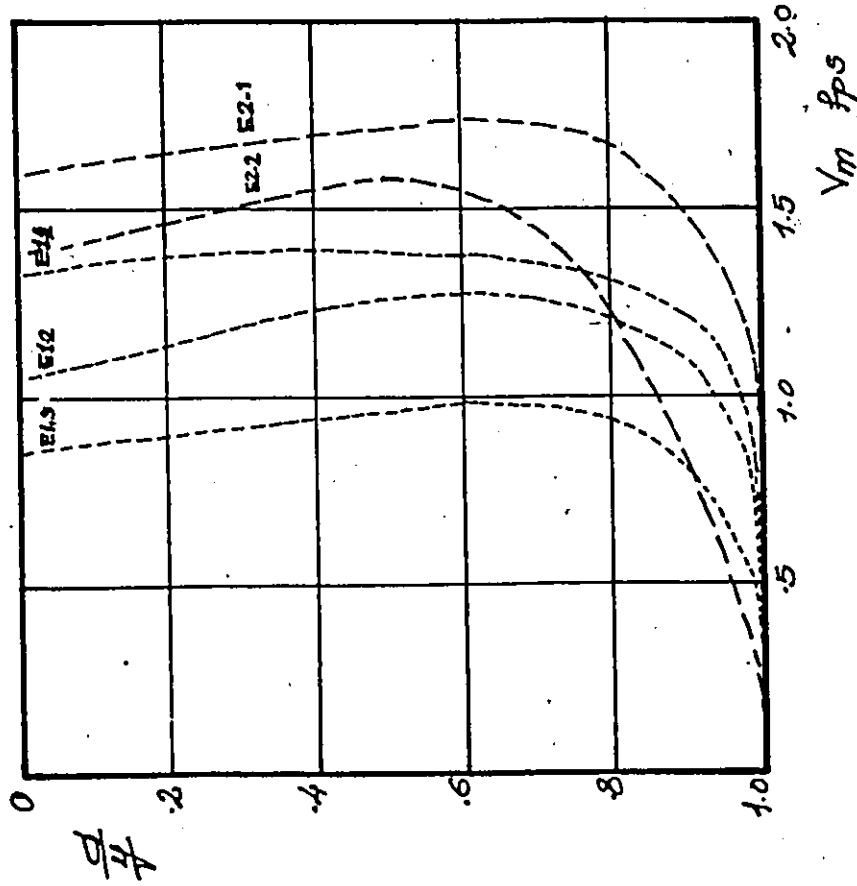
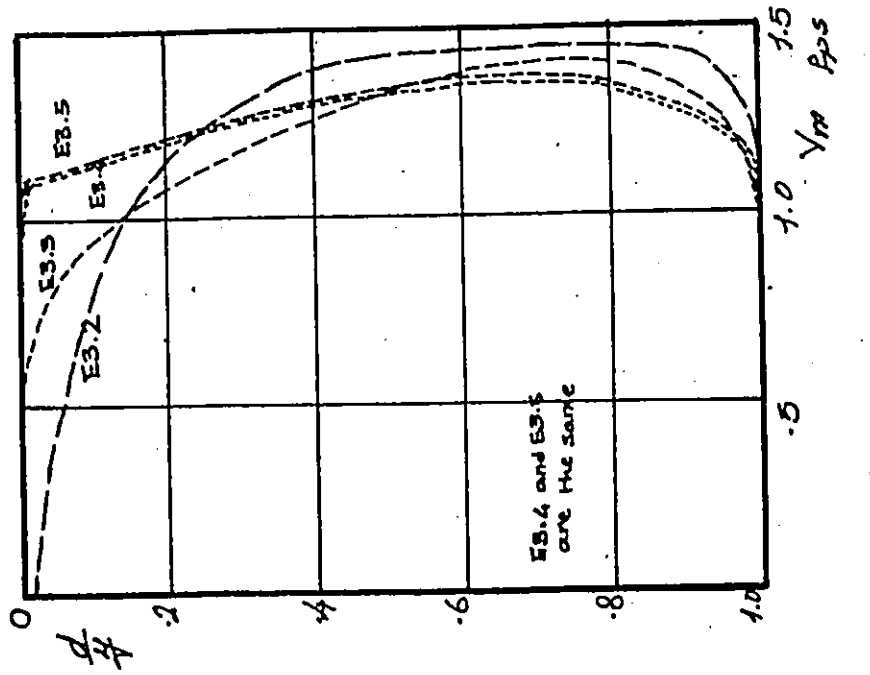


FIG. (E.1). Measured Velocity Profiles for Experiments E1, E2, and E3.

TABLE E-5
 VERIFICATION OF VELOCITY PROFILES

Run No.	Q	y	$\beta \times 10^3$	n	τ_2	V ₁	V ₂	V _{max}	d/y _{max}
E5-1	2.40	1.427	1.24	0.0161	0.04	0.85	0.91	1.06	0.58
E5-2	2.04	1.376	1.00	0.024	0.0182	0.94	0.86	0.97	0.45
E5-3	1.69	1.24	0.95	0.0246	0.0162	1.20	1.30	1.48	0.22
E5-4	2.38	1.135	2.2	0.0237	0.026	1.17	1.13	1.33	0.19
E5-5	2.04	1.08	2.25	0.0256	0.0166	0.98	1.00	1.07	0.50
E5-6	1.60	1.006	1.49	0.0243	0.0182	1.19	1.03	1.25	0.28
E5-7	1.22	0.75	2.34	0.0225	0.0316	1.24	1.15	1.35	0.18
E5-8	1.12	0.67	2.07	0.0228	0.023	1.24	1.15	1.35	0.18
E5-9	0.98	0.62	1.94	1.94	0.020	0.94	0.89	1.08	0.33

TABLE E-6
VERIFICATION OF COMPOSITE ROUGHNESS

Run No.	t	Q	τ	S	η	$E_{\eta} \%$ *
EG-1	1"	1.74	1.	0.0017	0.01967	25
EG-2	1	2.14	1.21	0.001	0.01939	29
EG-3	1	1.63	1.131	0.001	0.024	27
EG-4	1	1.37	1.068	0.0008	0.0231	34
EG-5	1	1.56	1.33	0.0005	0.0212	53
EG-6	1	2.25	1.41	0.0009	0.02176	31
EG-7	1	1.94	1.39	0.00058	0.01969	47
EG-8	1	1.60	1.33	0.00042	0.01890	64
EG-9	1	1.28	1.265	0.0005	0.0242	54
EG-10	1	2.38	1.577	0.00067	0.0202	42
EG-11	1	2.50	1.60	0.00083	0.0219	34
EG-12	1	1.27	1.29	0.00027	0.018	98
EG-13	2"	2.70	1.17	0.0018	0.0196	19
EG-14	2	1.93	1.34	0.00063	0.0195	44
EG-15	2	2.40	1.43	0.0009	0.0205	32
EG-16	2	1.69	1.24	0.00072	0.0215	38
EG-17	2	2.04	1.36	0.00117	0.025	26
EG-18	2	2.38	1.13	0.0022	0.0238	17
EG-19	2	1.42	0.75	0.00234	0.0226	16
EG-20	2	1.12	0.68	0.0021	0.0232	17
EG-21	2	0.98	0.62	0.00194	0.02282	18
EG-22	2	2.48	1.22	0.0018	0.0226	19
EG-23	2	0.89	0.82	0.0006	0.0215	43
EG-24	2	1.56	1.25	0.0005	0.0204	50
EG-25	2	1.94	1.32	0.0006	0.0189	43
EG-26	2	2.38	1.50	0.0007	0.0197	38
EG-27	2	2.50	1.52	0.0009	0.0213	32
EG-28	2	2.36	1.13	0.0016	0.0204	20
EG-29	2	2.12	1.09	0.0014	0.0202	22
EG-30	2	1.83	1.07	0.0011	0.0199	27
EG-31	2	2.20	1.26	0.0011	0.0207	27
EG-32	2	2.46	1.21	0.0013	0.0189	24
EG-33	2	1.82	0.91	0.0017	0.0199	20
EG-34	2	1.93	1.45	0.0008	0.0223	35
EG-35	2	2.39	1.42	0.0008	0.0192	34
EG-36	2	1.69	1.25	0.0008	0.022	40

* E_{η} is the maximum expected percentage error in the measured composite Manning's roughness coefficient.

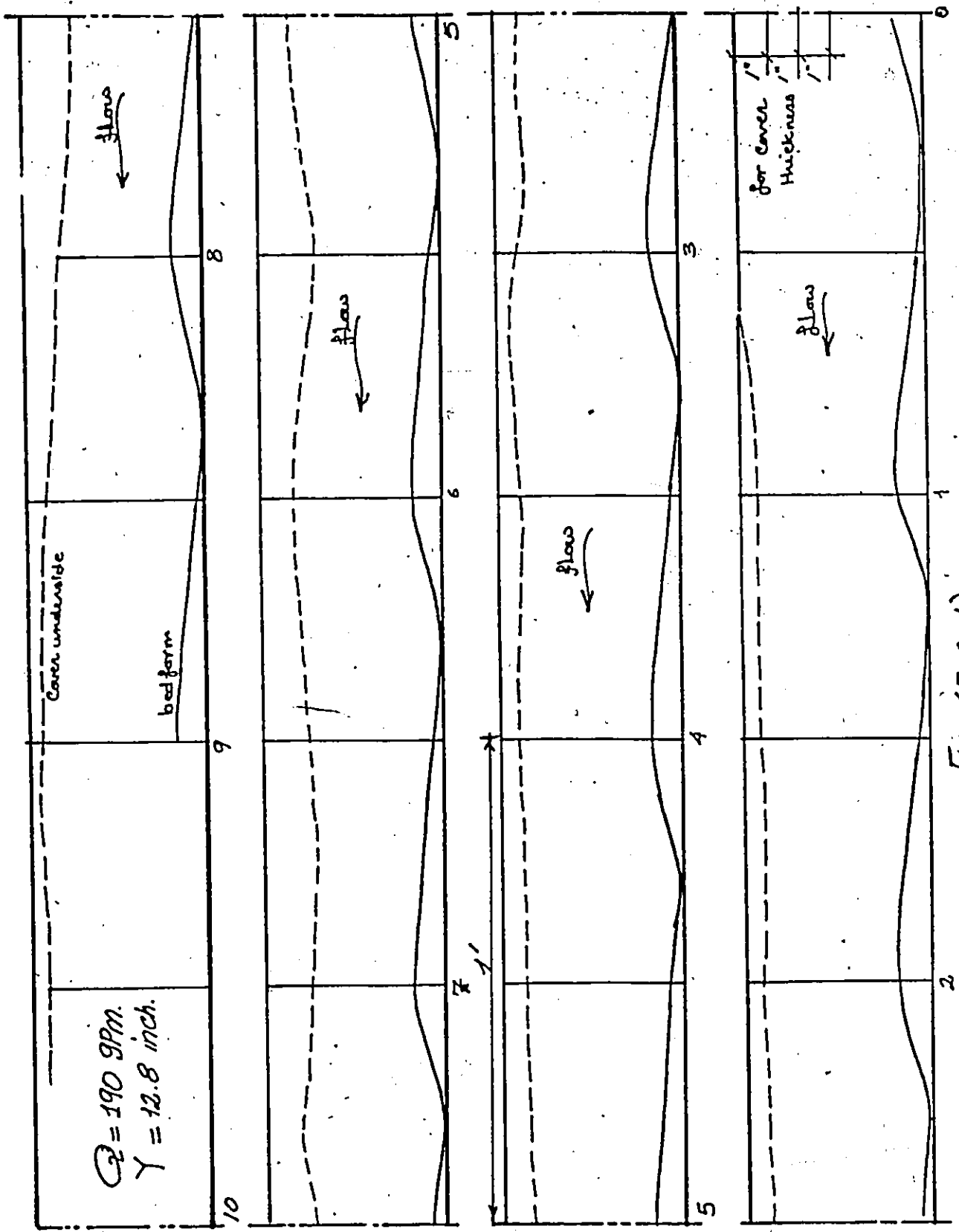


Fig. (E.2.1)

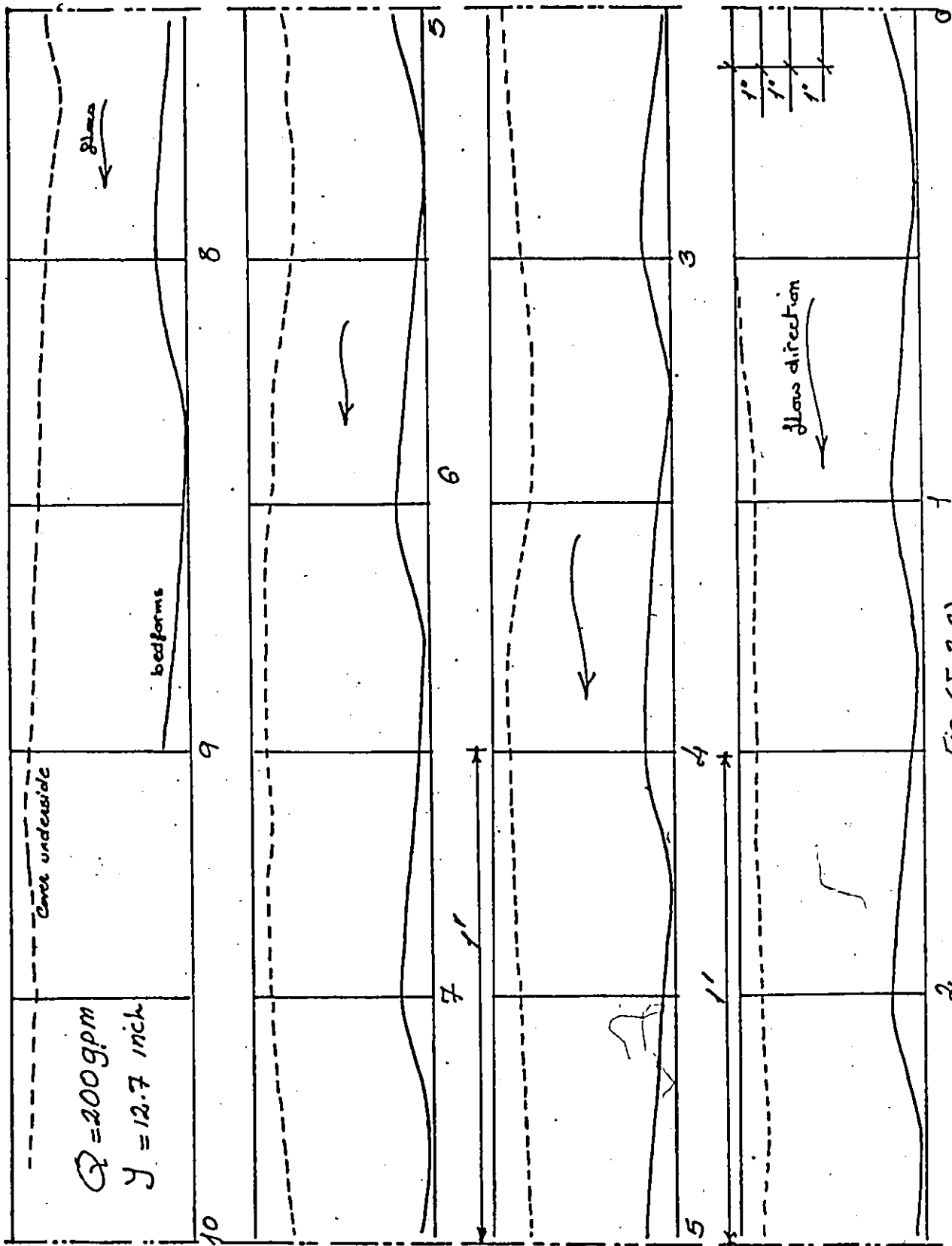


Fig. (E.2.2)

2

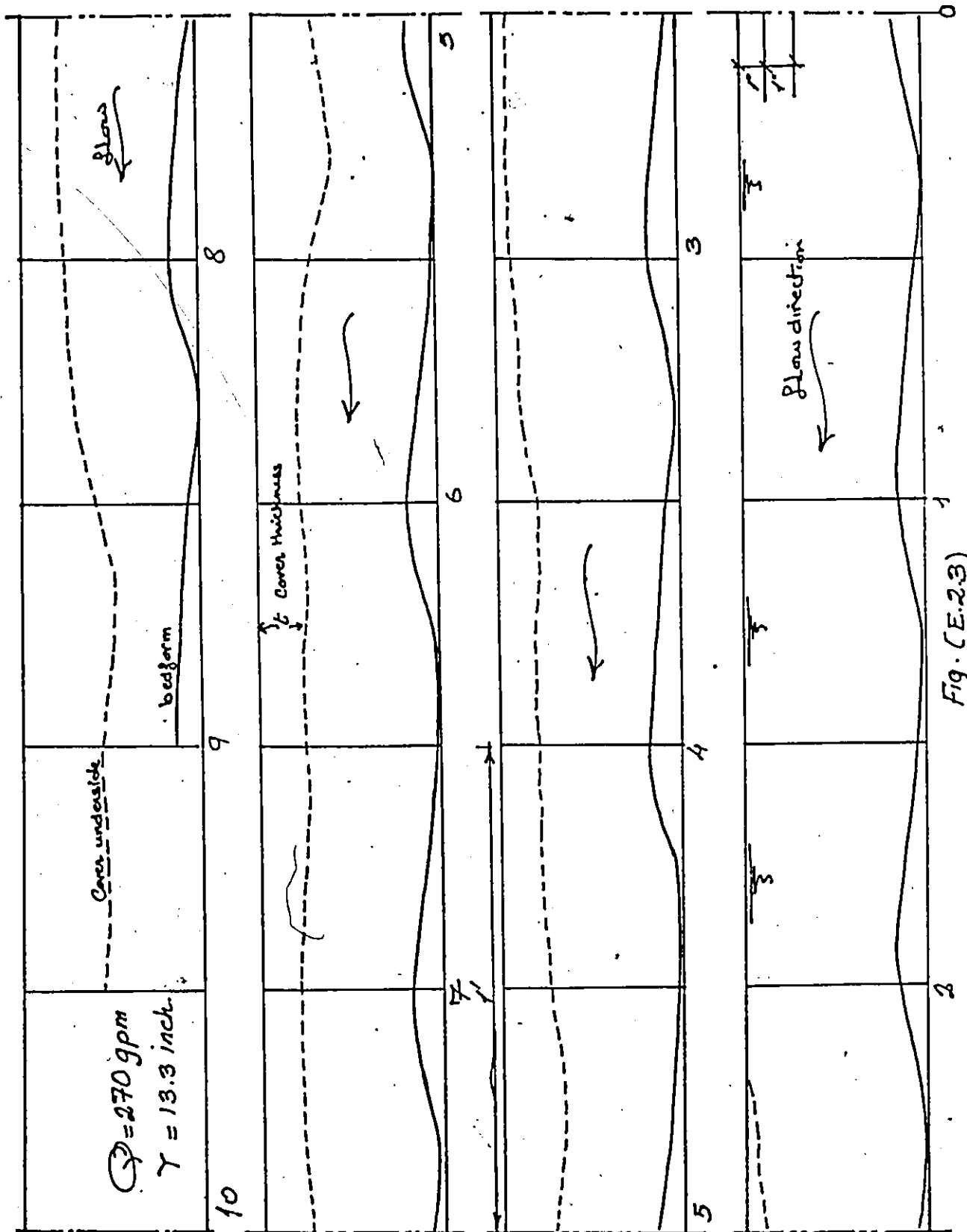


Fig. (E.2.3)

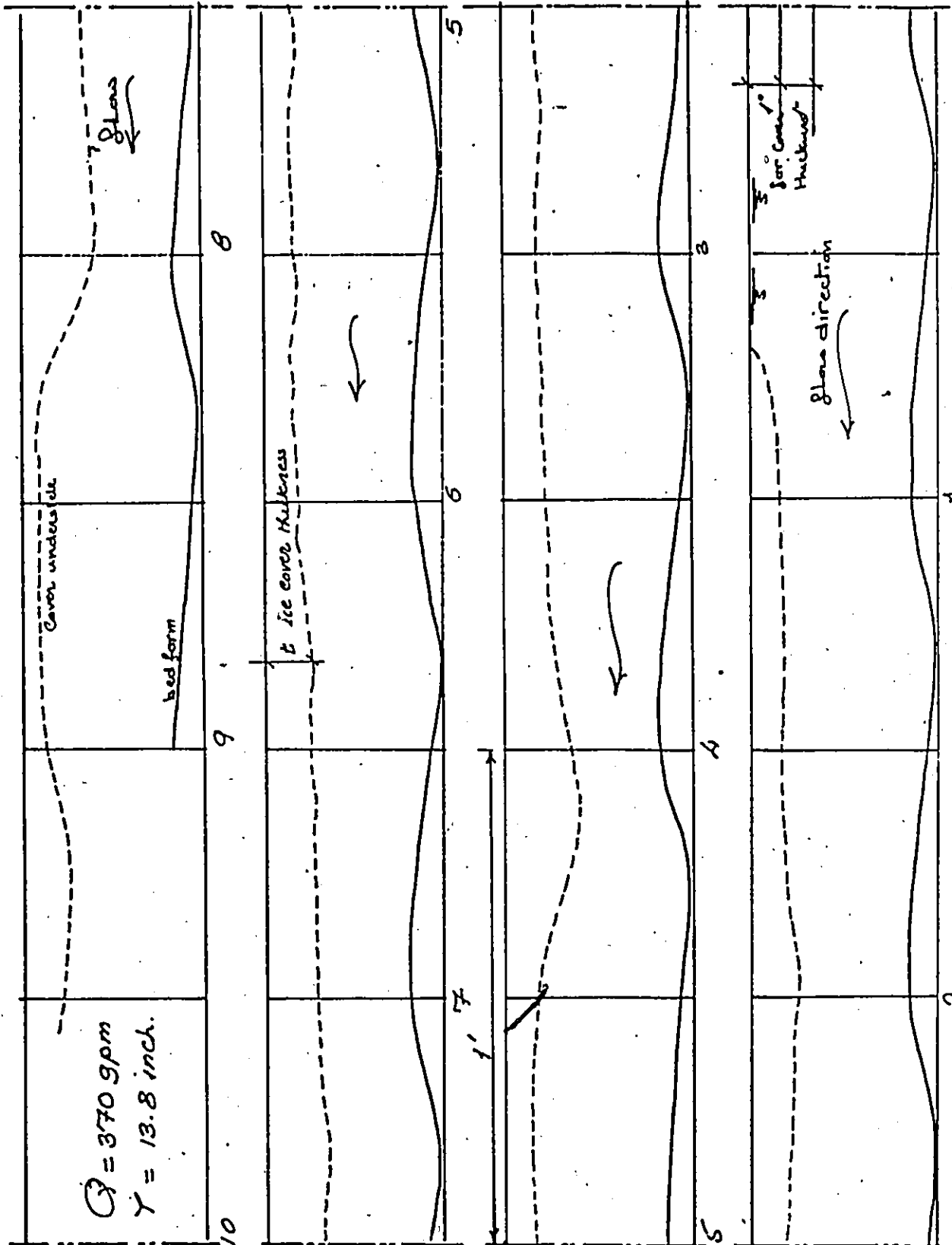


Fig. (E2.4)

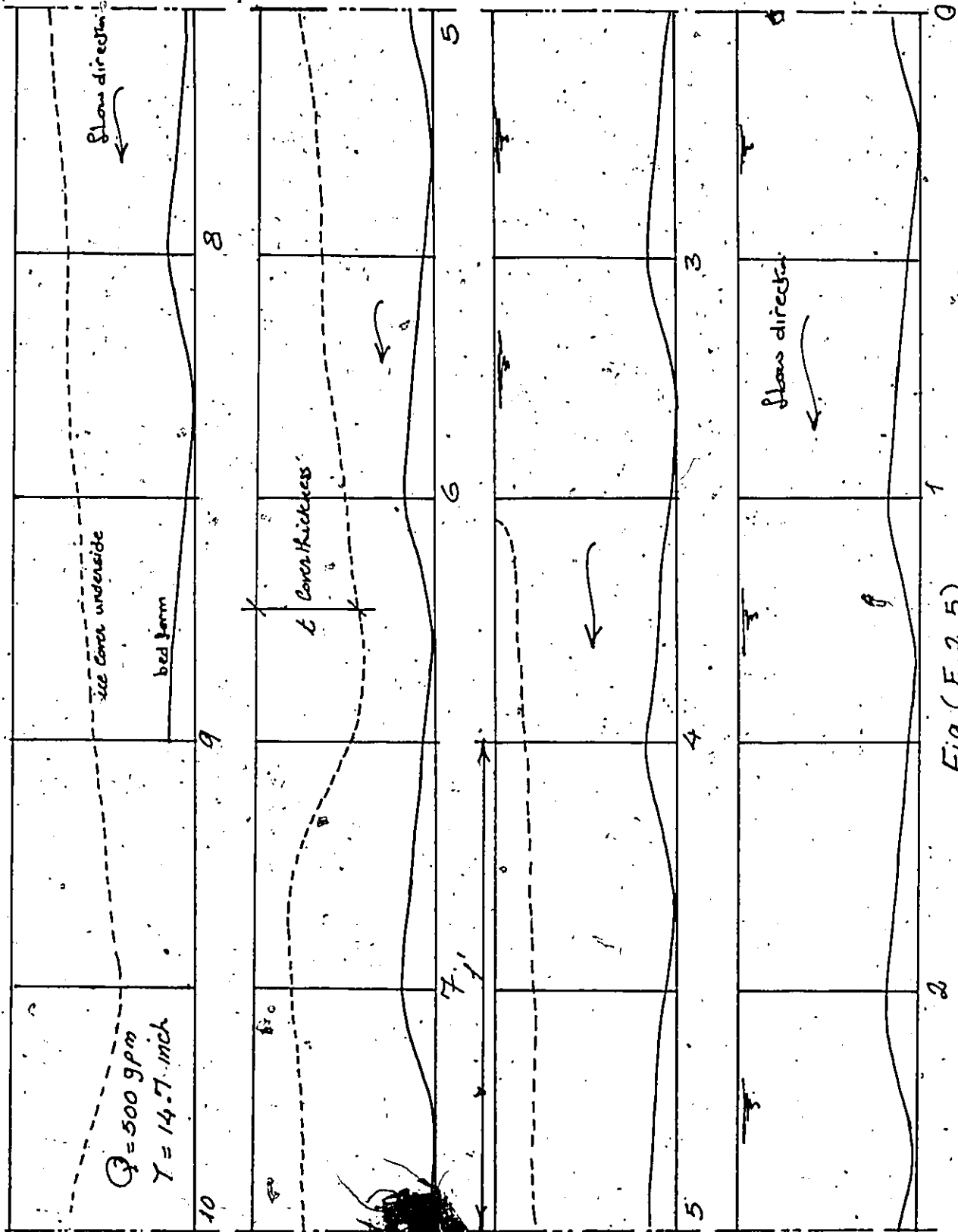


Fig (E.2.5)

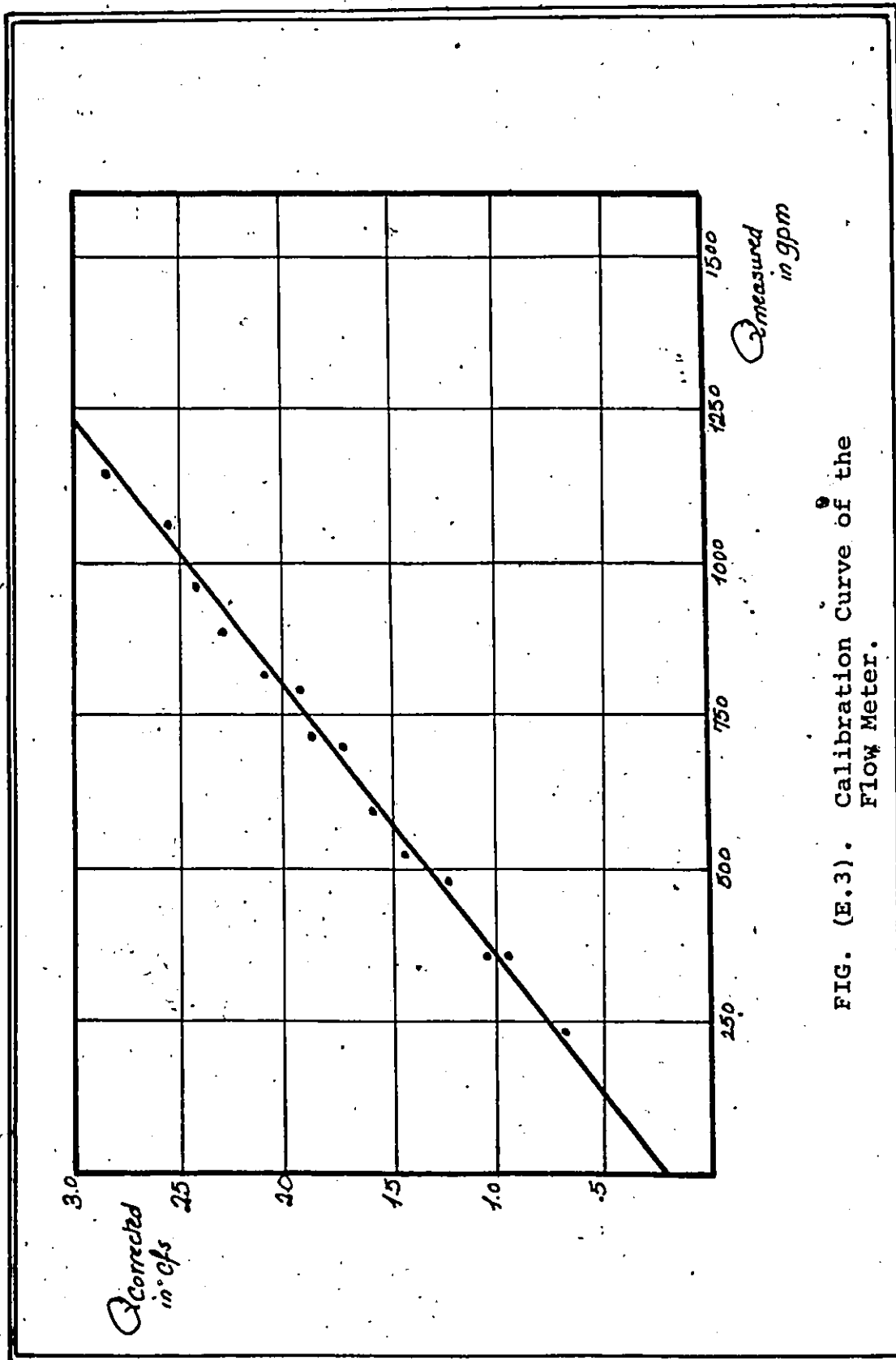


FIG. (E.3). Calibration Curve of the Flow Meter.

NOMENCLATURE

- A channel cross-sectional area, constant.
- A_1, A_2 cross-sectional area of channel and cover sub-sections respectively.
- a wetted perimeter ratio of P_1/P_2 .
- B channel top width.
- b channel bed width
- b bouyancy force.
- C Chezy's coefficient constant.
- C_1, C_2 Chezy's coefficients for channel and cover respectively.
- d local flow depth by Hancu.
- d_i roughness height for sub-section i.
- E absolute error
- E_R error in measuring hydraulic radius.
- E_S error in measuring the slope.
- E_V error in measuring the velocity.
- E_Y error in measuring flow depth.
- Exp. exponential ; $EXP(x) = e^x$.
- F special Froude number used by Uzuner.
- F_n Froude number.
- F_{ix} body forces in x-direction.
- f Darcey's-Wiesbach friction factor.
- f_{MOD} modified Darcey's-Wiesbach friction factor.
- g acceleration due to gravity.
- H height.

i	subscript takes the value 1 for channel sub-section and 2 for cover sub-section.
k	constant
k_i	roughness height for the boundary i .
L	length.
L	Prandtl mixing length.
M	Manning's index value.
n	composite Manning's roughness coefficient.
n_i	Manning's roughness coefficient for the boundary i .
P	channel wetted perimeter.
P_i	channel wetted perimeter for the boundary i .
P	pressure force.
Q	flow discharge with ice cover.
Q_0	flow discharge without ice cover.
R	channel hydraulic radius.
R_i	channel hydraulic radius for sub-section i .
R_n	Reynolds number.
r	general exponent for Chezy-Manning n relation.
S	slope of energy line.
S_0	slope of bed line.
t	cover thickness
u_i	local velocity at point i .
\bar{u}	average point velocity in x -direction.
u'	fluctuating point velocity in x -direction.
V	channel mean velocity.
V_i	mean velocity for sub-section i .
V_{*i}	shear velocity of sub-section i .

V_{\max}	maximum velocity in the cross-section and flow.
\bar{v}	average point velocity in y-direction.
v	fluctuating average point velocity in y-direction.
W	weight.
x	distance along x-axis.
Y	total flow depth.
Y_i	flow depth at sub-section i.
Y_{ij}	depth from point to boundary i.
z	exponent used by Yu.
α	angle.
α	wetted perimeter ratio P_1/P .
α_n	hydraulic division ratio used by
γ_i	laminar sub-layer thickness for boundary i.
γ	specific weight of the water.
ρ	density of specific weight of the water.
ρ	density of specific weight of the ice.
λ	hydraulic radius ratio R_2/R_1 .
λ_0	initial λ value used in numerical solutions.
λ	friction factor used by Hancu.
ϵ	relative depth.
ϵ_i	relative depth to boundary i.
μ	dynamic viscosity of fluid.
π	dimensionless term.
τ_L	laminar shear.
τ_t	turbulent shear.
τ_i	shear stress at boundary i.
τ_m	mean shear stress at ice underside.

κ

Von Karmen's constant.

 ϕ

general function.

LIST OF REFERENCES

1. Ashton, G.D. and J.F. Kennedy, "Ripples on Underside of River Ice Covers", J. of Hydraulics Division, ASCE, Vol. 98, No. HY9, September 1972, PP. 1603-1624.
2. Ashton, G.D., "Stability of Floating Ice Blocks", Discussion, J. of Hydraulics Division, ASCE, Vol. 99, No. HY11, November 1973, PP. 2142-2144.
3. Carey, K.L., "Observed Configuration and Computed Roughness of the Underside of River Ice, St. Croix River, Wisconsin". U.S. Geol. Survey Prof. Paper 550B, Geological Survey Research, 1966, PP. B192-B198.
4. Carey, K.L., "The Underside of River Ice, St. Croix River, Wisconsin", U.S. Geol. Survey Prof. Paper S75-C, Geological Survey Research, 167, PP. C195-C199.
5. Carey, K.L., "Analytical Approaches to Computation of Discharge of An Ice Covered Stream", U.S. Geol. Survey Prof. Paper S75-C, Geological Survey Research 1967, PP. C200-C207.
6. Chang, F.M., D.B. Simons and E.V. Richardson, "Total Bed-Material Discharge in Alluvial Channels", IAHR, PP. A17.1-A17.6.
7. Graf, W.H., "Hydraulics of Sediment Transport", McGraw-Hill, 1974.
8. Henderson, F.M., "Open Channel Flow", MacMillan, New York, 1966.
9. Hinze, J.O., "Turbulence", McGraw-Hill, New York, 1959.
10. Kartha, V., H.J. Leutheusser, "Distribution of Tractive Force in Open Channels", J. of Hydraulics Division, ASCE, Vol. 96, No. HY7, July 1970, PP. 1469-1483.

11. Khanna, Sat Dev, "Experimental Investigation of Form of Bed-Roughness", J. of Hydraulic Division, ASCE, Vol. 96, No. HY10, October 1970, PP. 2029-2040.
12. Komora, J. and J. Sumbal, "Head Losses in Channels With Ice Cover", IAHR, 1967, No. S25, PP. S25.1-S25.5.
13. Krishnamurthy, M. and B.A. Christensen, "Equivalent Roughness for Shallow Channels", J. of Hydraulics Division, ASCE, Vol. 98, No. HY12, December 1972, PP. 2257-2264.
14. Langhaur, H.L., "Dimensional Analysis and Theory of Models", Wiley, New York, 1964.
15. Larsen, P.A., "Hydraulic Roughness of Ice Covers", J. of Hydraulic Div., ASCE, Vol. 99, No. HY1, January 1973, PP. 111-119.
16. Larsen, P.A., "Head Losses Caused by an Ice Cover on Open Channels", J. of Civil Engineering, Hydraulic Section, Boston Society of Civil Engineers, November, 1966, PP. 45-67.
17. Neville, A.M., and J.B. Kennedy, "Basic Statistical Methods for Engineers and Scientists", International, Scranton, Pennsylvania, 1968.
18. Nezhikhovskiy, R.A., "Coefficients of Roughness of Bottom Surface of Sluche-Ice Cover", Soviet Hydrology: Selected Papers, No. 2; PP. 127-150, 1964.
19. Pariset, E. and R. Hausser, "Formation and Evolution of Ice Covers on Rivers", Trans. of The E.I.C., Vol. 5, No. 1, 1961, PP. 1-9.
20. Powell, Ralph W., "The Origin of Manning's Formula", J. of Hydraulic Div., ASCE, Vol. 94, No. HY4, July 1968, PP. 1179-1181.
21. Rouse, H., "Engineering Hydraulics", Wiley, New York, 1958.
22. Rouse, H., "Advanced Mechanics of Fluids", Wiley, New York, 1959.
23. Rouse, Hunter, "Critical Analysis of Open-Channel Resistance", J. of Hydraulic Div., ASCE, Vol. 91, No. HY4, July 1965, PP. 1-25.

24. Schiller, E.J., W.W. Sayre, "Vertical Temperature Profiles in Open Channel Flow", J. of The Hydraulics Division, ASCE, Vol. 101, No. HY6, June 1975, PP. 749-761.
25. Schlichting, H., "Boundary Layer Theory", McGraw-Hill, New York, 1955.
26. Smith, K.V.H., "Alluvial Channel Resistance Related to Bed Form", J. of Hydraulics Div., ASCE, Vol. 94, No. HYL, January 1968, PP. 59-69.
27. Sumbal, J., J. Komora, "Determination of the Tangential Stress Acting on the Ice Cover in a Rectangular Flume", IAHR, 1967, No. 5-21, PP. 255-259.
28. Uzuner, M.S., J.B. Kennedy, "Stability of Floating Ice Blocks", J. of Hydraulics Div., ASCE, Vol. 98, No. HY12, December 1972, PP. 2117-2133.
29. Uzuner, M.S., "The Composite Roughness of Ice Covered Streams", J. of Hydraulic Research, IAHR, Volume 13, No. 1, 1975, PP. 79-102.
30. Yen, Chin-Lien and D.E. Overton, "Shape Effects on Resistance in Flood-Plain Channels", J. of Hydraulics Div., ASCE, Vol, 99, No. HYL, January 1973, PP. 219-238.
31. Yu, K.H., W.H. Fraff and G. Levine, "The Effect of Ice on the Roughness Coefficients of the St. Croix River", Proc. 11th Conf. Great Lakes Res., Assoc. Great Lakes Res., 1968, PP. 668-680.
32. "River Ice Problems: A State-of-the-Art Survey and Assessment of Research Needs", Report of the Task Committee on Hydromechanics of Ice of the Committee on Hydrodynamics of the Hydraulics Division, J. of Hydraulics Division, ASCE, Vol. 100, HYL, January 1974, PP. 1-16.
33. "Friction Factors in Open Channels", Progress Report of the Task Force on Friction Factors in Open Channels of the Committee on Hydromechanics of the Hydraulics Division, J. of Hydraulics Division, ASCE, Vol. 89, No. HY2, March 1963, PP. 97-143.

VITA AUCTORIS

1951. Born on the 15th of May in Cairo Egypt.
- 1967 Matriculated from Ibrahimia Secondary School, Cairo, Egypt.
- 1972 Graduated with a Bachelor of Science (Honour) in Civil Engineering, Cairo University, Cairo, Egypt.
- 1972 Appointed as an Instructor of Civil Engineering in the Hydraulics and Irrigation Department, Cairo University, Giza, Egypt.
- 1974 Registered as a M.A.Sc. candidate in Civil Engineering at the University of Windsor, Windsor, Ontario, Canada.